The impact of placement method on Antifer-block stability

Master of Science thesis

May 2007

A.B. Frens

MSc Committee:
Prof. Dr. Ir. M.J.F. Stive
Dr. Ir. M.R.A. van Gent
Dr. Ir. W.S.J. Uijttewaal
Ir. J. Olthof
Ir. H.J. Verhagen

Preface

To accomplish the Master of Science programme in Civil engineering, at Delft University of Technology, the impact of the placement method on the stability of Antifer-block armoured breakwaters was studied. The preparation and evaluation of the experiments were performed at Royal Boskalis Westminster nv. The experiments have been carried out at the Fluid Mechanics Laboratory of the Faculty of Civil Engineering and Geosciences at Delft University of Technology.

I would like to thank my graduation committee for their supervision and motivating support during the whole process. Furthermore I thank Royal Boskalis Westminster nv. for their financial support during this complete research and WL|Delft Hydraulics for providing me the Antifer-blocks. Finally I would like to thank all the members of the support staff of the Fluid Mechanics Laboratory for their help and advice during the experiments and everyone who assisted me in the realisation of this research.

Arjan Frens
Delft, May 2007

Abstract

Between 1976 and 1978 the breakwater for the harbour of Antifer (France) was constructed. In the design study a series of tests was carried out, which showed that blocks with simple cubic shape did not ensure the stability of the armour layer. An investigation of other block geometries led to the choice of blocks grooved on four sides. These grooved cubes, now called Antifer-blocks, have been applied for other breakwaters all over the world. For these breakwaters different placement methods were applied, because the Antifer-block is not patented and there are no guidelines developed which describe the best placement method. Over the years different placement methods were used and researched, however there is still much indistinctness on this subject, because the obtained information is very fragmented.

The main objective of this research was to assess the impact of different placement methods, with different packing densities, on the stability of Antifer-block armour layers. This was done by experimental research in the wave-flume of the Fluid mechanics laboratory of the Faculty of Civil Engineering and Geosciences at Delft University of Technology. The wave flume had a length of 40 meters, a width of 0.80 meter and a height of 1.00 meter. A foreshore with a slope of 1:35 was present in the flume, starting 8.00 meters from the wave board. The toe of the model was placed on the slope after 6.30 meters and was constructed with large stones, which assured the toe stability. The used Antifer-blocks had a nominal diameter of 4.0cm and were placed by hand on the trunk-section, which had a slope of 1:1.5. The dimensions of the under layer and core material were determined with the rules of thumb recommended by VAN GENT, 2006. This resulted in stones with a nominal diameter of 1.96cm for the under layer and 1.08cm for the core. 17 experiments were performed with packing densities between 44.8 and 61.1 percent. For every experiment the under layer, toe and armour layer were rebuilt. The placement of Antifer-blocks over the slope without any contact between the blocks resulted in the sliding down and a more irregular positioning of the blocks. Therefore the blocks could not be placed within a square grid and it was very difficult to obtain a prescribed packing density for irregular placed blocks.

After building the model the flume was filled with 60cm of water. The placed Antifer layer was tested with eight irregular wave series with increasing significant wave heights from 9cm up to 20cm. The irregular waves were generated according to the JONSWAP spectrum. For all wave series the number of waves was between 1000 and 1500. The average wave steepness for these wave series was 3% (calculated with the peak period).

After each wave series digital photos of the armour layer were taken from a fixed position perpendicular to the slope. Through comparison of the images, with the overlay technique, different block movements could be counted within different reference areas, which determined the stability of the layer. The stability values for the placement methods were based on wave heights before failure (when much repair is necessary). For regular placements this was for zero displaced blocks, because the displacement of one block caused a chain reaction. The stability values for the irregular placement method were calculated for less than 5% displacements within a reference area of SWL (Still Water Level) $\pm 5 \cdot D_n$. The first displacements mainly occurred around SWL, which stresses the importance of the chosen reference area for the stability calculation. Also the reflection coefficients per wave series were calculated. The highest waves during the last wave series overtopped the model and were able to move the unprotected core material on the leeside. This deformation at the leeside resulted in a berm profile at SWL level. The length of this berm was an indication for the amount of overtopped water.

A total of 17 experiments were performed with different placement methods and packing densities. From these experiments followed that regular placement methods behave more stable than irregular placement methods with a similar packing density. Also the more irregular (less accurate) positioning of blocks within a regular placement method caused a decrease in stability. Higher packing densities for equal placement methods lead to higher stabilities and higher reflection coefficients. The resulting K_D-values were between 4.0 and 23.7. If the reflection coefficients during the first wave series were high, this resulted in a long berm length, which indicates that there is a positive correlation between the reflection and the overtopping.

Overall it could be concluded that, when the under layer and the toe are smooth and the blocks can be placed accurately, the best performing placement methods are the closed pyramid placement method, figure 1, for packing densities around 45% and 50% and the double pyramid placement method, figure 2, for packing densities around 55% and 60%. The size of the openings to the under layer, of the double pyramid placement method, influenced the reflection coefficients. When the second layer was shifted half a nominal diameter upwards, as in figure 2, the reflection coefficients were minimal. It is recommended to investigate the possible negative influence of oblique incoming waves on the stability of the double pyramid placement method.
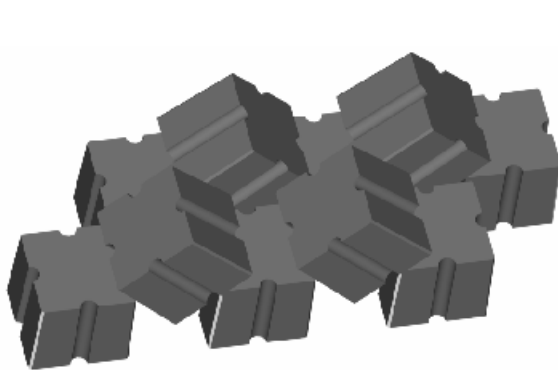
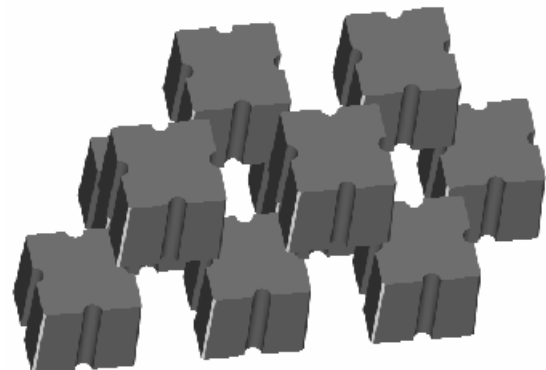Figure 1: Closed pyramid placement method   Figure 2: Double pyramid placement method

The eventual choice of the placement method and packing density depends on the allowed reflection and/or overtopping and the construction costs. The construction costs can be divided into the production costs, the placement costs and the constant costs. For equal constant costs and equal or small differences in placement costs the placement with the higher packing density and accompanying stability value is cheaper for high design wave heights. When the placement costs decrease for both placements or only for the placement with the higher packing density, then the placement with the higher packing density becomes also cheaper for lower wave heights.

Table of contents

List of symbols

a	Bottom width of Antifer-block	m
b	Top width of Antifer-block	m
B	Taper angle of Antifer-block	°
c	Depth of groove of Antifer-block	m
C_r	Reflection coefficients	-
d	Solid armour density	-
D_n	Nominal diameter of the armour unit	m
D_{n50}	Nominal diameter of the rocks	m
D_1	Displacement ratio, for displacements between 1 and $2 \cdot D_n$	-
D_2	Displacement ratio, for displacements above $2 \cdot D_n$	-
D_t	Total displacement ratio $(>1 \cdot D_n)$	-
E	Constant costs ratio	-
$E(f)$	Frequency spectrum	m²·s
F_D	Drag force	N
F_G	Gravitational force	N
F_I	Inertia force	N
F_L	Lift force	N
Fr	Froude number	-
g	Gravitational acceleration	m/s²
h	Water depth	m
H_s	Significant wave height	m
H_{m0}	Measured incoming significant wave height	m
H_{Rm0}	Measured reflected significant wave height	m
k_Δ	Layer thickness coefficient	-
K_{DH}	Stability parameter, Hudson	-
K_{D0}	Stability parameter, zero damage	-
$K_{D<5\%}$	Stability parameter, less than 5% damage	-
L	Length	m
M	Mass	kg
MI	Mesh grid	m
M_1	Movement ratio, for movements between 0 and $0.5 \cdot D_n$	-
M_2	Movement ratio, for movements between 0.5 and $1 \cdot D_n$	-
M_t	Total movement ratio $(0\text{-}1 \cdot D_n)$	-
n	Number of layers	-
N	Number of waves	-
N_{BL}	Number of blocks	-
N_{PBL}	Maximum possible number of block volumes	-
N_{od}	Damage number	-
N_s	Stability parameter	-

N_t	Required number of blocks per surface	-
P	Porosity	-
r	Radius groove of Antifer-block	m
Re	Reynolds number	-
R_{Nt}	Ratio for the required number of blocks	-
R_{Vb}	Ratio for the required block volumes	-
R_{Vt}	Ratio for the required volumes of concrete	-
S_d	Damage spreading ratio	-
s	Wave steepness	-
t	Layer thickness	m
T_p	Peak period	s
T_m	Average period	s
U	Velocity	m/s
V_b	Required volume per block	m³
V_t	Required volume of concrete per surface unit	m³/m²
Z	Placement costs ratio	-
α	Slope angle	º
β	Wave incident angle	º
Δ	Relative density	-
ρ_s	Density of the armour unit	kg/m³
ρ_w	Density of the water	kg/m³
ϕ	Packing density	-
ϕ_1	Number of blocks per unit area	-/m²
ϕ_2	Ratio between the real and the maximum number of blocks per unit area	-
ψ_S	Surface packing density	-
ξ	Surf similarity parameter	-

hyd²oRonamic

TUDelft

1 Introduction

Between 1976 and 1978 the harbour of Antifer (France) was constructed. To ensure a safe entrance a breakwater was required for the protection against waves, swell and to limit current velocities in the manoeuvring and berthing areas. In the design study a series of tests was carried out. The tests on the breakwater, exposed to wave action, showed that blocks with simple cubic shape did not ensure the stability of the armour layer. An investigation of other block geometries, combinations of different blocks and weights and finally accepting flow of water inside the protective layer, led to the choice of blocks grooved on four sides. MAQUET, 1985 concluded that, as a result of the hydraulic action of the grooves and the improved friction caused by them, the stability of the protective layer was noticeably improved compared to the plain block. Subsequently, all profiles were designed with grooved blocks.

"The Antifer Breakwater may in its design as well as in its construction be considered being one of the most advanced structures in the world. So far it has fulfilled its obligations without flaws – and with little maintenance, mainly in the head-section as it could be expected. It is an example of meticulous planning, design & execution." [MAQUET, 1985]

The grooved cubes, now called Antifer-blocks, have been applied for other breakwaters all over the world, see figure 1.1 (courtesy Delft Hydraulics). For these breakwaters different placement methods were applied, because the Antifer-block is not patented and there are no guidelines developed which describe the best placement method. The practical importance of the placement method has an economical background. When, for example, a placement method is applied with the same stability for the same units, but with a lower packing density (units per area), expenses on concrete and execution can be saved. Over the years different placement methods were used and researched, however there is still much indistinctness on this subject, because the obtained information is very fragmented.

Figure 1.1: Sines (Portugal) breakwater under wave attack

The main objective of this research is to assess the impact of different placement methods, with different packing densities, on Antifer-block stability. This will be done by experimental research in the wave-flume of the Fluid mechanics laboratory of the Faculty of Civil Engineering and Geosciences at Delft University of Technology. Irregular waves will perpendicular attack the double layered armour of Antifer-blocks placed on a trunk-section with a slope of 1:1.5 and a stable toe.

This report describes the performed study. In chapter 2 a study of literature is presented to gain insight into the current knowledge on Antifer-blocks, stability and placement methods. Chapter 3 deals with the set-up of the model and chapter 4 with the procedure of the performed experiments. This implies the construction of the model, the test procedure and the analysis. In chapter 5 the 17 performed experiments are analysed and they are evaluated in chapter 6. In chapter 7 a cost analysis is presented which is applied on the best performing placements from chapter 6. Finally the conclusions and recommendations which followed from this research are presented in chapter 8.

2 Literature study

2.1 Introduction

Breakwaters have a sheltering effect, which is established through a reduction or cut-off of the incident wave energy. This is done by both the reflection of waves and by turbulent dissipation of the wave energy. An important dissipation mechanism is wave breaking. Wind generated waves usually break on a sloping structure since the decrease in depth causes a reduction in wave celerity. The wave breaks when the particle velocity exceeds the wave celerity. Another effective dissipation mechanism is the turbulent flow in a porous structure. The combination of both mechanisms leads to a rubble mound breakwater in its simplest form, a homogenous mound of rocks. The structure however must consist of stones large enough to withstand displacement by wave forces. This in return will lead to a very permeable breakwater with considerable wave penetration and transmission. Additionally, large stones are expensive because most quarries yield a lot of finer material and only relatively small amounts of large rock material. In practice therefore the structure consist of fine materials armoured by large stones. Because of technical, transportation or economical limitations of natural stone many breakwaters are armoured with concrete armour units. In order to prevent the wash-out of the core material, filter layers are often required.

During the design process of a breakwater all failure modes of a structure must be identified and assessed. Figure 2.1 shows the most common failure mechanisms of a conventional breakwater. This thesis focuses on the hydraulic stability of the double Antifer armour layer for different placement methods. In this chapter the present knowledge on Antifer-blocks will be presented and discussed; first the Antifer-block, then the hydraulic stability and the chapter will be concluded with the placement method.
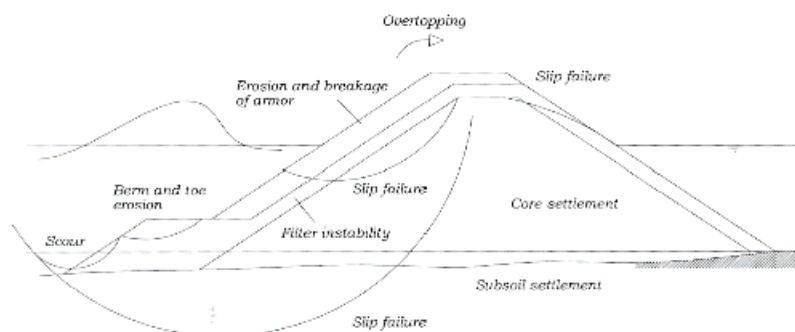

Figure 2.1: Failure modes of a conventional rubble mound breakwater

2.2   The Antifer-block

2.2.1   General information

Many breakwaters are armoured with concrete armour units. These units can be divided in the following categories related to their structural strength: massive, bulky, slender and multi-hole, see figure 2.2.
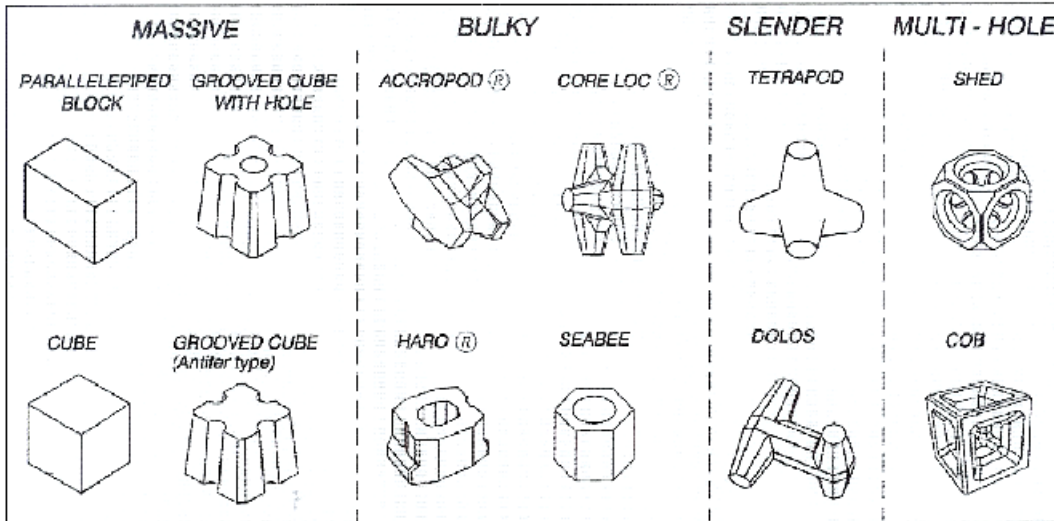

Figure 2.2: Examples of concrete armour units [CEM, 2006].

Compared to bulky, slender and multi-hole units, an armour layer of massive units requires more concrete. VAN DER MEER, 1999 made a comparison of different concrete units based on a weight around 30 ton, see table 2.1. The stability coefficient (K_D-value) in this table is derived with the Hudson method, which is described in paragraph 2.3.2. The packing density (ϕ) is described in paragraph 2.4.2.

Type of Armour	Accropode	Core-loc	Tetrapod	Cube
Slope, $\cot\alpha$	1.33	1.33	1.5	1.5
Number of layers	1	1	2	2
Stability coefficient, K_D	12	16	7	7
packing density, ϕ	0.61	0.56	1.04	1.17
Relative volume of concrete	100%	81%	208%	220%

Table 2.1: Comparison of different concrete units [VAN DER MEER, 1999]

The necessity to use a stronger crane and problems with tension-cracks, caused by the high level of hydration heat and subsequent thermal stresses, are also disadvantages of massive blocks. Despite of these disadvantages, irregular placed massive blocks have specific applications where they are useful. Such as:
-construction quality is expected to be difficult to control
-high uncertainty in the wave climate
-expected instability of the foundation

In these cases interlocking blocks, like dolos and core-loc, may be unreliable due to potential breakage, because of their thin profile. Block breakages cause the armour layer to loose its function earlier than expected and increase the uncertainty of the life of the structure.

The Antifer-block, figure 2.3, is a massive armour unit and was created during tests for the breakwaters of the harbour of Antifer in 1976 by Maquet. The block has four grooves and a slightly tapered shape, so it is easier released from the mould. MAQUET, 1985 concluded that as a result of the hydraulic action of the grooves and the improved friction caused by them, the stability of the protective layer was noticeably improved compared to the plain cube. There are designers who prefer the plain cube, because the moulds are less complex and in their opinion the interlocking capability and the difference in stability is minimal.
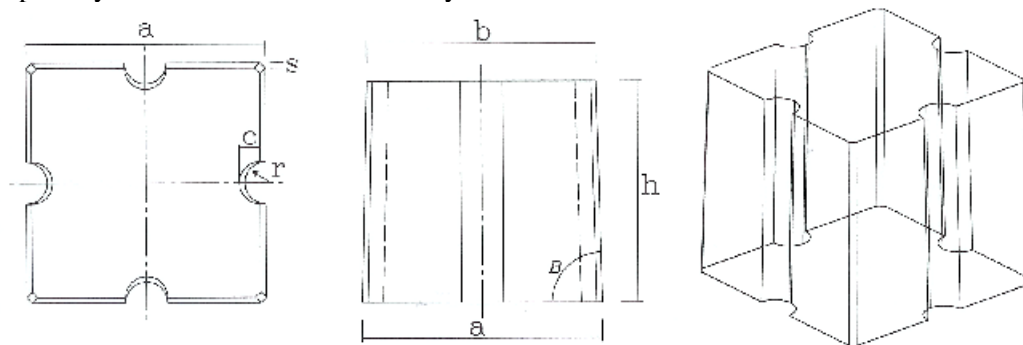
$a = 1.076 \cdot \sqrt[3]{V}$	width bottom
$b = 0.9254 \cdot a$	width top
$h = 0.921 \cdot a$	height
$r = 0.1115 \cdot a$	radius groove
$c = 0.0877 \cdot a$	depth groove
$s = 0.022 \cdot a$	width corner side
$B = 87.7°$	taper angle

Figure 2.3: Geometric characteristics Antifer-block

2.2.2   Production

GÜNBAK, 1999 recommends for Antifer-blocks the use of non reinforced concrete with a specific weight between 2.2 and 2.4 t/m³ and a compression resistance within a range of 200-250 kg/cm². According to Günbak it is advisable to cast the concrete with 50% or higher blast furnace cement and with a water/cement ratio lower than 0.45 for obtaining a durable unit at marine environment. The generally used moulds are steel single piece lift-off moulds, with bottom and top open. The moulds must be heavy enough so that they will not rise with the negative pressure developed by the inclined side walls. They should be constructed from steel of sufficient thickness or braced well from outside so that they do not deform under pressure.

For the construction of a breakwater in Brunei [JONES *et al.*, 1998] the moulds were placed on a well prepared concrete surface. Hereafter the concrete was poured in from the top and compressed with thickness vibrators. Insulation was placed between the form boundaries, the bottom and the concrete, so the water could not drain out the form. After a minimum of 6 hours the form had to be pulled upwards (like a mud pie). Sometimes assistance is necessary in breaking the bond between the cube and the mould. This can be done with a hydraulic jack or a lever arrangement pushing the block downwards from the top, see figure 2.4. Problems with mould releases in the smaller cube sizes can be resolved by introducing a slight increase in taper. After stripping, the blocks were covered with burlap and were kept wet by trickle hose irrigation. 3 days later they were lifted and moved to the stockpiles where the blocks were kept for a minimum of 27 days more. The duration of the drying process depends on the reduction of hydration heat and subsequent thermal stresses, which cause tension-cracks. The blocks can be moved with a large tong arrangement, with a part placed in the vertical groove for lateral stability. For small cubes the tong is placed under the base and for large cubes sockets can be cast into the sides to allow a grip at a higher level. Also hydraulic clamps or wires are used, see figure 2.5.
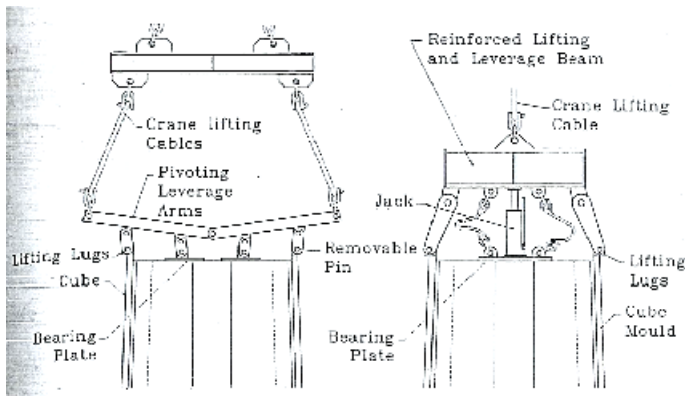
Figure 2.4: Form stripping devices [JONES *et al.,* 1998]

Figure 2.5: Production line in Hisaronu, Turkey

2.2.3 Placement technique

The placing of Antifer-blocks is done from sea or from land. Usually placement from sea brings more difficulty in positioning and safe placement due to waves, currents and wind. For a placement method with a regular grid the Antifer-block placing plan is prepared with the space coordinates of each block being defined on a local grid referred to the breakwater control survey line or by map grid coordinates for offshore placement.

The Antifer-blocks can be placed in different ways, such as:
1. Using a rope sling system with a clamp. This was done for the reconstruction of the Arzew Breakwaters, see figure 2.6. An experienced crane operator can place the units with reasonable accuracy. However, the crane operator cannot see under water when visibility is poor. In this case, a diver can provide help to the crane operator.
2. Using two steel hooks on top of the Antifer-block and a rope sling system connected to these. This technique is expensive due to the steel hooks, which are susceptible to steel corrosion and therefore block deterioration. Also blocks with one steel hook on top are used e.g. for the maintenance of the breakwaters in the harbour of Antifer, see figure 2.7.
3. Using a large crane with an orange peel. To improve grip on the tapered cube, two opposing grab tynes can be pointed inwards more than the other diagonal which provide location control.

4. Using a specially designed groove on the top of the block where a steel attachment can go in which is connected to the block by turning. The block is lifted by pulling the rope connected to the attachment. By a reverse process the attachment is released. For the groove a special form has to be installed into the top of the block.

5. Using two hydraulic arms which fit into two horizontal side grooves. This technique may cause concrete surface injuries at the grab surfaces because of the squeezing arms. It was used in Dos Bocas, Mexico, see figure 2.8.

6. Using a hydraulic clamping system which squeezes the top of the block. This is a very new method, which makes it possible to place the blocks very accurate, see figure 2.9.
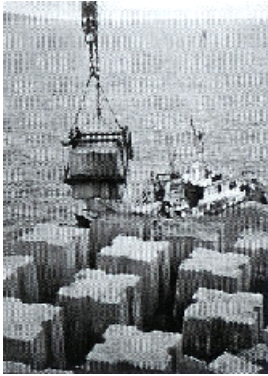
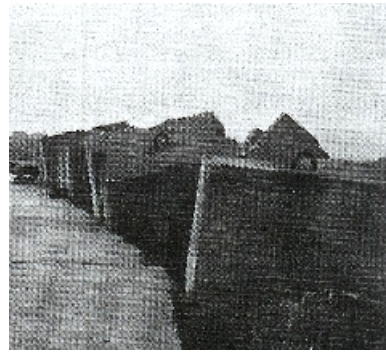Figure 2.6: Rope sling with clamp

Figure 2.7: Antifer-blocks with a steel hook

Figure 2.8: Two horizontal side grooves

Figure 2.9: Hydraulic clamping system

2.3   Hydraulic stability

2.3.1   General information

Hydraulic instability is the movement of armour units caused by wave forces. These movements can be:
- Rocking: cyclical rolling of a single block
- Settling: displacement from the original position on a slope greater than half a unit dimension, but remaining in a stable position in the armour
- Displacement: the displacement of units out of the armour layer
- Sliding: the sliding of a group of armour units

The wave-generated flow forces on armour units might be expressed by an equation containing a drag force F_D, a lift force F_L and an inertia force F_I (the vectorial sum of these can be interpreted as a resulting flow force F_F). Furthermore the stabilizing gravitational force F_G and the reaction forces acting at the contact points with neighbouring units, see figure 2.10.
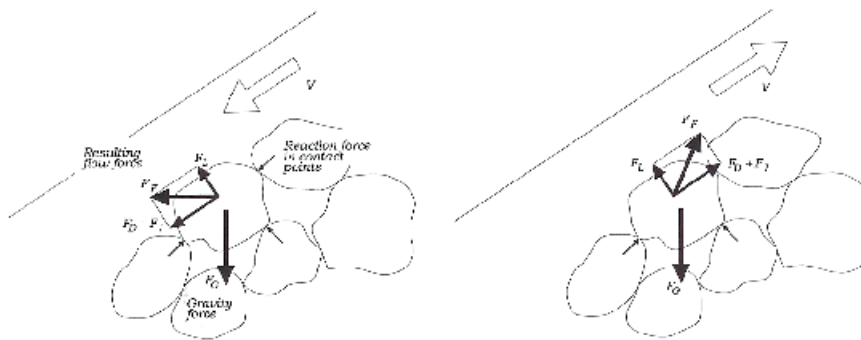
Figure 2.10: Forces on armour units

For complex interlocking types of armour, like dolosses, the forces in the contact points between the units increase the overall stability. In 1979 Price [CEM, 2006] found by dry pull-out tests that the interlocking ability of complex slender units increases with the slope angle. In 1993 Burcharth and Thompson [CEM, 2006] showed that dolos armour placed on a horizontal bed and exposed to oscillatory flow is not more stable than rock armour of similar weight. The difference in stability between interlocking and non-interlocking armour is illustrated in figure 2.11. The Antifer-block is a massive block, but because of grooves the interlocking and the friction are greater than for cubes.
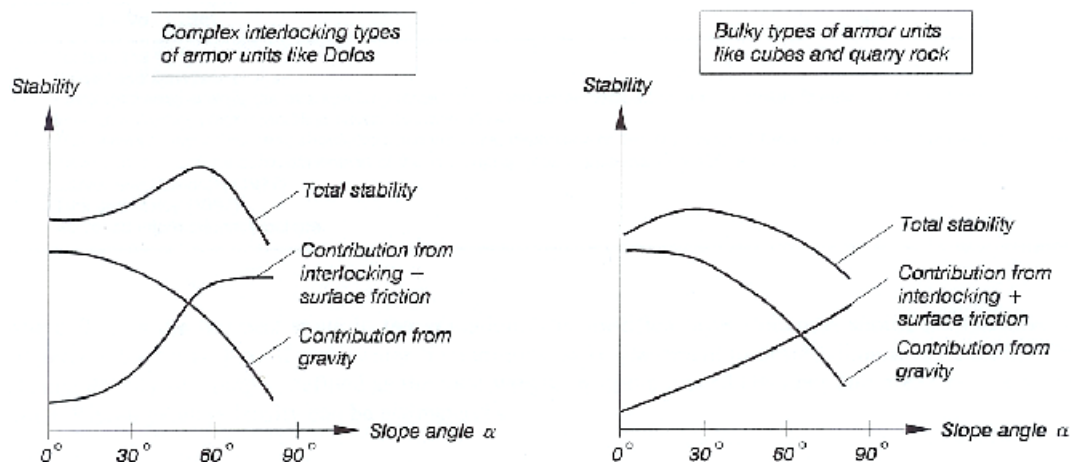
Figure 2.11: Influence of slope angle on the different stabilizing effects [CEM, 2006]

The flow around the units is non-stationary in both direction and velocity, thus all the forces, with exception of the gravitational force, vary in size and direction with time. The velocity of the flow depends on the properties of the incoming waves and its action on the slope. Furthermore, it is affected by the permeability and surface roughness of the structure. A common way to express these flow forces on a unit is:

$$F_D \approx C_D \cdot \rho_w \cdot A \cdot \overline{v} \cdot |v|$$

$$F_L \approx C_L \cdot \rho_w \cdot A \cdot \overline{v} \cdot |v| \qquad\qquad (2.1)$$

$$F_I \approx C_I \cdot \rho_w \cdot V \cdot \frac{d\overline{v}}{dt}$$

C_D, C_L and C_I are empirical coefficients. A is the cross sectional area of the units at right angles to $\overline{v}$ and V is their volume. It becomes quite evident that when, beside the complexity of the flow field, also the shape of the Antifer-block and its variable positioning on the under layer is considered (within a regular or irregular placement), deterministic calculation of the instantaneous armour unit stability conditions cannot be performed. This is why stability formulae are based on hydraulic model tests. The latter statement results in a stochastic approach in which the response of the armour units is related directly to the properties of the incident waves. However, some qualitative considerations of the involved forces can be used to explore the structure of stability formulae. The properties of the waves are captured in environmental parameters. Environmental parameters are boundary conditions which in most cases cannot be influenced by the designer. Because of this, a good insight in the effects of these parameters on the armour is of high importance. Environmental variables are characterized by:

- Characteristic wave heights: H_s, $H_{1/3}$, H_{m0}, etc.

- Characteristic wave steepness: s_m, s_p, etc., derived from the wave period $s = 2 \cdot \pi \cdot \dfrac{H}{g \cdot T^2}$

- Water depth, h
- Wave incident angle, β
- Number of waves, N
- Mass density of water, ρ_w
- Shape of the wave spectrum; JONSWAP, P-M, TMA etc. and double peak spectra.
- Wave asymmetry
- Wave grouping

Structural parameters on the other hand, describe the resistance of the Antifer-block breakwater against the wave loads. The whole of these parameters represents the strength of the breakwater. The most significant structural parameters of the armour layer are given by:

- Seaward profile of the structure, including armour layer slope angle α, freeboard, the height and width of the crest etc.
- Mass density of armour units, ρ_s
- Mass M and shape of armour units
- Placement method, packing density, interlocking and layer thickness of the main armour
- Porosity, permeability and thickness of under layers, filter layer(s) and core
- The ratio of diameter between armour, under layer and core material

When simple expressions are made about the geometry of the units and the flow, it is possible to derive some expressions for the stability. The first simplification is the characterization of an equivalent cube length concerning the unit's geometry.

$$D_n = \left(\frac{M}{\rho_s} \right)^{1/3} \tag{2.2}$$

A second assumption is to consider the flow quasi-stationary. The inertia forces can then be neglected. A qualitative stability ratio thus becomes.

$$\frac{F_D + F_L}{F_G} \propto \frac{\rho_w \cdot v^2}{g \cdot (\rho_s - \rho_w) \cdot D_n} = \frac{v^2}{g \cdot \Delta \cdot D_n} \tag{2.3}$$

Where $\Delta = \dfrac{\rho_s}{\rho_w} - 1$ and v is the characteristic flow velocity.

By inserting $v \approx \sqrt{g \cdot H}$, for a breaking wave height of H, in equation 2.3 the following stability parameter, N_s, is obtained.

$$N_s = \frac{H}{\Delta \cdot D_n} \tag{2.4}$$

A certain degree of damage, or non-exceedence of instability, can then be expressed in the general form:

$$N_s = \frac{H}{\Delta \cdot D_n} \leq K_1^a \cdot K_2^b \cdot K_3^c \dots \tag{2.5}$$

The K-factors depend on all the other environmental and structural parameters, except H, Δ and D_n, influencing the stability. The stability formulae does not contain explicitly all these parameters. This together with the stochastic nature of wave load and armour response introduces uncertainty in any stability formula. This uncertainty is in most cases included in equation 2.5 in the form of a Gaussian distributed stochastic variable with a specified mean value and standard deviation.

There has been done much research on the stability of armour layers with hydraulic model tests. This stability is based on a certain allowed degree of damage. The definition for damage is not unambiguous, but interpreted in different ways by the different researchers. In the next two paragraphs the stability-theory and damage interpretation for Hudson and Van der Meer are discussed.

2.3.2   Hudson

HUDSON, 1959 and 1979 investigated the stability of armour layers and derived his formula from the analysis of a large data set of model tests with regular waves on rock armour. This resulted in following formula, which is also applicable for armour units:

$$M = \frac{H^3 \cdot \rho_s}{K_D \cdot \cot\alpha \cdot \left(\dfrac{\rho_s}{\rho_w} - 1\right)^3} \qquad (2.6)$$

M = mass of armour unit
H = characteristic wave height
ρ_s = density armour unit
ρ_w = density water
K_D = Hudson stability parameter
$\cot\alpha$ = slope of the armour layer

When equation 2.6 is rearranged the stability parameter, N_s, is found:

$$N_s = \frac{H}{\Delta \cdot D_n} = (K_D \cdot \cot\alpha)^{1/3} \qquad (2.7)$$

The Hudson formula, initially based on monochromatic wave tests, is extended to irregular wave conditions, by substituting H (characteristic wave height) with H_{m0} (significant wave height) or with $H_{1/10}$, as suggested in various textbooks.

Hudson's formula has been used for irregular placed concrete armour units by selection of appropriate K_D-values derived from hydraulic model tests. This approach can be dangerous, because many concrete units rely for their stability upon factors which are not included in Hudson's formula. The formula doesn't considerate the influence of wave period, type of breaking (spilling, plunging, surging), duration of storm (i.e. number of waves), the permeability of the breakwater and the part played by interlocking between the units in the stability of an armour layer. The effect of such interlocking is to increase the apparent stability of a unit allowing the use of lighter weights than would otherwise be the case for a given wave height. However, an increase in wave height can have a greater effect on reducing the stability of these lighter, interlocked units than on massive units, because of the structural damage to the units. The Antifer-block is a massive unit with small interlocking capacity from its grooves. In this report the possible structural damage and resulting reduction in stability is not taken into account.

In the design of a concrete armour layer Hudon's formula should be regarded as no more than a device for comparing the stability of different types of units, and K_D-values published from previous hydraulic model testing should be used only as guidance for preliminary selection of armour sizes for full hydraulic model testing. When using these K_D-values attention should be paid to the damage ratio and damage level upon which the value is based. In literature there are different interpretations about damage levels, such as:

- Initiation of damage [LOSADA *et al.*, 1986]: The condition when a certain number of armour units are displaced from their original position to a distance equal to or larger than a unit length. It also corresponds to the situation in which the outer armour layer displays holes larger than the average pore size on its surface.
- Iribarren's damage, stated by Iribarren in 1965 [LOSADA *et al.*, 1986]: Failure, covering an area so extensive in the upper layer of the armour (10-15%) as to allow the extraction of units from the lower one (2-layer armour).
- Initiation of destruction, stated by Vidal in 1991 [YAGCI AND KAPDASLI, 2002]: A small number of units, two or three, in the lower armour layer are forced out and the waves work directly on pieces of the under layer.
- Destruction [LOSADA *et al.*, 1986]: The failure is large enough to uncover the under layer. The armour units leave the mound continuously, and if the test is not stopped, the whole cross-section will be destroyed after a sufficiently long period.

In this thesis damage for irregular placement is defined in the following way [CEM, 2006]:
- No damage: No units are displaced.
- Initial damage: A few units are displaced.
- Intermediate damage ranging from moderate to severe damage: Units are displaced but without causing exposure of the under layer to direct wave attack.
- Failure: The under layer is exposed to direct wave attack.

For designing an irregular placed armour layer a little damage is allowed. The K_D-value is based on the initial damage. To compare the different K_D-values a specified definition has to be made for "the displacement of a few units". This is done with the relative displacement within an area, called the damage ratio.

$$DamageRatio = \frac{number\_of\_displaced\_units}{Total\_number\_of\_units\_within\_reference\_area} \qquad (2.8)$$

The displacement of units has to be defined, e.g., as the movement of a block more than distance D_n, or as a displacement out of the armour layer. The reference area has to be defined as the complete armour area or as the area between two levels, e.g., $SWL \pm H_s$, where H_s corresponds to a certain damage, or $SWL \pm n \cdot D_n$.

HUDSON, 1959 based his K_D-values in his 'Laboratory investigation of rubble-mound breakwaters' on the removal of up to one percent of the total number of armour units in the cover layer and considered this to be 'No damage'. The 'Initial damage' according to the definition of CEM, 2006 corresponds to the no-damage level used in SPM 1977 and 1984 in relation to the Hudson formula stability coefficient (K_D). Here the no-damage level is defined as 0-5% displaced units. This corresponds to the wave height level were the first blocks are displaced more than the nominal diameter and this is always below a damage ratio of 5%. The zone wherein this happens extends for rocks from the middle of the crest height down the seaward face to a depth below SWL equal to a H_s-value which causes the damage 0-5%. For cubes this zone is $SWL \pm 6 \cdot D_n$.

The CEM, 2006 listed K_D-values (based on the SPM, 1984) for the modified cube, for the trunk, of 7.5 for non-breaking waves and 6.5 for breaking waves. For the head only a value of 5 was listed for non-breaking waves. These values are also used by designers of Antifer-block armour layers, however they are originally based on the modified cube, see figure 2.12, which was developed in the USA in 1959.
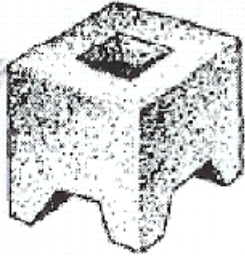
Figure 2.12: Modified cube

The BRITISH STANDARD, 1991 listed K_D-values for Antifer-block armour layers from 6-8, without any further specifications.

Günbak performed in 1996 a study on K_D-values for existing Antifer-block armour layers for the initial damage. He did backward calculations for different breakwaters and model tests if the value was not defined and used a concrete unit weight of 2.4 (if not defined). The findings of this study are summarized in table 2.2. GÜNBAK, 1999 recommended after his study the use of the following K_D-values: Trunk K_D=7 for breaking and non-breaking, Head K_D =6 for non-breaking, K_D=5 for breaking conditions.

Reference	Slope 1:x	Trunk	Head	Wave Type	Note
Maquet1976	1.4	6.56	5.24	-	-
Maquet1976	1.4	7.36	5.65	Non-Breaking	-
Abdelbaki1983	1.33	6.90	-	Non-Breaking	-
SPM 1984	5	7.5	5	Non-Breaking	For Modified Cube
Paolella	3	4.36	-	Non-Breaking	-
Bruun1984	2	6.34	-	Breaking	-
Bonnin1988	1.33	6.13	-	Non-Breaking	-
Estramed 1990	1.33-2	11.9	9	-	% damage
DeMeyer 1990	1.5-2	5	10	-	uncertain
Jackson1991	1.5	12.55	-	Non-Breaking	-
FRH1993	1.5	7.4	3.75	Breaking	-
STFA1993	1.5-2.5	7.4	4.5	Breaking	-
FRH1993	1.5	7.57	4.54	Breaking	-
Abdelbaki1993	1.5	8	5	-	-
Rouck1994	1.5-2	6.50	-	-	-
Juhl1995	1.5	6.0	-	-	-
Galland1995	1.33	4.4	-	Non-Breaking	-
					for 2% damage

Table 2.2: Stability numbers, K_D, used for Antifer-blocks (for initial damage level)

The above discussed K_D-values are all for a double layered, irregular placed, Antifer-block armour layer with a porosity of 46-47% and are calculated with the same damage ratio and level. In literature and practice there are a lot of misunderstandings within the comparing of K_D-values because of the use of different damage ratio's, different damage levels, different placement methods and different porosities (porosity-definitions). A few of these different approaches are presented below. In paragraph 2.4 the placement methods and porosity will be discussed.

YAGCI *et al.*, 2003 characterized the damage on the armour layer and came with a different way of calculating the damage ratio. Three different types of block movements were considered and it was assumed that each type has a different contribution to the damage. They included rocking with an arbitrary chosen weighing factor of 0.25 and turning (movement less than D_n) with an arbitrary chosen weighing factor of 0.5 in the damage ratio. The displacement (movement longer than D_n) of a unit was called rolling.

$$DamageRatio = \frac{0.25RBN + 0.5TBN + RLBN}{TNOB} \qquad (2.9)$$

RBN=Rocking number of blocks
TBN=Turning number of blocks
RLBN=Rolling number of blocks
TNOB=Total number of blocks on seaward slope

Yagci, using equation 2.9, found a K_D-value for Antifer-blocks varying between 3.52 (for cota=1.5) and 2.69 (for cota=2) for a damage ratio of 0.03. These values were obtained for the irregular placement technique using irregular waves and are less than the K_D-values found by Günbak. This is because of the inclusion of rocking and turning blocks the damage ratio increases and the maximum damage ratio was taken lower (3% in stead of 5%). YALCINER *et al.*, 1999 drew regression curves for the damage ratio (Hudson) against the wave height. He determined the stability coefficient for the wave height which causes exact 5% damage by using the Hudson formula, in stead of taking the wave height at the start of damage (0-5%). Another difference is that the blocks were placed in a slightly different way than was done by Günbak. Both placement methods were irregular, however Yalciner placed the blocks of the first layer with their grooves perpendicular to the slope, while GÜNBAK, 1999 placed several blocks in the first layer on their side. The obtained stability-values are presented in table 2.3. For the less critical damage ratio the expected K_D-values should be higher. The presented values are, however, on the low side compared to the results from Günbak. This acknowledges the importance of the used placement method, which will be further discussed in paragraph 2.4.

Slope	Breaking waves		Non-Breaking waves	
Cot a	Trunk	Head	Trunk	Head
1.5	4	3.5	5	4
2.0	5.5	4.5	7	5.5
2.5	6.5	5.5	8	6.5
3.0	7.5	6.5	9	7.5

Table 2.3: K_D-values from 2D and 3D tests for 5% damage [YALCINER *et al.*, 1999]

2.3.3 Van der Meer

VAN DER MEER, 1988a presented an empirical formula based on small and large scale model tests on rock armour.

$$\frac{H_s}{\Delta \cdot D_n} = f\left(S^{n1} \cdot \xi^{n2} \cdot N^{n3} \cdot \alpha^{n4} \cdot P^{n5}\right) \tag{2.10}$$

Where S signifies the damage level, ξ represents the wave kinematics, N is the number of waves (storm duration), α is the slope angle and P is an empirical coefficient which signifies the permeability of the slope. Van der Meer assumed the effect of the wave period to be connected with the shape and intensity of breaking waves. He therefore used the Iribarren parameter:

$$\xi = \frac{\tan \alpha}{\sqrt{s}} \tag{2.11}$$

In which $s = 2 \cdot \pi \cdot \dfrac{H}{g \cdot T^2}$.

Using the characteristic values for irregular waves; H_{m0}, measured at the toe and T_p or T_m, measured in deep water, this leads to the use of ξ_{s0p} and ξ_{s0m} respectively.

Contrary to Hudson, Van der Meer found a clear influence of the storm duration, the longer the storm, the more damage. This can easily be explained by the model technique. Hudson used regular waves. A longer storm duration leads to a higher probability of the occurrence of extremely high waves. These extremely high waves are responsible for ongoing damage.

For cubes on a 1:1.5 slope VAN DER MEER, 1988b presented a method found by hydraulic model tests. The damage number was generated by the number of moving units related to the width of the model and the nominal diameter:

1. No movement
2. Rocking of single units.

$$N_{o<0.5} = \frac{N_r}{B / D_n}$$

3. Sliding: Movement of units from their initial position by a certain distance ($0.5 \cdot D_n$ to $2.0 \cdot D_n$).

$$N_{o>0.5} = \frac{N_{sl}}{B / D_n}$$

4. Units displaced from their initial positions (movement of more than $2.0 \cdot D_n$).

$$N_{od} = \frac{N_o}{B / D_n}$$

The movement of the units is not uniformly distributed over the slope. In general, all movement takes place within the levels SWL ± Hs. Therefore a reference area was chosen that takes into account this non-uniformity of movement. VAN DER MEER, 1988b chose the complete slope as reference area to facilitate the comparison of the various experimental results. Rocking was

disclosed from the damage evaluation for cubes, because this is only relevant for the evaluation of breakage of units (structural damage). This resulted in the following definition for movement:

$$N_{o,mov} = N_{od} + N_{o>0.5}$$

With the results from the tests the following equations for movement and displacement were formulated. The damage levels are presented in table 2.4.

$$\frac{H_s}{\Delta \cdot D_n} = \left[6.7 \cdot \frac{N_{od}^{0.4}}{N^{0.3}} + 1.0 \right] \cdot s_{om}^{-0.1} \tag{2.12}$$

$$\frac{H_s}{\Delta \cdot D_n} = \left[6.7 \cdot \frac{N_{omov}^{0.4}}{N^{0.3}} + 1.0 \right] \cdot s_{om}^{-0.1} - 0.5 \tag{2.13}$$

N = number of waves

s_{om} = wave steepness, based on the mean period, $s_{om} = \dfrac{2 \cdot \pi}{g} \cdot \dfrac{H_s}{T_m^2}$

	Start of damage	Initial damage (needs no repair)	Intermediate damage (needs repair)	Failure (under layer exposed)
N_{od}	0	0-0.5	0.5-1.5	>2

Table 2.4: Damage levels

Van der Meer's formula can be used as a general check for the preliminary design of Antifer-block armour layers. This is only a check, because the formula has been derived from a limited number of laboratory tests, and only for standard cubes. Because of the greater interlocking effect of Antifer-blocks there is no technical justification for a direct design with the Van der Meer formula.

CHEGINI AND AGHTOUMAN, 2001 performed model tests on Antifer armour layers and applied the above described method (Van der Meer) to the results. They derived the following formulae for Antifer-blocks on a slope of 1:1.5 with the same damage levels:

$$\frac{H_s}{\Delta \cdot D_n} = \left[6.951 \cdot \frac{N_{od}^{0.443}}{N^{0.291}} + 1.082 \right] \cdot s_{om}^{-0.082} \tag{2.14}$$

$$\frac{H_s}{\Delta \cdot D_n} = \left[6.951 \cdot \frac{N_{omov}^{0.443}}{N^{0.291}} + 1.082 \right] \cdot s_{om}^{-0.082} - 0.5 \tag{2.15}$$

The test results from Chegini and Aghtouman for a slope of 1:1.5 are presented in figure 2.13. They are based on tests with storm durations of 1000, 2000 and 3000 waves with different wave steepness. Also the outcome of the derived formulas for Antifers and cubes for 2000 waves and a wave steepness of 5% are drawn in this figure. It can be concluded that the obtained formula for Antifer-blocks differs minimal from the formula for cubes and seen the scattering of the test results the additional value is low.
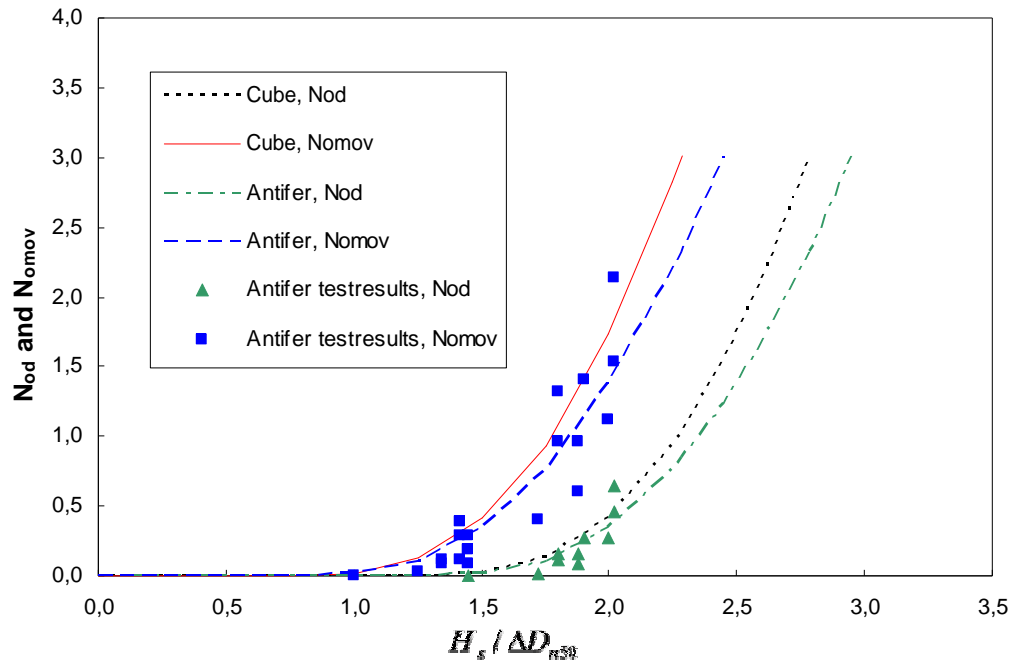
Figure 2.13: Comparison of formulas for cubes and Antifer-blocks

2.4   Placement method

2.4.1   Introduction

"The placement technique of the blocks of the armour layer is one of the most significant parameters affecting the stability" [HUDSON *et al*., 1979]

The placement method is an important structural parameter which influences the stability. Therefore the stability coefficients differ per placement method. With the stability coefficient the required block volume can be calculated. The volume of the blocks determines the armour layer thickness and together with the necessary number of Antifer-blocks per unit area this results in the porosity. In literature there are many different ways in which these values are used, which leads to misunderstandings. In the different design guides (CEM, BS, etc.) there is no difference made in placement method. The design coefficients (K_D -value, layer thickness coefficient, supposed porosity) for Antifer-blocks are given for a double layered random placing method. This is the most commonly used placement method. The term "Irregular" is preferred over "random" since the Antifer-blocks are placed individually by a defined schedule. Besides the irregular placement method there's the regular placement method. In this paragraph first the definition for porosity will be discussed, after which the focus will lie on the different types of placement methods.

2.4.2   Porosity

When Maquet did his tests for the Antifer-breakwater in 1976 he discovered that the porosity of the armour layer had an effect on the stability [MAQUET, 1985]. He described the existence of a value, above which there was insufficient stability and below there occurred a 'paving' action. This 'paving' action reinforced the reflection of waves and increased the vulnerability of the structure because of the risk of destruction of entire sections of the protective layer. Maquet determined this value to be about 50% and used it for all the construction works. The porosity stands for the percentage of void spaces in the armour layer. For calculating the porosity it is necessary to define the armour layer thickness. In literature there are many discussions over the armour layer thickness. There are a few options for deriving the thickness, namely to measure; the highest points of the top layer, the lowest points of the top layer or an average thickness between these two. To calculate the layer thickness the block volume is needed, which follows from the Hudson-equation:

$$V = \frac{H^3}{K_D \cdot \cot \alpha \cdot \left(\dfrac{\rho_s}{\rho_w} - 1 \right)^3} \tag{2.16}$$

The armour layer thickness is:

$$t = n \cdot k_\Delta \cdot V^{1/3} \tag{2.17}$$

n = number of layers
k_Δ = Layer thickness coefficient
$V^{1/3} = D_n$ = Nominal diameter

A parameter which is used to calculate the porosity and defines the spreading of the blocks is, ϕ, the number of Antifer-blocks per unit area:

$$\phi = \frac{N}{B \cdot L}$$
(2.18)

N = number of blocks in the defined area
B = Width of area
L = Length (on slope) of area
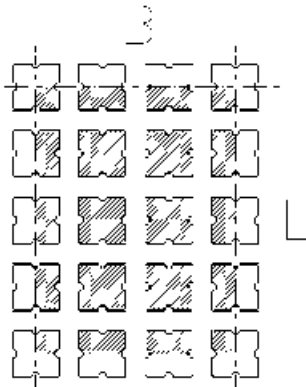See figure 2.14, where the hatched area stands for the included number of blocks.

Figure 2.14: Definitions for the calculation of ϕ

The porosity, P (%), follows from:

$$P = (1 - \frac{N \cdot V}{B \cdot L \cdot t}) \cdot 100 = (1 - \frac{V \cdot \phi}{t}) \cdot 100$$
(2.19)

There are a few misinterpretations within this theory such as:
-There are two commonly used values for the layer thickness coefficient which lead to different layer thicknesses and consequently different porosities. The CEM, 2006 and the BS, 1991 specify a layer thickness factor for cubes (modified) of 1.10. In literature (e.g. YALCINER *et al*., 1999 and GÜNBAK, 1999) the following definition for layer thickness is often found:

$$t = 2 \cdot a = 2 \cdot \left(\frac{V}{0.8024} \right)^{1/3} = 2 \cdot 1.076 \cdot (V)^{1/3}$$
(2.20)

Layer thickness coefficient = 1.076
Both layer thickness coefficients are mentioned for a double layered, irregular placed, armour with a porosity of 46% [GÜNBAK, 1999] or 47% [CEM, 2006 and BS, 1991]. In literature there is a greater variety on porosity values, these values vary between the 40 and 50%.

-The above defined porosity calculation (equation 2.19), with a layer thickness coefficient of 1.10 or 1.076, is only suitable for double layered, irregular placed armour. In literature this calculation is also used for other types of placement methods, like the regular method. This is incorrect, because these layers have, most of the time, a different thickness. For the comparison of the spreading it is a correct method (only then the use of the thickness is redundant, see the definition of ϕ). However, the values should not be published as porosity, because this stands for the void spaces.

-In literature the term density is used for the solid armour density and for the packing density. Further more the packing density is calculated in different ways. Therefore it is important when using values from the literature to make sure which density is used. Below a few examples of different densities are presented.

Solid armour density:

$$d = \frac{N \cdot V}{B \cdot L \cdot t} \cdot 100 = (1 - P) \qquad (2.21)$$

Packing density:
-Number of blocks per unit area:

$$\phi_1 = \frac{N}{B \cdot L} = \frac{t \cdot (d/100)}{V} = \frac{n \cdot k_\Delta \cdot (d/100)}{V^{2/3}} \qquad (2.22)$$

-Ratio between the real and the maximum number of blocks per unit area:

$$\phi_2 = \frac{N \cdot D_n^2}{B \cdot L} = \frac{t \cdot (d/100)}{V^{1/3}} = n \cdot k_\Delta \cdot (d/100) \qquad (2.23)$$

Most researchers use the second packing density, ϕ_2, nevertheless different values for packing densities are found in literature. To illustrate this, the packing densities used by GÜNBAK, 2000, VAN DER MEER, 1999 and DE ROUCK *et al*., 1987 are compared in table 2.5.

Unit Type	Antifer	Cube	Rock	Tetrapod	Accropode	Core-loc	Dolos
ϕ_2, Günbak	1.21	1.32	1.26	1.04	0.66	0.58	-
ϕ_2, Van der Meer	-	1.17	-	1.04	0.61	0.56	-
ϕ_2, De Rouck et al.	1.21	-	-	1.04	0.76	-	0.82

Table 2.5: Packing densities used by Günbak, Van der Meer and De Rouck *et al*.

2.4.3 Irregular placement method

The advantages of the Antifer-block named in paragraph 2.2 are based on an irregular placement method, see figure 2.15. If construction quality is expected to be difficult to control, or when there is high uncertainty in the wave climate or instability of the foundation is expected then it is better to choose an irregular placement method instead of a regular method. When for example the first layer of a regular placement is deformed due to instability, this deformation directly affects the form and stability of the second layer. Another advantage of the irregular method is that the damage is easy to repair by adding extra blocks to the armour layer.

Figure 2.15: Examples of irregular placement

The irregular placement method was used for the construction of the breakwaters at the harbour of Antifer [MAQUET, 1985], see figure 2.16. The Antifer-blocks were placed in two layers with the grooves mainly perpendicular to the slope, see figure 2.17. As mentioned in the previous paragraph Maquet determined during the tests a porosity of 50%, which above there was insufficient stability and below there occurred a 'paving' action. After realisation the placement was checked by visual observations and by the delivered quantities of Antifer-blocks. The porosity turned out to be between 45 and 50%.
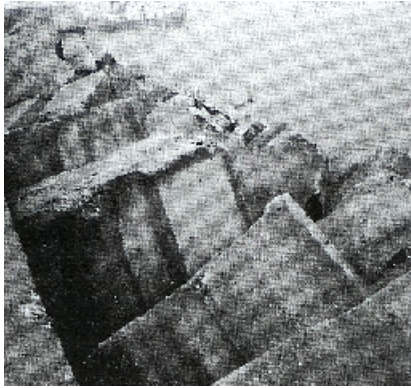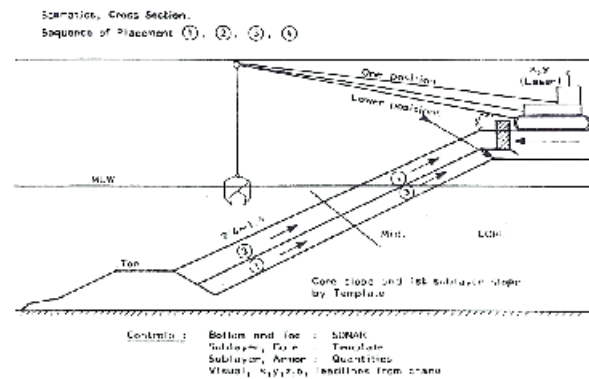

Figure 2.16: Irregular placement   Figure 2.17: Schematics of block placement

From later tests on the irregular placement method by GÜNBAK, 2000 also followed that it is very difficult to obtain the desired porosity. An intended porosity of 46% often turned out smaller (sometimes 40%). This problem is caused by the placing of the first layer. For a breakwater slope of 1:1.33 or 1:1.5 (the slope used in this thesis) the placing of the first layer is very important for obtaining the required porosity and roughness of the armour layer. If the Antifer-blocks are placed too close to each other or if they slide down during construction and become more densely packed, the second layer becomes automatically also more densely packed, so less porosity is obtained. Field and hydraulic model experience by GÜNBAK, 1999 demonstrated that it is very important to place the first layer of blocks in an irregular configuration as irregular as possible by not aligning the sides to each other as well as by placing several blocks on their side instead of on their bottom (as done by Maquet). The second layer placement will then generate the required thickness, layer porosity and irregular surface texture. When compared to the results from YALCINER et al., 1999 the placement by Günbak turned out to be also more stable (see paragraph 2.3.2, table 2.3). This can be explained by the better interlocking between the two layers because of the higher roughness of the first layer.

YAGCI et al., 2003 found with hydraulic model tests, figure 2.18, that the armour has a greater auto-restoring capability with low porosity, than with high porosity. Similar to LOSADA et al., 1986 they placed the blocks, per complete layer, by letting them fall from an approximate height of 30 cm. In their report recommendations are given for the placement of the first row on the toe. This thesis focuses on the stability of the placing method and not on the toe placement.
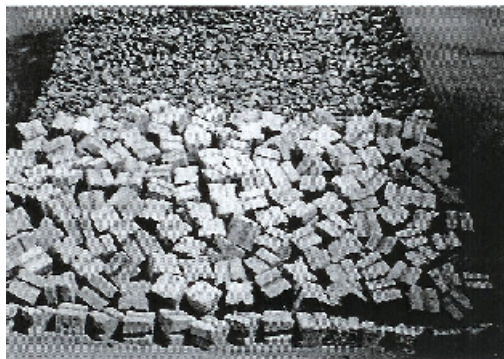

Figure 2.18: Irregular placed first layer [YAGCI et al., 2003]

To obtain a uniform distribution of blocks with the desired porosity it is necessary to control the irregular Antifer-block placement. For this reason a regular placing grid where the blocks of the first layer have to be placed or dropped is often determined from the necessary number of blocks per unit area.

For a breakwater in Brunei [JONES *et al*., 1998] the design was based on a theoretical solid armour density of 56%. During the tests it was noted that the appearance of the outer layers was fairly sensitive to this density and that for a solid armour density lower than 56% visible holes started to appear in the layer. When these holes were repaired the solid density was approximately 56%. Solid armour densities higher than 56% tended to produce individual blocks above the second layer. The grid spacing was calculated by finding the length of the side of a square area that would produce this packing density in a single layer.

$$GridSpacing = \sqrt{\frac{AntiferVolume}{0.56 \cdot layerthickness}} \qquad (2.24)$$

For the actual placement the Antifer-blocks were lowered to the seabed within 0.5m of the theoretical location and then released. To improve interlocking and reduce block movement after release, rows of block locations (up slope and in the layer above) were offset along the breakwater from the adjacent rows. For a straight breakwater section, the set out grid for one layer appeared as drawn in figure 2.19. Across the profile, rows of blocks were placed starting at the bottom of the slope on the most seaward row. From here rows of blocks were located at the grid spacing up the slope in 2 layers. Rows were placed in the sequence shown in figure 2.20 until the top of the slope was reached. This is different compared to the harbour of Antifer, where the armour was placed per half layer. The placement could be interrupted at intermediate levels for construction scheduling of other operations, provided that the basic sequence was followed for a particular segment.
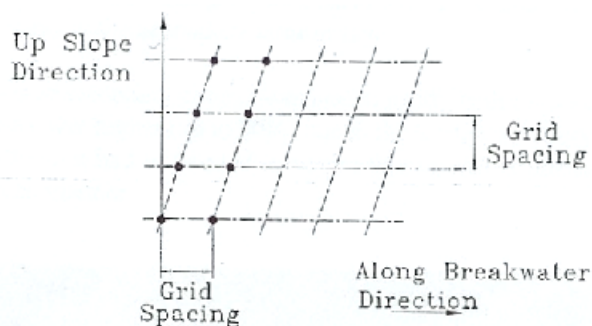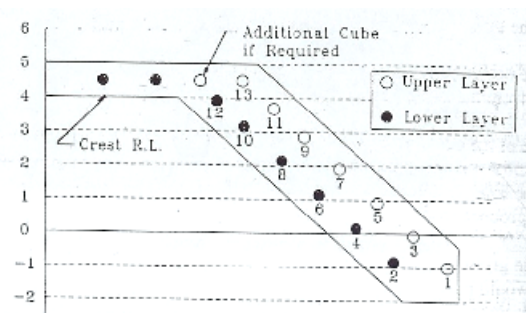

Figure 2.19: Placement grid   Figure 2.20: Cross-section with block locations

Position fixing of the location was done by using Differential Global Positioning Systems (DGPS), GPS receivers were mounted on the placing cranes with the antenna mounted on the boom tip. After a section was completed it was visual checked. If required additional blocks were added. It was noted that the achieved solid armour density on site was approximately 58%, when additional blocks to fill obvious gaps were included. The density was influenced by the surface roughness of the secondary armour layer. In areas where secondary armour was placed neatly with a smooth outer surface, the achieved density was higher (up to 60%) due to the tendency of cubes to slide down the slope. Careful attention had to be paid to ensure that operators placed the secondary armour in a random manner, see figure 2.21 [JONES *et al*., 1998].
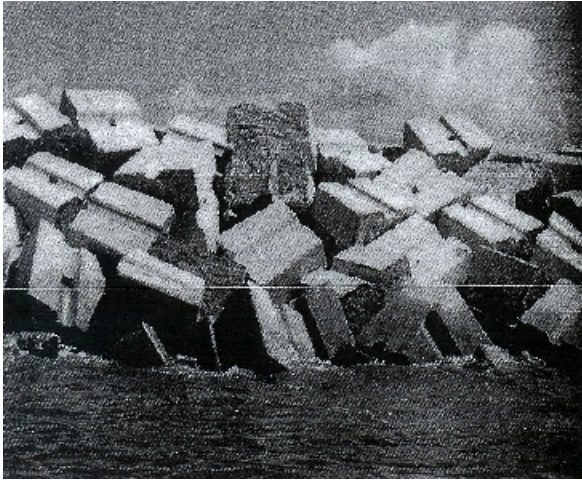
Figure 2.21: Random manner placed second layer

2.4.4   Regular placement method

The regular placement method can be defined as the placement of the Antifer-blocks of both layers in a regular pattern and often also in a regular position. Because of the development of more accurate placing techniques (paragraph 2.2.3) it is now possible to place the blocks in regular patterns in contrary to, for instance, the placement technique used for the harbour of Antifer in 1976.

When the first layer of Antifer-blocks is placed very regularly, by placing blocks on their bottom with block surfaces parallel to each other, the blocks of the second layer will intrude very deep between the blocks of the first layer. The thickness together with the porosity of the armour layer will then decrease [GÜNBAK, 1999]. In these cases it is not correct to use the prescribed layer thickness coefficient from the design guides (CEM and BS) for the calculation of the porosity. The obtained value can be used as a comparing value, a higher 'porosity' indicates a smaller amount of used blocks, but does not represent the void ratio.

There has been done some research on regular placement. In this paragraph the "sloped wall placement method", the "alternative placement method", the "square-grid placement method" and the "double second layer placement method" will be discussed.

Sloped wall placement method
The sloped wall placement method was presented by YAGCI, 2003. In the first layer, Antifer-blocks were placed adjacent to each other with their grooves perpendicular to the slope. The second layer is placed straight onto the first layer using the same method. Figure 2.22 presents a top view of this method. In this figure the x-direction points along the slope and the y-direction points upwards the slope. (a) stands for the first layer and (b) stands for the second layer.
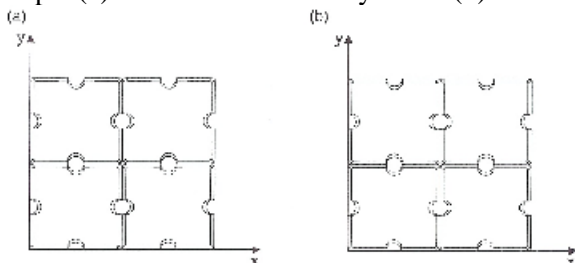

Figure 2.22: The sloped wall placement method

This method uses many blocks per surface area and because of the low roughness and low porosity Yagci observed a high wave reflection, run-up and overtopping.

Alternative placement method

The alternative placement method was presented by YAGCI AND KAPDASLI, 2002. The Antifer-blocks in the first layer were placed perpendicular with their grooves on the filter layer. The distance between neighbouring blocks was equal to 'a/2'. In the second layer, the neighbouring blocks were placed adjacent to each other, see figure 2.23 and 2.24.
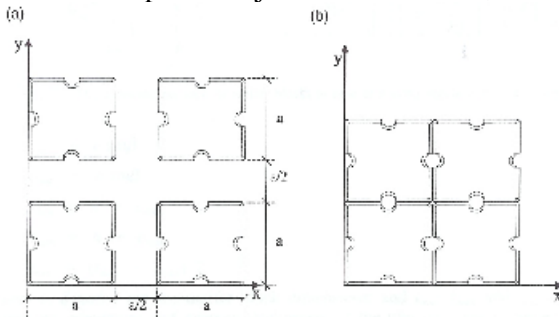

Figure 2.23: The alternative placement method   Figure 2.24: General view of 1st and 2nd layer

YAGCI *et al*., 2003 compared this method with the irregular placement method for a low porosity and found a similar stability performance. They also observed that there was not much difference in the wave run-up, in spite of the low roughness on the second layer. This is because the water, which enters through the semi-cylindrical holes of the Antifer-blocks on the second layer, creates turbulence in the holes between the Antifer-blocks of the first layer. Critical condition is that the filter material is possibly subject to erosion. YAGCI *et al*., 2003 evaluated this method as a superior method over the irregular method with low porosity when armour layer stability, prototype placement, clarity of the placement methods definition, armour layer cost and wave run-up were all taken into consideration.

When this method is used for a slope of 1:1.5, the Antifer-blocks of the first layer will possible slide down which decrease the porosity. If a block from the first layer slides down it creates a hole bigger than 'a/2'. This makes it very difficult to place the block of the second layer straight. This together with the high amount of blocks used per surface area makes this method in my opinion not suitable for a slope of 1:1.5.

Square-grid placement method

For a Middle-East harbour project tests were performed by Sogreah. The employed square-grid placement method was recommended by the HR Wallingford institute. For the square-grid placement method the Antifer-blocks in the first layer are placed in a square grid with mesh M1 with their grooves perpendicular to the slope. The second layer is placed in the same way, only shifted 0.5·M1 along the slope. In this way the blocks of the second layer are placed over the gapes between the blocks of the first layer, see figure 2.25 and figure 2.26. In the figures the blocks were dropped from 2 to 3 cm above the slope and the first layer was placed 2 rows ahead. This is why some blocks are not on their base and the positioning of the blocks is a little irregular.
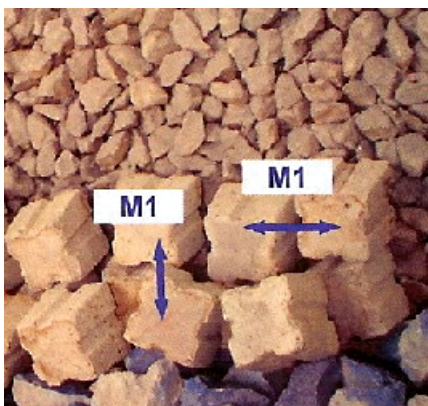

Figure 2.25: Square-grid placement   Figure 2.26: General view

The square grid that was used was defined according to the following expression:

$$d = \frac{2 \cdot V}{MI \cdot MI \cdot t} \qquad (2.25)$$

d = solid armour density
V = block volume
MI = mesh grid, respected horizontally and vertically
t = layer thickness

The following placing ratio is also used:

$$d = \frac{a^2}{MI^2} \qquad (2.26)$$

a = base dimension

Combining equation (2.21) and (2.22) with $t = n \cdot k_\Delta \cdot V^{1/3}$ and $V = 0.8024 \cdot a^3$ results in:

$$\frac{2 \cdot V}{MI \cdot MI \cdot (n \cdot k_\Delta \cdot V^{1/3})} = \frac{2 \cdot (0.8024 \cdot a^3)}{MI \cdot MI \cdot (2 \cdot k_\Delta \cdot \sqrt[3]{0.8024} \cdot a)} = \frac{a^2}{MI^2}$$

With $k_\Delta = \dfrac{0.8024}{\sqrt[3]{0.8024}} = 0.8645$

A layer thickness coefficient of 0.87 is impossible for this placement method, because the second layer does not intrude the first layer, so the coefficient can't be smaller than 1. This placing ratio (equation 2.26) should therefore never be confused with the packing density. This emphasizes the importance of defining the way the density was calculated, see also paragraph 2.4.2.

For the tests the Antifer blocks were placed with a 55% solid armour density. In practice the density turned out higher, because the Antifer-blocks tend to slide down on the filter layer, which makes the layer more compact. A disadvantage of this method is that the vertical gap, MI, is not reliable because of the sliding. In my opinion it should be better to define a constant value for the vertical mesh. In this way the real density is derived from the horizontal spreading.

Double second layer placement method
This placement method is characterized as a two layer armour of which the second layer is placed in two steps, because of this it is sometimes called a three layer placement. The placement pattern is based on a rectangular grid and is scheduled in figure 2.27.
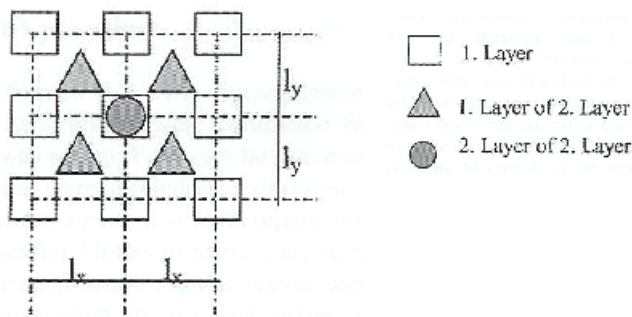

Figure 2.27: Plan view of the double second layer placement method

The placement grid dimensions for the placement of the first layer, as illustrated in figure 2.27, can be computed with the following equations [GÜNBAK, 1999]:

$$c_{min} = e \cdot \sin \beta$$

$$c_{max} = d \cdot \sin \beta$$

$$t_{min} = h + c_{min} \qquad \text{, minimum thickness}$$

$$t_{max} = h + c_{max} \qquad \text{, maximum thickness}$$

$$t_{ave} = (t_{min} + t_{max})/2 \quad \text{, average thickness}$$

$$S_r = (1 - P) \qquad \text{, the solid ratio of the armour layer}$$

$$l_x \cdot l_y = \frac{V}{S_r \cdot \left(\dfrac{t_{ave}}{2}\right)} \tag{2.27}$$

Where e, d and h are the Antifer-block dimensions and β is the angle between the upper surface of the first armour layer and has a value 72.5º, see figure 2.28.
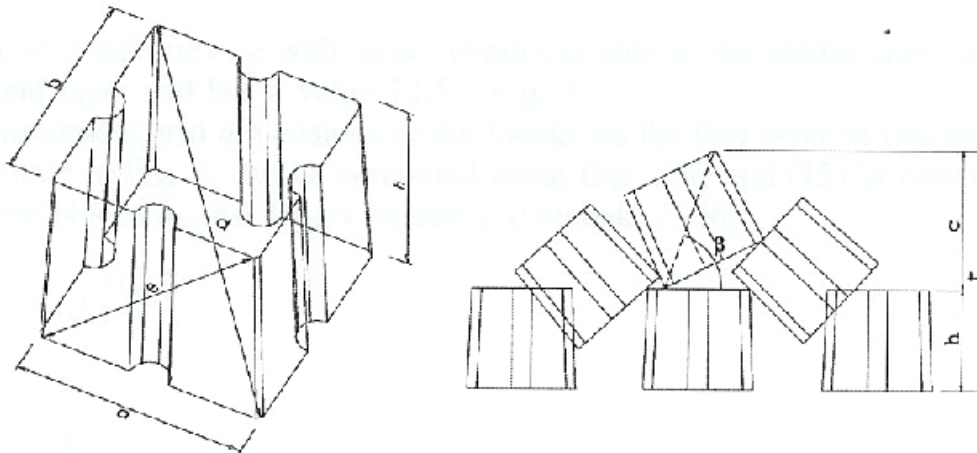

Figure 2.28: The cross-section view for the double second layer placement method.

The double second layer method has a low stability compared with other placement techniques, but also a lower number of required blocks per surface unit. The pattern is well defined and easy to apply to the prototype. However, this type of placement was found convenient to use only for the low values of the incident wave. With this method it was also found difficult to obtain a high porosity. Due to the sliding of the Antifer-blocks on a steep filter layer slope the armour layer becomes less permeable and more blocks than predicted have to be used. For the Ormara breakwaters in Pakistan, the Sines breakwater repair in Portugal and several breakwaters in Turkey the double second layer method was used; some applications resulted in a low porosity of 35% [GÜNBAK, 2000].

3 Model set-up

The experiments for this thesis are not based on a real prototype, which has to be scaled and tested. The main objective of this study focuses on the comparison of processes. It is therefore better to speak of process-orientated experiments instead of scale experiments. The model-dimensions and wave characteristics are scaled to the provided Antifer-blocks within the limitations of the facilities (wave flume and wave generator). Assumed is that the experiments are similar influenced by the possible scale effects. This chapter deals with the scaling of the model and the governing parameters which determine the dimensions of the model and the required wave characteristics.

3.1 Scaling

First the theory on similarity and the type of scaling is presented. In paragraph 3.1.2 the accompanying scale effects and the way to reduce them are described.

3.1.1 Similarity

Laboratory models should ideally behave in all respects like a controlled version of the prototype. This similar behaviour is achieved when all influential factors are in proportion between prototype and model, while those factors that are not in proportion are supposed to be so small that they are not significant to the process. Requirements of similitude will vary with the problem being studied and the degree of accuracy in model reproduction of prototype behaviour. In fluid mechanics, similarity generally includes three basic classifications: geometric similarity, kinematic similarity and dynamic similarity [DE VRIES, 1977 and HUGHES, 1993].

Geometric similarity
When the ratios of all corresponding linear dimensions between the prototype and the model are equal the model is geometrically similar:

$$K = \frac{x_M}{x_P} = \frac{y_M}{y_P} = \frac{z_M}{z_P} \tag{3.1}$$

This relationship is independent of motion of any kind and involves only similarity in form.

Kinematic similarity
The science of kinematics studies the space-time relationship. Kinematic similarity consequently indicates a similarity of motion between particles in model and prototype. If the velocities at corresponding points in the model and prototype are in the same direction and differ by a constant scale factor, the model is regarded as kinematic similar to the prototype.

Dynamic similarity
Dynamic similarity between two geometrically and kinematically similar systems requires that the ratios of all vectorial forces in the two systems are the same. To achieve complete similarity all relevant dimensionless parameters must have the same corresponding values for model and prototype. A systematic procedure for forming a complete set of dimensionless products from a given set of variables is the Buckingham Pi Theorem, which means:

$$\pi_P = \pi_M = f(\pi_1, \pi_2, ..., \pi_r) \tag{3.2}$$

In which the π's are a complete set of dimensionless products.

For practically all coastal engineering problems the forces associated with surface tension and elastic compression are relatively small, and can thus be safely neglected. The Froude and Reynolds numbers are, therefore, the most important dimensionless products.

The Froude number is represents the relative influence of inertial and gravity forces in a hydraulic flow. To achieve similarity the Froude number must be equal in model and prototype:

$$Fr = \left(\frac{U}{\sqrt{g \cdot L}} \right)_P = \left(\frac{U}{\sqrt{g \cdot L}} \right)_M \qquad (3.3)$$

Where U stand for velocity and L for length.

With $K_U = U_M / U_P$, $K_L = L_M / L_P$ and $K_g = 1$ (gravity remains unscaled), equation 3.3 can be written as:

$$K_U = \sqrt{K_L} \qquad (3.4)$$

The Froude scale law is intended for modelling flows in which the inertial forces are balanced primarily by the gravitational forces (gravity waves), which happen to be most flows with a free surface.

The Reynolds number represents the relative importance of the inertial force on a fluid particle to the viscous force on the particle. To obtain similarity the Reynolds number for both the model and prototype must be equal:

$$\text{Re} = \left(\frac{U \cdot L}{v} \right)_P = \left(\frac{U \cdot L}{v} \right)_M \qquad (3.5)$$

Where v stands for the kinematic viscosity.

With $K_U = U_M / U_P$, $K_L = L_M / L_P$ and $K_v = v_M / v_P = 1$ (modelling is done with water), equation 3.5 can be written as:

$$K_U = \frac{1}{K_L} \qquad (3.6)$$

The Reynolds scale law is intended for modelling flows where the viscous forces predominate. In free-surface flow, gravity is considered dominant over viscosity and therefore, this wave flume experiment is Froude-scaled. The required wave heights are derived with the Hudson-method from the provided Antifer-blocks.

3.1.2   Scale effects

If a small Froude-scaled model is tested in the same fluid as the prototype, equations 3.4 and 3.6 cannot be fulfilled at the same time. This leads to a viscous scale effect. Other scale effects are: surface tension, friction and aeration. These scale effects will be discussed in this paragraph.

Viscous scale effect

The linear geometric scaling of material diameter, which follows from the Froude-scaling, may lead to too large viscous forces corresponding to too small Reynolds numbers. The related increase in flow resistance reduces the flow in and out of the under layer and the core. Wilson and Cross concluded in 1972 that this is why models with a too low Reynolds number generally reflect relatively more wave energy from the model structure and transmit relatively less wave energy through the model structure than in their prototype-scale equivalent [HUGHES, 1993]. Also up-rush and down-rush velocities are relatively larger. As a result, run-up levels will be too high and armour stability too low [BURCHARTH *et al.*, 1999], which leads to safer stability coefficients. This is corrected in the model by increasing the size of the core material, than called for by the geometric length scale. In this research the core and under layer are scaled to the provided Antifer-blocks with ratios advised by VAN GENT, 2006. In present-day model testing these ratios are used by representative institutes (e.g. Delft Hydraulics, Sogreah and DHI), which makes the results comparable. After scaling the Reynolds number is calculated. When the Reynolds number in the core is higher than $2*10^3$ the flow in the structure is turbulent, conform to prototype situation, and the viscous scale effects are negligible [HUGHES, 1993].

Surface tension scale effect

The scale effect due to surface tension forces becomes important when the water waves are very short or the water depth is very shallow. Rules of thumb, presented by Le Méhauté in 1976, are that surface tension effects must be considered when wave periods are less than 0.35 seconds and when water depth is less than 2 cm [HUGHES, 1993]. At these parameter values, the restoring force of surface tension begins to be significant and the model will experience wave motion damping that does not occur in the prototype. For this research both wave period and water depth are considerably higher, so the scale effects by surface tension forces are negligible.

Friction scale effect

Bottom friction scale effects are possible in a coastal structure model if the wave propagation distance is very long. This is typically not a consideration for rubble-mound structure models because of the relatively large length scales. Other friction scale effect arises from the contact friction between adjacent armour units. In prototype rubble-mound structures, contact frictional forces are usually considered negligible compared to the dominant forces affecting the structure's response to wave action. However, in a small-scale physical model, the frictional forces between units may not be in similitude with the prototype because the armour unit surface can be relatively rougher than the large-scale units. Few systematic studies of the contact friction scale effect have been reported, and the standard practice is to reduce the friction between armour units as much as possible by making the model units smooth. Painting the units provides a smoother surface, as well making identification of damage areas easier. HUDSON AND DAVIDSON, 1975 noted that slightly conservative stability results would be provided if the model units are relatively smoother than the prototype.

Aeration scale effect

Hall conducted in 1990 an experimental program that examined the entrainment and movement of air bubbles which were pushed into the voids of rubble-mound models by waves breaking directly on the structure and by flow separation as water moves rapidly past the solid armour units [HUGHES, 1993]. Hall noted that entrained air bubbles would not be similitude in small-scale physical models because of lack of similarity of the Weber number ($We = \dfrac{\rho \cdot U^2 \cdot L}{\sigma}$, where $\sigma =$ surface tension) between prototype and model. This results in air bubbles that are relatively larger in the model than in the prototype, which in turn leads to too much energy dissipation in the model. Therefore, the total energy dissipation on the rubble-mound slope will be greater than it should be, and wave run-up will be somewhat affected.

3.2   Governing parameters

In this paragraph the governing parameters which determine the stability and therefore the setup of the model will be discussed. First the model-dimensions are determined by the facilities were the experiments were executed and by the structural parameters. As discussed in paragraph 2.3.1 there are structural and environmental parameters which affect the stability. In paragraph 3.2.3, the environmental parameters will be discussed. They determine the wave-properties and water height for the tests. In the last paragraph the instrumentation is discussed.

3.2.1   Facilities

The physical model tests were performed in the Fluid mechanics laboratory of the Faculty of Civil Engineering and Geosciences at Delft University of Technology. The used wave-flume has a length of 40 meter, a width of 0.80 meter and a height of 1.00 meter. The waves are generated by an electrical driven wave board. The wave board has an automatic reflection compensation system (ARC), which absorbs the reflected waves from the model based on the measurement of the free surface displacement at three locations on the wave board. This prevents the re-reflection of waves by the wave-board and thus allows the control of the created incident wave field of an experiment.

3.2.2   Structural parameters

Seaward profile of the structure
A slope of 1:35 was present in the flume, starting 8.00 meters from the wave board. The toe of the model is placed on the slope after 6.30 meters, so the slope will act as a foreshore, see figure 3.1. This means that the toe of the structure starts 14.3 meters from the wave board at a height of 0.18 meter. The crest height, of the under layer, was set to 0.90 meter to insure a minimum of overtopping, so almost all the wave-energy is concentrated on the front slope. It follows from this that the structure height is 0.72 meter. The width of the tested area is 0.80 meter, this is the maximum possible width in the wave flume. The recommended, and commonly used, slope angle for Antifer-block armour layers (and most other concrete units) is; $\cot a = 1.5$. Therefore all the experiments will be done with this slope angle. The influence of the slope angle on the stability of the structure will not be treated in this research.

This results in a fixed slope length of $\dfrac{0.72}{\sin(\tan^{-1}1.5)} = 0.87$ meter.

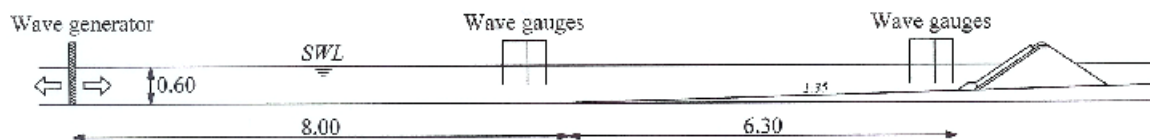The model-dimensions are presented in figure 3.2, they will be explained in this paragraph.

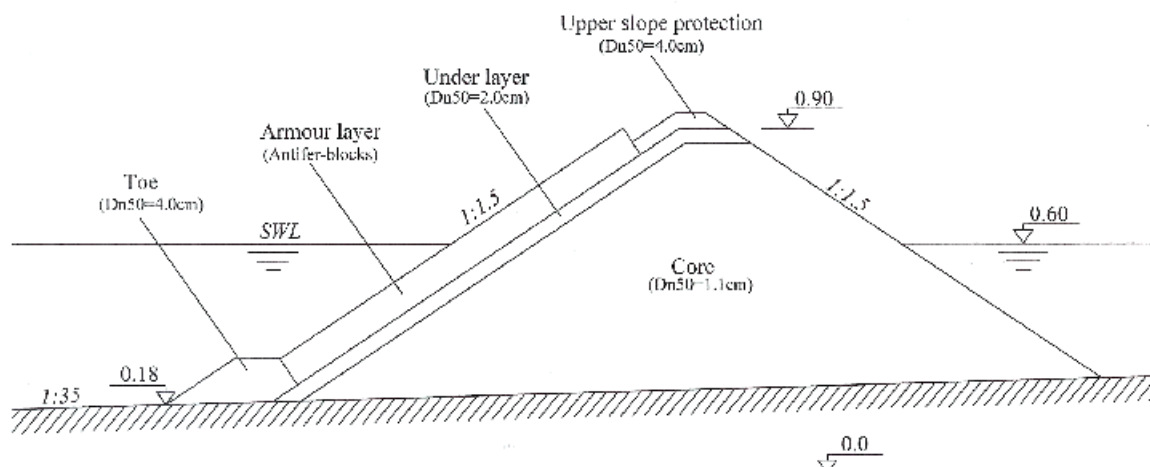Figure 3.1: Set-up of the wave-flume

Figure 3.2: Cross-section of the model

Armour layer
425 Antifer-blocks are made available by Delft Hydraulics. The blocks are made of aluminium, filled up with a plastic cylinder and were painted (smooth surface, no friction scale effect) in the colours red, yellow and blue, see figure 3.3. They have an overall mass, M, of 162.7 gram, a mass density, ρ_s, of 2507 kg/m³ and a volume of 64.9 cm³, see appendix I; Properties of the materials.

This results in a nominal diameter, D_n, of 4.0cm. In table 3.1 the block dimensions are presented.

Width bottom	$a = 4.4$ cm
Width top	$b = 4.0$ cm
Height	$h = 4.1$ cm
Radius groove	$r = 0.5$ cm
Depth groove	$c = 0.4$ cm

Figure 3.3: Used Antifer-block   Table 3.1: Block dimensions of used Antifer-blocks

For every experiment an attempt is made to place the centre of the armour layer on the still water level (SWL). This is done because the block movements will be counted within a reference area with the same distances under and above SWL.

Under layer
The standard Froude scaling method for the under layer is based on a relation between the armour-block weight and the under layer material weight, $M_{armour} / M_{50,underlayer}$. VAN GENT AND SPAAN, 1998 found that for this relation a value between 10 and 20 gave reliable results. The CEM, 2006 recommends the use of a weight ratio around 10. A relation based on the nominal diameter of the armour and the under layer, $D_{n,armour} / D_{n50,underlayer}$, is also commonly used. VAN GENT, 2006 recommended a ratio between 2 and 2.5. This resulted in the selection of calcareous rubble (sold under the name Yellow Sun) with a weight, M_{50}, of 20.62 gram, a mass density, ρ_s, of 2663 kg/m³ and a nominal diameter, D_{n50}, of 1.96 cm. The gradation wide (D_{n85} / D_{n15}) is 1.21 and the porosity of the under layer is 0.4. The sieve curve is given in Appendix I; Properties of the materials.

This results in a weight ratio with the armour layer of:

$$\frac{M_{armour}}{M_{50,underlayer}} = \frac{162.7}{20.62} = 7.89$$

The nominal diameter ratio is:

$$\frac{D_{n,armour}}{D_{n50,underlayer}} = \frac{4.0}{1.96} = 2.0$$

The thickness of the under layer has to be: $t_u \geq 2 \cdot D_{n50,underlayer}$ [CEM, 2006]. A thickness of 4.0cm with a maximum positive deviation of 1.0cm ($0.5 \cdot D_{n50,underlayer}$) is required for the experiments.

Core
The CEM, 2006 recommends for three layer sections a weight ratio for the armour and the core, $M_{armour} / M_{50,core}$, between 200 and 4000. In present-day model tests a ratio between the under layer and core, $M_{50,underlayer} / M_{50,core}$, between 5 and 10 is mostly used. VAN GENT, 2006 recommended a nominal diameter ratio between the under layer and core, $D_{n50,underlayer} / D_{n50,core}$, of 1.5. This resulted in the use of calcareous rubble (sold under the name Yellow stone) with a weight, M_{50}, of 3.47 gram, a mass density, ρ_s, of 2643 kg/m³ and a nominal diameter, D_{n50}, of 1.08cm. The gradation width (D_{n85} / D_{n15}) is 1.34 and the porosity of the core is 0.4. The sieve curve is given in Appendix I; Properties of the materials.

The weight ratio with the under layer is:

$$\frac{M_{50,underlayer}}{M_{50,core}} = \frac{20.62}{3.47} = 5.94$$

The nominal diameter ratio with the under layer is:

$$\frac{D_{n50,underlayer}}{D_{n50,core}} = \frac{1.96}{1.08} = 1.81$$

The viscous scale effects are negligible when the Reynolds number is higher than 2·10³. The Reynolds number is calculated in the following way, with the wave data from paragraph 4.2:

$$\text{Re} = \frac{U \cdot D}{v}$$

D is the characteristic dimension (10% smaller) of the core material and v is the kinematic viscosity, which for water of 10 degrees is 1.33*10⁻⁶ m²/s.

$$U = \frac{P \cdot H_i \cdot L}{2 \cdot h \cdot T}$$

This velocity calculation was presented by Keulegan in 1973 and represents the maximum seepage velocity at the entrance face of the structure [HUGHES, 1993]. P is the porosity of the core material, H_i, the incident wave height at the toe, L, the incident wave length, h, the water depth and T, the average wave period at the toe.

The resulting Reynolds number is 600 for the lowest wave-series and 2100 for the highest wave-series. From this follows that the porous flow inside the structure is not fully turbulent for all wave series and minor viscous scale effects are expected. This is accepted, because the experiments are process-orientated and the model is comparable with models from the representative institutes. Furthermore is assumed that every experiment is influenced in the same way by these scale effects, which cause the stability coefficients to be on the safe side.

The lea side of the model will consist of the unprotected core material with a slope angle of $\cot a = 1.5$. In this way the overtopping will generate a natural berm at the still water level (SWL). The length of this berm will be measured and qualitative compared for all experiments.

<u>Toe</u>
The stability of the toe of the structure is not part of the research. To guarantee the toe stability, it is made of a stone-class comparable to the nominal diameter of the Antifer-blocks. The selected stones have a weight, M_{50}, of 172.67 gram, a mass density, ρ_s, of 2678 kg/m³, a nominal diameter, D_{n50}, of 3.96 cm and a gradation wide (D_{n85}/D_{n15}) of 1.23. The sieve curve is given in Appendix I; Properties of the materials. The thickness of the toe should be more than $2 \cdot D_{n50,toe} =$ 8cm and the top of the toe should be more than $1.5 \cdot H_s = 30$cm beneath the still water level (SWL) [CEM, 2006]. The toe-height will differ for the experiments, because of the determined number of Antifer-blocks (425), the different placement methods (with different packing densities) and the placement of the centre of the armour layer on SWL. The width of the toe has to be larger than $3 \cdot D_{n,Armour} = 12$cm and smaller than $2 \cdot H_s = 40$cm [CEM, 2006]. Because of the guaranteed stability and the differing heights of the toe, a smaller width can be used, so the toe will less influence the incoming waves on the armour.

<u>Upper slope protection</u>
As mentioned before, the number of Antifer-blocks is determined and the centre of the armour layer will be placed on SWL. The length of the unprotected part of the under layer above the armour layer will therefore differ for the different experiments. For equal up- and down-rush and comparable amounts of overtopping this part together with the crest is filled with one layer of the same stones which are used for the toe (nominal diameter in accordance with Antifer-blocks).

<u>Placement method</u>
The placement method is a structural parameter which has a high influence on the stability and is closely bound with the packing density, interlocking and layer thickness of the main armour. The impact of the placement method on the stability is the main objective of this research; the employed placement methods will be discussed in chapter 5.

3.2.3 Environmental parameters

The experiments are performed with irregular waves, based on a realistic wave field. Compared to regular waves this gives more valuable results for practice. The use of a wave-flume makes it only possible to simulate wave attack with an incident angle, β, of 90 degrees to the slope. This perpendicular wave attack is often regarded as the most severe condition for the stability of the armour layer. In this paragraph the most determining environmental parameters will be discussed. Because of limitations in time and resources wave grouping and wave asymmetry are not examined.

Shape of the wave spectrum
The irregular wave field is best described with a variance-density spectrum. This type of spectrum provides a statistical description of the fluctuating wave height caused by wind. Much empirical research has been done to predict and generate a realistic wave field. In the early seventies a large field experiment in the North Sea led to the JONSWAP-spectrum. The JONSWAP-spectrum is used for the experiments and is also commonly used in other wave flume experiments, which makes the laboratory data accessible for comparison. The JONSWAP-spectrum does not represent a fully developed sea (fetch limited to about 100km.). Its expression was generated by enhancing the Pierson-Moskowitz spectrum with a peak-enhancement function [HOLTHUIJSEN, 2002]. This resulted in the following equation:

$$E_{JONSWAP}(f) = \alpha \cdot g^2 \cdot (2\pi)^{-4} \cdot f^{-5} \exp\left\{\frac{5}{4} \cdot \left(\frac{f}{f_{peak}}\right)^{-4}\right\} \cdot \gamma^{\exp\left\{-\frac{1}{2}\left(\frac{f-f_{peak}}{\sigma \cdot f_{peak}}\right)^2\right\}}$$

(3.8)

With $\sigma = \sigma_a$ for $f \leq f_{peak}$ and $\sigma = \sigma_b$ for $f > f_{peak}$.

The energy scale parameter, α, the shape parameters, γ, σ_a and σ_b, and the frequency scale parameter, f_{peak}, are free parameters. The mean values of the shape parameters of the JONSWAP observations were; γ =3.3, σ_a =0.07 and σ_b =0.09. These values are also used for the experiments within this research. The significant wave height, H_{m0}, can be determined from the variance-density spectrum with the following equation:

$$H_{m0} = 4 \cdot \sqrt{m_0}$$

(3.9)

With the total area of the spectrum being equal to the total variance:

$$m_0 = \int_0^\infty E(f) df$$

(3.10)

Characteristic wave steepness
The wave steepness is a parameter which includes the characteristic wave height and the wave length. The wave length is often written as a function of the wave period, see equation 3.11.

$$s = \frac{H_s}{L_0} = \frac{2 \cdot \pi}{g} \cdot \frac{H_s}{T^2}$$

(3.11)

Where s is the wave steepness, H_s the significant wave height and T the wave period.

In previous research VAN GENT *et al.*, 1998 was concluded that there was no clear and consistent influence of the wave steepness on the stability. VAN GENT, 2006 recommended a steepness for the peak period between 3 and 3.5%. This is comparable to a steepness of 5% for the mean period. Per test the significant wave height will be gradually increased until the maximum possible to generate wave height is reached. The peak periods in the input files for the different wave heights are calculated with a constant wave steepness of 3.3%.

Number of waves
VAN DER MEER, 1988a showed in his research the importance of the storm duration (number of waves, N) on the armour layer stability. Because of limitations in time the total number of generated waves is set between 1000 and 1500. Assumed is that if no damage occurs after 1000-1500 waves, more waves will neither develop damage. It is also assumed that the JONSWAP-spectrum will be fully developed after this number of waves.

Characteristic wave height
Per test the incoming significant wave height at the toe will be gradually increased, to obtain damage (instability). In this way the stability can be compared according the wave height were the structure failed. To determine the significant wave heights, H_s , which are required for the experiments, the Hudson formula is applied. In this way the wave height where initial damage will possibly occur for the irregular placement method can be found. A K_D -value of 7 is used, as recommended by GÜNBAK, 1999, see paragraph 2.3.2.
This leads to the following calculation:

$$H_s = \sqrt[3]{V \cdot K_D \cdot \cot \alpha \cdot \left(\frac{\rho_s}{\rho_w} - 1 \right)^3} = \sqrt[3]{64.9 \cdot 7 \cdot 1.5 \cdot \left(\frac{2507}{1000} - 1 \right)^3} = 13.3 \, \text{cm}$$

To check this wave height the derived formula by VAN DER MEER, 1988b for cubes and the formula for Antifer-blocks from CHEGINI AND AGHTOUMAN, 2001, as presented in paragraph 2.3.3, are used.

Van der Meer formula for cubes:

$$H_s = \left[6.7 \cdot \frac{N_{od}^{0.4}}{N^{0.3}} + 1.0 \right] \cdot s_{om}^{-0.1} \cdot \Delta \cdot D_n$$

Derived formula by Chegini and Aghtouman for Antifer-blocks:

$$H_s = \left[6.951 \cdot \frac{N_{od}^{0.443}}{N^{0.291}} + 1.082 \right] \cdot s_{om}^{-0.082} \cdot \Delta \cdot D_n$$

The results for 1000 waves, N , and a wave steepness, based on the mean period, of 5% are presented in table 3.2.

	N_{od}	H_s (cm), cubes	H_s (cm), Antifer
Start of damage	0	8.2	8.4
Initial damage (needs no repair)	0-0.5	8.2-13.4	8.4-13.7
Intermediate damage (needs repair)	0.5-1.5	13.4-16.3	13.7-17.0
Failure (under layer exposed)	>2	>17.3	>18.2

Table 3.2: Van der Meer method for cubes and Antifer-blocks

All formulas confirm that the start of serious damage will occur for a significant wave height between 13.3 and 13.7cm. Significant wave heights from 9 to 20cm are used for the experiments. A 20cm significant wave height is about 150% of the wave height determined by the Hudson formula for the initial damage. This is assumed to be enough to guarantee damage for economical (a porosity above 40%) placement methods.

Water depth

The water depth h should be at least $3 \cdot H_s$, which results in a water depth of minimal 60cm. It is possible for the wave-board to generate the required JONSWAP spectrum with a significant wave height of 20cm in a water depth of 60cm. When the water depth is higher, the chance for overtopping increases, which influences the wave attack (and stability) on the armour. Since the focus of this research lies on the stability the experiments are performed with a water depth of 60cm.

3.2.4   Instrumentation

Two arrays of wave gauges are installed on the wave flume. One array is placed in front of the foreshore to measure the deep water wave. The other is placed in front of the toe of the structure to measure the wave attack on the structure. Every array consists of 3 wave gauges. This makes it possible to accurately split the recorded surface elevation over time into incident and reflected wave information.

4 Experimental procedure

Every experiment consists of 3 parts; constructing the model, testing the model and analysing the obtained data. These three parts will be discussed in this chapter.

4.1 Model construction

First the model dimensions were drawn on the glass of the flume. It was necessary to sieve and wash the stones for the core and the under layer before placing them. This was done to obtain the required stone dimensions and to make sure the water stays clear during the tests. The core was placed within the drawn dimensions and was not compressed, see figure 4.1. This is comparable with the real construction and a high porosity is obtained. The under layer was placed again for each experiment, because of the possible compression of the layer by the Antifer-blocks during placement and tests. Before placing the Antifer-layer the theoretically length of the layer was calculated for the regular placement methods, with the packing density, and estimated for the irregular placement method. In this way the necessary height of the toe was determined because it was attempted to place the centre of the Antifer-layer for every experiment on the still water level. After placing the toe in a stable way the Antifer-blocks were placed one by one. For the regular placement methods the required distances between the blocks depended on the pattern and the packing density. They were loosely placed on the under layer at the intended position. For the irregular placement the blocks were placed by letting them fall free from a few centimetres above the intended position. This was done to increase the irregularity of the placement. LOSADA, 1986 and YAGCI *et al*., 2003 placed the blocks by dropping them from a height of 30cm. This however is not standard practice and does not replicate real construction. As mentioned in paragraph 2.2.3 it is possible to place the blocks in reality with a high accuracy. For both methods the units were placed in coloured bands, to improve the visualization of the displacement, which determines the damage. After placing the Antifer-layer the upper part of the slope was filled up with one layer of the same stones the toe was constructed with.

When the building of the model was completed the actual length and the heights of the extreme points of the Antifer-layer were measured. Ropes were tightened on the side of the flume to visualize the different heights (reference areas). Thereupon photos were taken from the front and the side of the structure, see figure 4.2. Finally the wave flume was filled with water up to a height of 60cm and the wave gauges were calibrated.

Figure 4.1: Core of the model

Figure 4.2: Side view of the model

4.2   Test procedure

For all the experiments the same wave series were applied. The different significant wave heights were determined as described in paragraph 3.2.3 and the associated peak periods for a wave steepness of 3.3% were calculated. With these values the input files for the wave generator were computed. The measured incoming significant wave height came out a little lower than was put in. Because the wave steepness for the peak period lied within the limit of the recommended 3-3.5%, the input files were not adapted. Wave characteristics measured in front of the foreshore (deep water wave) and in front of the toe, averaged over all experiments, are presented in table 4.1. The obtained wave spectra from the two measuring places for the first experiment for an input wave-height of 14 cm are presented in figure 4.3 and 4.4. For all wave data per experiment is referred to Appendix III; Obtained data.

Input		Output; incident wave at deep water							Output; incident wave at the toe						
H_{m0}	T_p	H_{m0}	T_p	$T_{m0,1}$	$T_{m-1,0}$	s_p	$s_{m0,1}$	$s_{m-1,0}$	H_{m0}	T_p	$T_{m0,1}$	$T_{m-1,0}$	s_p	$s_{m0,1}$	$s_{m-1,0}$
(cm)	(s)	(cm)	(s)	(s)	(s)	(%)	(%)	(%)	(cm)	(s)	(s)	(s)	(%)	(%)	(%)
10	1.39	9.45	1.38	1.20	1.27	3.2	4.2	3.7	9.15	1.38	1.21	1.28	3.1	4.1	3.6
12	1.53	11.31	1.52	1.32	1.40	3.1	4.2	3.7	11.06	1.52	1.34	1.40	3.1	4.0	3.6
14	1.65	13.11	1.65	1.42	1.51	3.1	4.2	3.7	12.88	1.65	1.44	1.50	3.0	3.9	3.7
16	1.76	14.93	1.75	1.51	1.61	3.1	4.2	3.7	14.67	1.75	1.53	1.60	3.1	3.9	3.7
18	1.87	16.61	1.86	1.61	1.70	3.1	4.1	3.7	16.26	1.87	1.59	1.69	3.0	3.9	3.7
20	1.97	18.32	1.97	1.66	1.77	3.0	4.3	3.7	17.59	1.99	1.61	1.75	2.9	4.0	3.7
22	2.07	19.88	2.05	1.73	1.86	3.0	4.3	3.7	18.90	2.07	1.63	1.82	2.8	4.2	3.7
24	2.16	21.34	2.16	1.77	1.95	2.9	4.3	3.6	20.05	2.18	1.63	1.89	2.7	4.4	3.6

Table 4.1: Wave characteristics
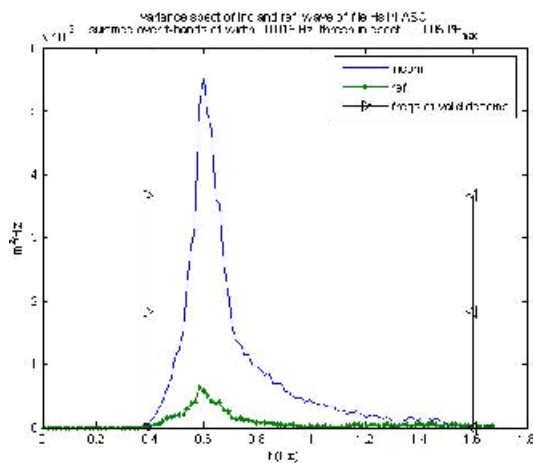
Figure 4.3: Wave spectrum at deep water
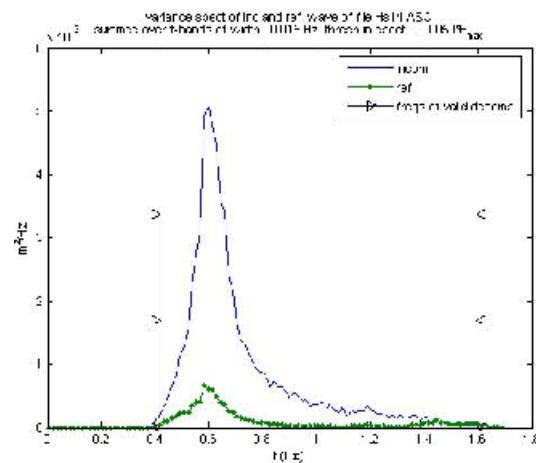
Figure 4.4: Wave spectrum at the toe

For every run a standard procedure was followed. First a photo was taken of the armour layer from a fixed position perpendicular to the armour layer. Hereafter the video camera was turned on for the first five minutes and the wave-generator was started. When the first waves reached the structure the measuring programme (Dasylab) for the wave gauges was started. During the test the armour layer was closely observed and block movements were noted down.

4.3 Experiment analysis

This paragraph discusses how every test is analysed. After the construction of the model the packing density and the porosity are determined. Thereafter the model is tested and the wave characteristics and the stability are calculated. All the analyses for the performed experiments are presented in the next chapter.

4.3.1 Packing density

In paragraph 2.4.2 was already mentioned that there are many different methods for computing the porosity and the density. A packing density, based on the surface occupation ratio, will be used for this research. An advantage of this method is that together with the damage value, which determines the block volume, the total required volume of concrete and the required number of blocks per surface can be simply calculated. This, among other things, determines the suitability of the placement method. The use of the surface packing density makes it also possible to compare the irregular with the regular placement methods. The standard porosity calculation does not give such a good insight in the density of the layer because of the different layer thicknesses.

The packing density, ψ_S, is the ratio between the real number of blocks and the maximum possible number of block volumes per surface unit averaged per layer and is expressed as:

$$\psi_S = \frac{N_{BL}}{N_{PBL}} = \frac{N_{BL} \cdot D_n^2}{B \cdot L} \qquad [\text{m}^2/\text{m}^2] \qquad (4.1)$$

N_{BL} = number of blocks in area B*L per layer

$N_{PBL} = \dfrac{B \cdot L}{D_n^2}$ = maximum possible number of block volumes in area B·L per layer

$D_n = \sqrt[3]{V_b}$ = nominal diameter block

V_b = volume per block

B = width of area

L = length (on slope) of area, which was measured for every experiment

See figure 4.5, where the hatched area indicates the number of blocks.
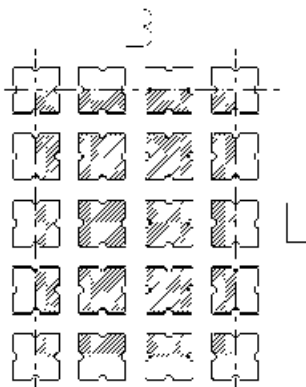
Figure 4.5: Definitions for the calculation of ψ_S

For a regular placement method it is possible to apply a different packing density per layer, ψ_{S1} and ψ_{S2}. The overall packing density then follows from:

$$\psi_S = \frac{\psi_{S1} + \psi_{S2}}{2} \qquad (4.2)$$

For the irregular placement method all the blocks in the area are counted and divided by the number of layers (2) to get the N_{BL}.

This method gives the same results as a solid density, d, calculation with an armour thickness; $t = n \cdot k_\Delta \cdot \sqrt[3]{V_b}$, where the layer thickness coefficient, k_Δ, is equal to 1. For a solid density calculation the total volume of concrete per surface is divided by the volume of the armour layer for that area:

$$d = \frac{n \cdot N_{BL} \cdot V_b}{B \cdot L \cdot t} = \frac{N_{BL} \cdot V_b^{2/3}}{B \cdot L \cdot k_\Delta} = \frac{\psi_S}{k_\Delta}, (V_b^{2/3} = D_n^2) \qquad (4.3)$$

For a breakwater design the total required volume of concrete per surface unit, V_t, can be calculated by multiplying the packing density (surface-occupation) by the number of layers and the required nominal block diameter, which follows from the damage coefficient. This results in:

$$V_t = \psi_S \cdot n \cdot \sqrt[3]{V_b} \qquad [\text{m}^3/\text{m}^2] \qquad (4.4)$$

Where ψ_S is now a constant value, depending on the chosen placing pattern. The corresponding stability parameter determines the block volume.

The required number of Antifer-blocks per surface, N_t, is calculated by dividing the volume of concrete per surface unit by the required block volume. This results in:

$$N_t = \frac{V_t}{V_b} = \frac{\psi_S \cdot n}{V_b^{2/3}} \qquad [\text{-/m}^2] \qquad (4.5)$$

4.3.2 Porosity

The porosity has no use for directly comparing the different placement methods because of the different layer thicknesses. The void ratio, however, is a meaningful property of a placement method. The real porosity for the placement methods is calculated. Therefore the layer thickness has to be determined for every experiment. The real porosity, P_r, is expressed as:

$$P_r = 1 - d = 1 - \left(\frac{\psi_S}{k_\Delta}\right) \qquad (4.6)$$

For the irregular placements the layer thickness coefficient is specified by the CEM, 2006 and the BS, 1991 as 1.10 for (modified) cubes. A commonly used coefficient for irregular placed double layered Antifer-armour is 1.076. This follows from a layer thickness, $t = 2 \cdot a$:

$$t = n \cdot k_\Delta \cdot \sqrt[3]{V_b} \tag{4.7}$$

$$t = 2 \cdot a = 2 \cdot \left(\frac{V}{0.8024} \right)^{1/3} = 2 \cdot 1.076 \cdot (V)^{1/3}$$

For regular placed blocks the layer thickness coefficient is different because of the possible intrusion of the second layer into the first layer. The porosities will be determined for every placement method, by measuring or calculating the layer thickness.

4.3.3 Wave characteristics

For every wave series the wave characteristics were calculated, from the measured data from the wave gauges, with Matlab. The wave characteristics from the measuring point in front of the toe of the structure are used for the stability analysis. Per wave series the data consist of the incoming significant wave height, H_{m0}, the reflected significant wave height, H_{Rm0}, and three periods, namely the peak period, T_p, and the average periods, $T_{m0,1}$ and $T_{m-1,0}$. With these values the associated wave steepness, the reflection coefficients, C_r, and the stability parameter, $N_s = \frac{H_s}{\Delta \cdot D_n}$ are calculated. The wave steepness can be included in the stability analysis by employing the dimensionless Iribarren surf similarity parameter, $\xi = \frac{\tan \alpha}{\sqrt{s}}$ [SCHIERECK, 2001]. In this research the value for the wave steepness and the storm duration (1000-1500 waves) is kept constant for every test and will therefore be not included in the stability analysis.

4.3.4 Stability

For the calculation of the armour layer stability the Hudson formula is applied, see equation 4.8. This formula is based on the significant incoming wave height at the toe were the last tolerable damage ratio appears.

$$K_D = \frac{H_{m0}^3}{V_b \cdot \cot \alpha \cdot \left(\frac{\rho_s}{\rho_w} - 1 \right)^3} \tag{4.8}$$

The damage ratio is calculated with equation 4.9, in which displacement is defined as the movement of a block more than one nominal diameter.

$$DamageRatio = \frac{number\_of\_displaced\_units}{Total\_number\_of\_units\_within\_reference\_area} \tag{4.9}$$

The reference area has to be defined, because the movement of the units is not uniformly distributed over the slope. In general, most movements take place within the levels SWL ± Hs. This results in a reference area for the calculation of K_D of SWL ± 20cm. This is the maximum tested significant wave height and is equal to SWL $\pm 5 \cdot D_n$. For every experiment the different damage ratios will also be graphical presented as values of different reference areas.

To visualize the movements within the layer, the overlay technique was used. Photos were made after every test-run, when the water was tranquil again, from exact the same location. These photos were printed on overhead-slides and the block positions were visual compared, by overlaying, with the positions on the photo that was taken before the first test-run. The moving blocks in the second layer were counted. The blocks connecting to the glass of the flume were not included, because of the possible wall-effect. They are at one side not connected to the other blocks in the armour layer, which may influence their stability. Other blocks which move because of the movement of these wall-blocks are also not included. In this way 4 different types of movement were counted for the different reference areas. The 4 types of movement are expressed in relation to the nominal diameter: 0.0-0.5·D_n, 0.5-1.0·D_n, 1.0-2.0·D_n and >2.0·D_n. Movements of the type >1·D_n are called displacement.

For placement methods which are easy to repair, the stability parameter K_{DH} (the H stands for Hudson), is calculated. Easy repairable placement methods are the irregular placement and placements where the holes of the first layer are irregular filled up with the second layer. The stability parameter, K_{DH}, is based on the significant wave height were the first displacements appear within a damage ratio of 0-5%. If this first damage exceeds the damage ratio of 5%, the significant wave height from the preceding wave-series is applied to calculate the K_{DH}-value. This method was also used by Hudson, as described in paragraph 2.3.2. When one block of an irregular placement method displaces during the first wave attack the block is not included, because the layer always settles a little during the first waves. A displacement is then not a sign of instability of the layer but of an individual badly placed block.

For regular placement methods a different damage level is required. This is also noted in the BS, 1991. The displacement of a few units in a regular placed armour layer is very problematic, because the method obtains its stability from a strict pattern. When this pattern is disturbed it results in a chain reaction. The layer cannot be repaired by filling up the hole, because the upper blocks tend to slide down. Blocks from the upper rows, which rested on the displaced block, have to be removed to repair the layer. Therefore a damage ratio of 0% is required. The significant wave height before the wave-series in which the first displacement appeared is applied for the calculation of the stability parameter, K_{D0}, for regular placement.

To compare the irregular placement with the regular placement methods another stability parameter is required. From the tests on the irregular placement methods was observed that after the initial damage occurred there is a wave series where the damage ratio suddenly rapidly increases and exceeds the 5%. In this stage also a chain reaction of settlement takes place and repair is necessary. The K_D-value is calculated with the significant wave height where the damage ratio was still below 5%, $K_{D<5\%}$. This $K_{D<5\%}$-value for irregular placement is comparable to the K_{D0}-value for regular placement, because both values are based on the wave-series before failure (great repair work).

For every experiment the damage development is presented in N_s and K_D-values. This is done by calculating these values for a damage ratio of 0, 1, 3, 5, 10 and 15 percent. The K_D-values are calculated with the N_s-values, which are derived by interpolation. Also graphs are drawn with the movement ratios for the movements; 0.0-$0.5 \cdot D_n$, 0.0-$1.0 \cdot D_n$, 0.0-$2.0 \cdot D_n$ and $>0.0 \cdot D_n$, versus the dimensionless stability parameter, N_s. In this way a visual impression of the damage development is given.

Rocking is not specified in the stability analysis, because rocking is mostly problematic for slender armour units, for which it can result in breakage of the units. In this report the possible structural damage and resulting reduction in stability is not taken into account.

5 Performed experiments

The experiments were not all planned in advance. For the first experiments a schedule was made with different placement methods, which could be tested. With the results from the analyses of these tests new experiments were planned. In the first paragraph of this chapter the followed programme is discussed, the second paragraph describes the way the experiments are presented and thereafter all 17 performed experiments are presented. In Appendix II an overview is given of the performed experiments and in Appendix III all the obtained data is presented on a CD.

5.1 Experiment programme

A placement is determined by three choices; the pattern for the first layer, the pattern for second layer and the way the blocks are placed, per row or per layer. At the start of the research a schedule was drawn with a general overview of the possible placement methods, see figure 5.1. In this schedule the pictures for the regular placement are top views, wherein distance X directs along the slope and distance Y directs over the slope. When after placing the average values for X and Y are calculated the packing density can be calculated with:

$$\psi_s = \frac{D_n^2}{X \cdot Y}$$

(5.1)

The pictures for the placement are side views. When the blocks are placed per layer first 4 rows of the first layer are placed and thereafter 4 rows of the second layer are placed. This continues for the whole slope.
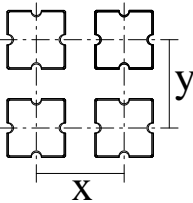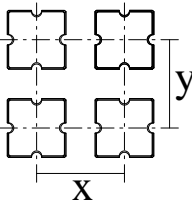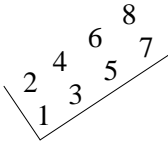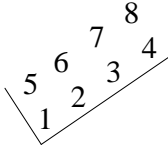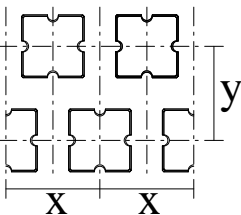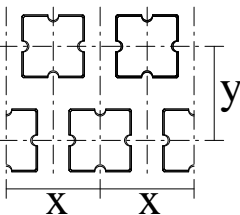
First layer	Second layer	Placement
-1, Irregular	-a, Irregular	-A, Row by Row
Regular -2, Square grid	*Regular* -b, Square grid	
-3, Pyramid	-c, Pyramid	-B, Layer by Layer
	-d, Filling up the holes	

Figure 5.1: General overview placement methods

There are more options for the regular placement of the first and second layer. The blocks can be placed on their side, top or under an angle. In this research the Antifer-blocks are placed on their bottom. Alternatives are considered for the square-grid and pyramid pattern by turning the blocks over 45 degrees, see figure 5.2.
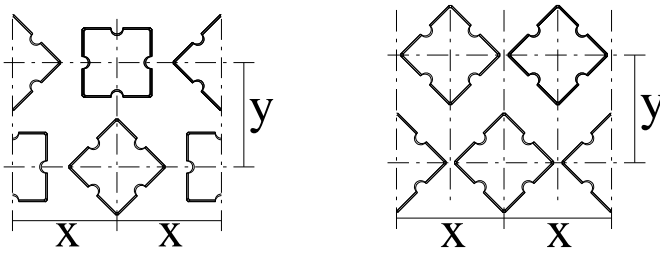
Figure 5.2: Turned blocks within the square-grid and pyramid pattern

With the schedule from figure 5.1 the first experiments were planned and with the results new experiments were planned. A short description of the followed programme is given beneath. An overview with packing densities can be found in Appendix II. In the following paragraphs all the experiments are discussed in detail.

1. 3dA, closed pyramid method, the blocks of the second layer direct to a different side per row.
2. 1aA, irregular placement, placed row by row.
3. 2bB, column method with spreading over the slope (distance Y).
4. 3dB, filled pyramid method, the blocks of the second layer are irregular placed in the holes
5. 1aB, irregular placement, placed layer by layer.

From experiment 3 followed that the blocks did slide down the slope. So experiment 3 was repeated without spreading over the slope.

6. 2bB, column method with Y=bottom length.
7. 3cB, double pyramid method with spreading over the slope.
8. 3bB column method under an angle, testing oblique wave attack.
9. 3cB, double pyramid method with Y=bottom length.

After the first nine experiments was concluded that with spreading over the slope (distance Y) the methods became less stable for the same packing density. For the irregular methods experiment 5 turned out to be the most stable. For the regular placement the column method and the double pyramid method turned out to be the most stable. The column method has as disadvantage the high overtopping, the instability due oblique incoming waves and the high pressures on the toe. Therefore further testing was done to optimise the double pyramid method. Both alternatives with turned blocks are not performed because of the sliding down of the blocks and the disadvantages of the column method.

10. 3cB, double pyramid method, experiment 9 with lower packing density.

In experiment 10 the second layer was placed a little shifted over the slope (? -¼ · D_n) on the first layer. This resulted in lower reflection coefficients. More tests were planned with the staggered double pyramid placement.

11. 3cB, double pyramid method, experiment 10, now placed around ½ · D_n staggered.
12. 3cB, double pyramid method, experiment 10 with lower packing density.
13. 3dA, closed pyramid method, experiment 1 with higher packing density.
14. 3dA, closed pyramid method, experiment 1 with lower packing density.
15. 3cB, double pyramid method, experiment 10, now placed around ¾ · D_n staggered.

The last two experiments are chosen to test the reproducibility of the experiments.

16. 1aB, irregular placement layer by layer, experiment 5 with a little lower packing density
17. 3cB, double pyramid method, experiment 10, now 0-? $\cdot D_n$ staggered.

It was considered to test the double pyramid method with different packing densities for both layers. This however would result in the turning of the blocks of the second layer into the holes of the first layer, which makes regular placement of the second layer impossible. Also the turning of blocks over 45 degrees for a complete row was considered. This however would result in a far higher packing density, which is not efficient.

5.2   Experiment presentation

For every performed experiment a description, a visualisation and the layer properties, which follow from the model construction, are given. The layer properties are expressed with the horizontal spreading ratio, X / D_n (only for regular placement), the diagonal spreading ratio, Y / D_n (only for regular placement), the packing density, the layer thickness, the layer thickness coefficient, the solid density and the porosity. The way the layer thickness is derived is presented in a figure. Thereafter the model was tested. The wave characteristics obtained at the toe of the structure, the stability parameter, N_s, and the derived characteristics of the placement method are presented in a table. The wave characteristics are represented by the incoming significant wave height, H_{m0}, and the different wave steepness', s_p, $s_{m0,1}$ and $s_{m-1,0}$. The characteristics of the placement method are expressed with the reflection coefficient, C_r, and the damage ratios. The presented damage ratios are obtained by the overlay method within the reference area SWL±20cm (or SWL$\pm 5 \cdot D_n$). The damage ratios for the movements 0.0-0.5$\cdot D_n$, 0.5-1.0$\cdot D_n$ and 0.0-1.0$\cdot D_n$ are indicated with M_1, M_2 and M_t respectively. The damage ratios for the displacements 1.0-2.0$\cdot D_n$, >2.0$\cdot D_n$ and >1.0$\cdot D_n$ are indicated with D_1, D_2 and D_t respectively. Hereafter the observed phenomena during the tests are described, the stability is analysed and the K_D-value is calculated. The damage development is presented in N_s and K_D-values for the damage ratios: 0, 1, 3, 5, 10 and 15 percent. Graphs are drawn with the movement ratios for the movements; 0.0-0.5$\cdot D_n$, 0.0-1.0$\cdot D_n$, 0.0-2.0$\cdot D_n$ and >0.0$\cdot D_n$, versus the dimensionless stability parameter, N_s. In this way a visual impression of the damage development is given. The displacement ratio D_t is also plotted for different reference areas. These graphs show if the damage is equal divided over the slope or if most displacements take place around SWL, which means: the larger the reference area, the lower the damage ratio.

5.3   Experiment 1

The Antifer-blocks are placed row by row. The blocks in the first layer are placed with fixed horizontal distances from one another and in a regular position, with their grooves perpendicular to the slope. The blocks of the second layer are placed diagonal for the first row directing to the left, for the second row to the right and so on. They fill up the gaps between the blocks of the first layer. The blocks of the second layer are clamped by the blocks from the next row of the first layer, which integrates both layers. The pattern has a triangular shape and the blocks of the second layer close up the holes in the first layer. Therefore this method is called, the closed pyramid method, see figure 5.3 and 5.4. The properties of the layer are presented in table 5.1 and figure 5.5 (measurements in cm.) and the test results are presented in table 5.2.
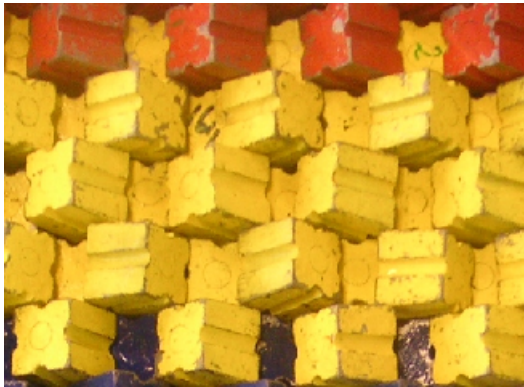
Figure 5.3: Photo of experiment 1
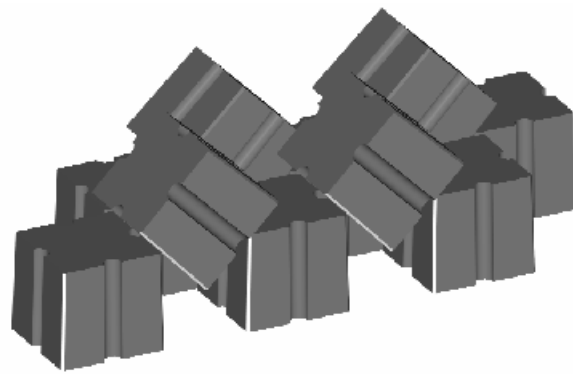
Figure 5.4: 3D drawing of experiment 1

|	
Hor. spreading ratio, X/D_n	1.88
Diag. spreading ratio, Y/D_n	1.07
Packing density, ψ_S	49.7 %
Layer thickness, t	8.1cm
Layer thickness coefficient, k_Δ	1.01
Solid density, d	49.3 %
Real porosity, P_r	50.7 %

Table 5.1: Layer properties
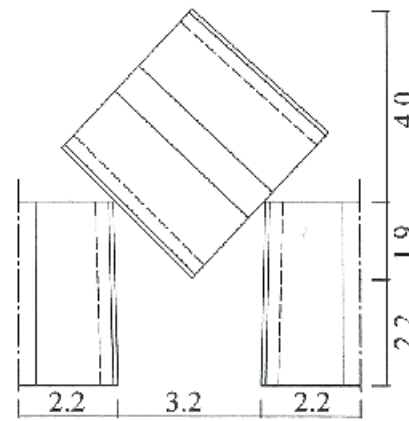
Figure 5.5: Thickness derivation

H_{m0} (cm)	s_p (%)	$s_{m0,1}$ (%)	$s_{m-1,0}$ (%)	C_r (%)	N_s (-)	M_1 (%)	M_2 (%)	M_t (%)	D_1 (%)	D_2 (%)	D_t (%)
9.06	3.01	4.06	3.52	33.8	1.50	0.7	0.0	0.7	0.0	0.0	0.0
11.03	3.09	3.97	3.57	34.9	1.82	3.9	0.0	3.9	0.0	0.0	0.0
12.87	3.02	3.88	3.64	36.1	2.13	6.6	0.0	6.6	0.0	0.0	0.0
14.63	3.03	3.90	3.67	38.9	2.42	7.2	0.0	7.2	0.0	0.3	0.3
16.12	3.03	3.86	3.63	41.7	2.66	21.1	0.0	21.1	0.0	1.3	1.3
17.57	2.89	4.13	3.72	46.7	2.90	25.3	0.0	25.3	0.7	3.6	4.3
18.91	2.77	4.16	3.67	48.6	3.12	28.0	1.3	29.3	0.7	7.9	8.6
20.10	2.70	4.34	3.59	50.5	3.32	31.9	0.3	32.2	1.0	11.2	12.2

Table 5.2: Test results within the reference area SWL ±20cm

During the wave series $H_{m0} = 14.63$cm, the overtopping started and the first block was displaced, while the movement ratio was still low. The first displaced blocks lay near SWL. From there on more blocks, upward the slope, were displaced (chain-reaction), see figure 5.6. The layer obtains its stability from the clamping of a block of the second layer by a block of the next row of the first layer. When a block of the second layer is displaced, the clamping block above, of the first layer, moves down al little. This loosens the block above of the second layer etc. The stability-value for this regular method is calculated from the last stability parameter where no displacements occurred, $N_s = 2.13$. From this follows:

$$K_{D0} = \frac{N_s^3}{\cot \alpha} = 6.4$$

For the presentation of the damage development the N_s- and K_D-values were calculated for different damage ratios, see table 5.3. In figure 5.7 the damage ratios for the displaced units, are presented for the different reference areas. From this figure follows that most displacements take place around SWL.

Damage ratio	0%	1%	3%	5%	10%	15%
N_s	2.13	2.59	2.80	2.94	3.20	-
K_D	6.4	11.6	14.6	16.9	21.8	-

Table 5.3: N_s- and K_D-values for different damage ratios (D_t)
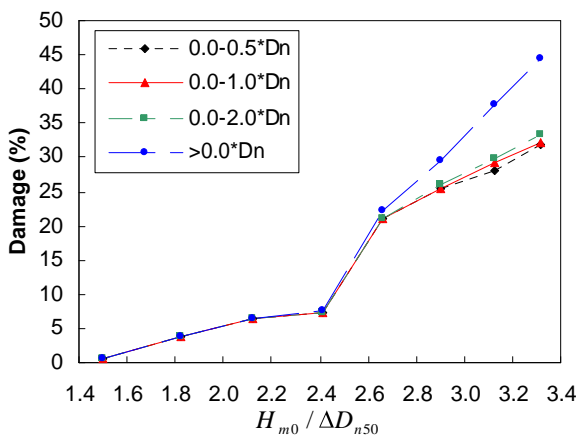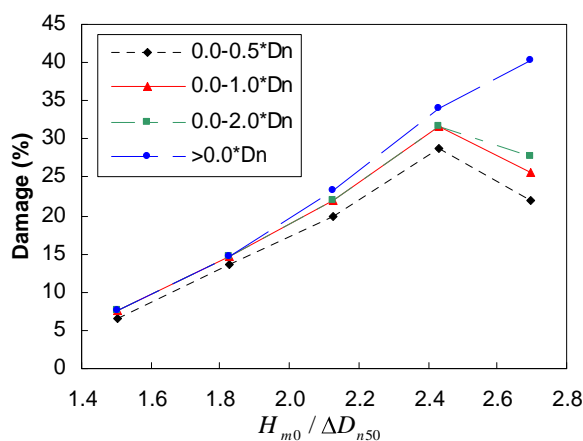

Figure 5.6: Damage for different movements   Figure 5.7: Damage for different reference areas
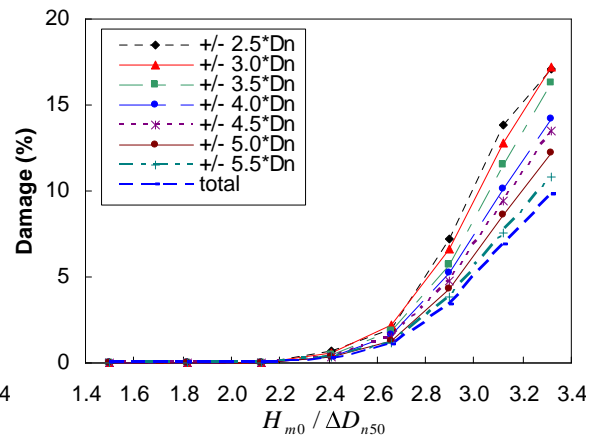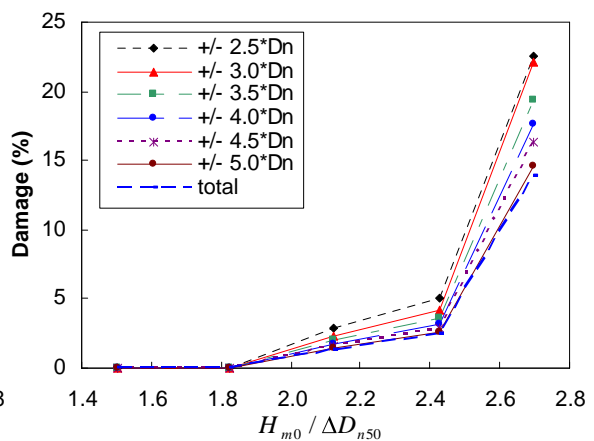
5.4   Experiment 2

The Antifer-blocks are irregular placed row by row. No pattern and no strict positioning is followed, see figure 5.8 and 5.9. The blocks were dropped individually from a few centimetres above the slope. An attempt was made to make the layer as porous as possible. The properties of the layer are presented in table 5.4. The layer thickness is determined from the photo by drawing a line at the average height of the layer, figure 5.10. The test results are presented in table 5.5.

Figure 5.8: Photo of experiment 2
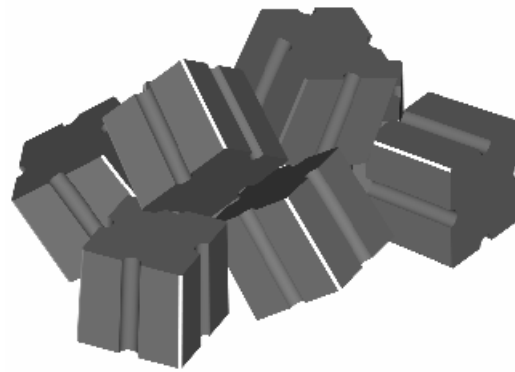
Figure 5.9: 3D drawing of experiment 2

Packing density, ψ_s	57.0 %
Layer thickness, t	8.7cm
Layer thickness coefficient, k_Δ	1.08
Solid density, d	52.7 %
Real porosity, P_r	47.4 %

Table 5.4: Layer properties
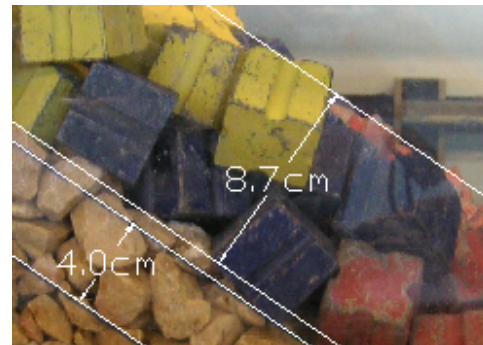
Figure 5.10: Thickness derivation

H_{m0} (cm)	s_p (%)	$s_{m0,1}$ (%)	$s_{m-1,0}$ (%)	C_r (%)	N_s (-)	M_1 (%)	M_2 (%)	M_t (%)	D_1 (%)	D_2 (%)	D_t (%)
9.12	3.10	4.04	3.55	30.4	1.51	6.5	1.1	7.6	0.0	0.0	0.0
11.06	3.03	3.94	3.58	31.7	1.83	13.5	1.1	14.6	0.0	0.0	0.0
12.87	3.02	3.88	3.62	32.5	2.13	20.0	2.0	22.0	0.0	1.4	1.4
14.71	3.04	3.91	3.67	35.0	2.43	28.7	2.8	31.5	0.0	2.5	2.5
16.33	3.06	3.94	3.69	35.9	2.70	22.0	3.7	25.6	2.0	12.7	14.6
17.70	2.86	4.22	3.76	39.2	2.92	-	-	-	-	-	-
19.04	2.91	4.24	3.73	41.9	3.14	-	-	-	-	-	-
20.25	2.84	4.39	3.64	44.9	3.34	-	-	-	-	-	-

Table 5.5: Test results within the reference area SWL ±20cm

During the first wave attack one block rolled down. The next wave-series no displacements were observed. Concluded is that this displacement was not a sign of instability of the whole layer but of an individual badly placed block. Therefore this block was not taken into account for the stability calculation.

The armour layer behaved very tough. There were a lot of movements (settlement of the layer) before the layer was damaged, see figure 5.11. The initial damage started at H_{m0} = 12.87cm in the middle of the layer between minus 10 cm. SWL and SWL. This centre of displaced units spread out to the sides. As a result the blocks from above, from the second layer, rolled down. In this stage great holes appeared in the upper part of the layer (repair is easy). At H_{m0} =16.33cm the layer completely failed. The layer obtained its stability from the downward directed pressure (gravity) and from interlocking. The Hudson stability-value for this irregular method is calculated from the stability parameter where the first real displacements occurred (below 5%), N_s = 2.13, where the damage ratio is 1.4%. From this follows:

$$K_{DH} = \frac{N_s^3}{\cot \alpha} = 6.4$$

The stability value before failure, which makes the irregular method comparable to the regular methods, is calculated with N_s = 2.43, where the damage ratio is 2.5%. From this follows:

$$K_{D<5\%} = \frac{N_s^3}{\cot \alpha} = 9.4$$

For the presentation of the damage development the N_s - and K_D -values were calculated for different damage ratios, see table 5.6. In figure 5.12 the damage ratios for the displaced units, are presented for the different reference areas.

Damage ratio	0%	1%	3%	5%	10%	15%
N_s	1.83	2.04	2.44	2.49	2.60	-
K_D	4.1	5.7	9.7	10.2	11.7	-

Table 5.6: N_s - and K_D -values for different damage ratios (D_t)
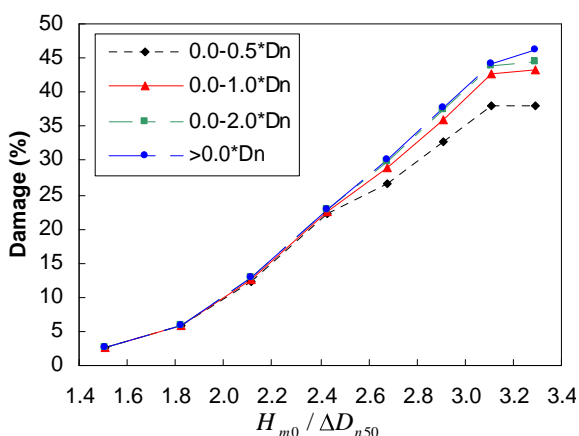

Figure 5.11: Damage for different movements   Figure 5.12: Damage for different reference areas
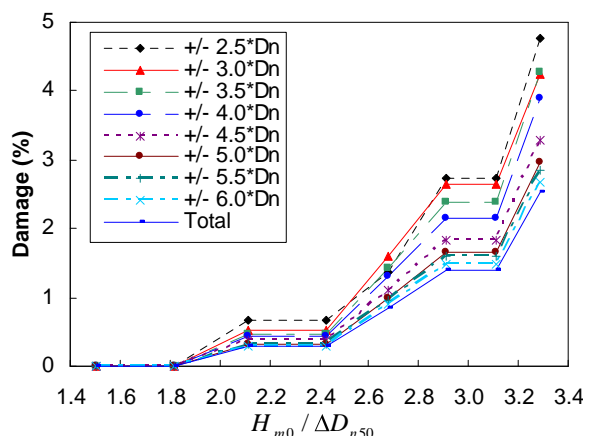
5.5   Experiment 3

For experiment 3 the Antifer-blocks are placed by the square-grid method, see paragraph 2.4.4. They are placed loosely on the slope, row by row. The blocks in the first layer are placed with fixed horizontal distances from one another and in a regular position, with their grooves perpendicular to the slope. An attempt is made to spread the different rows, by placing the blocks with distances in between over the slope. They were placed with a diagonal spreading ratio of 1.34, but they did slide down (as mentioned in paragraph 2.4) and this ratio became 1.18. In the prototype situation this will lead to the use of more blocks than planned. Because of the sliding down of blocks columns where formed and the positioning of the blocks became more irregular. Therefore this method will be referred to as the column method with irregular positioning. The blocks of the second layer are placed in the same grid as the first layer only horizontally moved, such that they are positioned over the gaps between the blocks of the first layer, see figure 5.13 and 5.14. The second layer does not intrude the first layer, but is placed on top of it. Therefore the layer thickness is equal to 2·h. The properties of the layer are presented in table 5.7 and figure 5.15 and the test results in table 5.8.

Figure 5.13: Photo of experiment 3
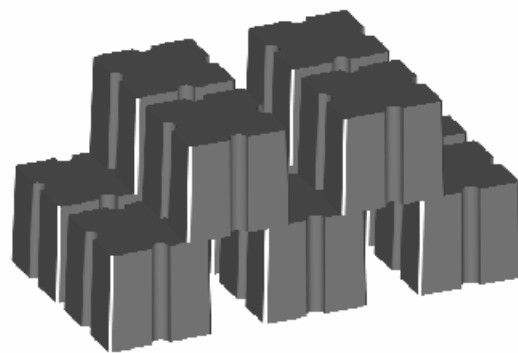
Figure 5.14: 3D drawing of experiment 3

Hor. spreading ratio, X / D_n	1.57
Diag. spreading ratio, Y / D_n	1.18
Packing density, ψ_S	54.2%
Layer thickness, t	8.2cm
Layer thickness coefficient, k_Δ	1.02
Solid density, d	53.1%
Real porosity, P_r	46.9%

Table 5.7: Layer properties
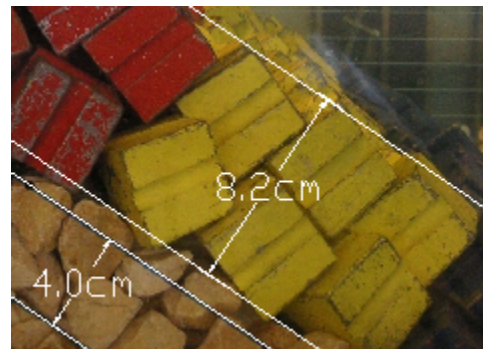
Figure 5.15: Thickness derivation

H_{m0} (cm)	s_p (%)	$s_{m0,1}$ (%)	$s_{m-1,0}$ (%)	C_r (%)	N_s (-)	M_1 (%)	M_2 (%)	M_t (%)	D_1 (%)	D_2 (%)	D_t (%)
9.13	3.10	4.11	3.57	31.3	1.51	2.6	0.0	2.6	0.0	0.0	0.0
11.02	3.09	3.97	3.57	31.2	1.82	5.9	0.0	5.9	0.0	0.0	0.0
12.79	3.01	3.91	3.62	32.0	2.11	12.2	0.3	12.5	0.3	0.0	0.3
14.71	3.12	3.92	3.67	34.4	2.43	22.1	0.3	22.4	0.3	0.0	0.3
16.23	3.05	3.90	3.68	37.5	2.68	26.7	2.3	29.0	0.7	0.3	1.0
17.61	2.90	4.17	3.73	43.6	2.91	32.7	3.3	36.0	1.3	0.3	1.7
18.85	2.88	4.20	3.67	46.7	3.11	38.0	4.6	42.6	1.3	0.3	1.7
19.92	2.67	4.36	3.56	49.5	3.29	38.0	5.3	43.2	1.3	1.7	3.0

Table 5.8: Test results within the reference area SWL ±20cm

The first displacements were observed between minus 10cm SWL and SWL. Because of the attempt to spread the blocks over the slope some blocks in this area were not pressed down well enough by blocks from above (they were on the top of small columns). The column above stayed stable because of the more irregular positioning the blocks rested on the edge of the top of the underlying block of the first layer. The first block was displaced during wave series $H_{m0} =$ 12.79cm. The overtopping started 2 wave series later. In the columns there is a downward directed pressure build up, which results in high forces on the toe. A block is clamped between two other blocks, without side-support. Oblique incoming waves can therefore be of great influence on the stability. During higher wave-series the columns at both sides of the layer completely failed because of the "wall-effect" (they were therefore not counted). This subscribes the possible high influence of oblique incoming waves. One block is pressed out and the rest of the column slides down (if the blocks don't rest on the edge of the top of blocks from the first layer). New blocks for repair can than be added at the top of what is left of the column. The centre of the slope turned out to be very stable. Graphs for the behaviour of the layer are drawn in figure 5.16. The damage ratio for the displaced blocks increased very slowly and for the complete test only 3% displacements occurred. The stability-value for this regular method is calculated from the last stability parameter where no displacements occurred, $N_s = 1.82$. From this follows:

$$K_{D0} = \frac{N_s^3}{\cot \alpha} = 4.0$$

This value alone does not give a good representation of the method, because the slow damage development is not included. For the presentation of the damage development the N_s - and K_D - values were calculated for different damage ratios, see table 5.9. In figure 5.17 the damage ratios for the displaced units, are presented for the different reference areas.

Damage ratio	0%	1%	3%	5%	10%	15%
N_s	1.82	2.68	3.29	-	-	-
K_D	4.0	12.8	23.7	-	-	-

Table 5.9: N_s - and K_D -values for different damage ratios (D_t)

Figure 5.16: Damage for different movements Figure 5.17: Damage for different reference areas

5.6 Experiment 4

For experiment 4 the blocks of the first layer are placed by the regular pyramid pattern. After every 4 rows of the first layer the second layer is placed by dropping the blocks above the holes. This method is therefore called the filled pyramid method, see figure 5.18 and 5.19. The irregular positioned second layer is not integrated with the first layer like the first experiment. The properties of the layer are presented in table 5.10 and figure 5.20. Because of the irregular positioned second layer the average is taken for the layer thickness, which is twice the height of the blocks. The test results are presented in table 5.11.

Figure 5.18: Photo of experiment 4
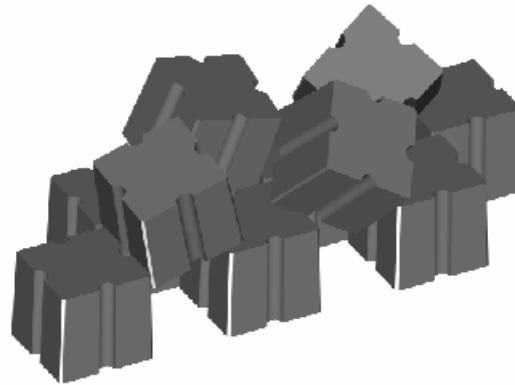
Figure 5.19: 3D drawing of experiment 4

|	
Hor. spreading ratio, X / D_n	1.88
Diag. spreading ratio, Y / D_n	1.08
Packing density, ψ_S	49.1%
Layer thickness, t	8.2cm
Layer thickness coefficient, k_Δ	1.02
Solid density, d	48.1 %
Real porosity, P_r	51.9 %

Table 5.10: Layer properties
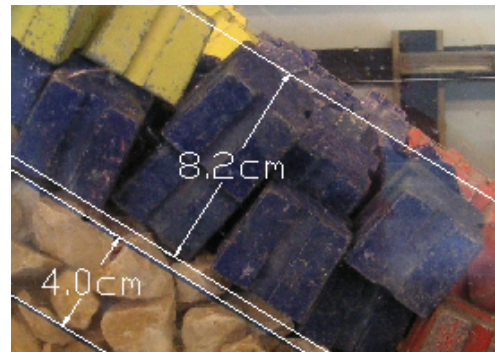
Figure 5.20: Thickness derivation

H_{m0} (cm)	s_p (%)	$s_{m0,1}$ (%)	$s_{m-1,0}$ (%)	C_r (%)	N_s (-)	M_1 (%)	M_2 (%)	M_t (%)	D_1 (%)	D_2 (%)	D_t (%)
9.13	3.03	4.11	3.56	0.313	1.51	8.6	0.0	8.6	0.3	0.0	0.3
11.02	3.09	3.96	3.58	0.321	1.82	23.7	0.3	24.0	1.0	1.0	2.0
12.94	3.04	3.91	3.66	0.329	2.14	31.9	1.0	32.9	0.7	3.3	3.9
14.71	3.11	3.95	3.69	0.350	2.43	30.9	7.2	38.2	0.7	5.9	6.6
16.29	2.99	3.93	3.69	0.362	2.69	28.3	5.9	34.2	1.0	13.5	14.5
17.89	2.88	4.20	3.78	0.411	2.95	-	-	-	-	-	-
19.12	2.92	4.19	3.72	0.436	3.16	-	-	-	-	-	-
20.32	2.72	4.32	3.62	0.456	3.36	-	-	-	-	-	-

Table 5.11: Test results within the reference area SWL ±20cm

Within the first wave series blocks are displaced around SWL. This is because the blocks of the second layer have no integration within their layer such as: downward pressure (like experiment 3) and interlocking (like experiment 2). There is also no integration with the first layer, like the clamping as in experiment 1. Repair however is very easy by placing a new block in the revealed hole. Because the first displacements already occurred at the start of the test, the start of damage was not indicated. Graphs for the behaviour of the layer are drawn in figure 5.21. The stability-value for this semi-regular method is calculated from the first wave series were the first displacement was observed, $N_s = 1.51$. From this follows:

$$K_{DH} = \frac{N_s^3}{\cot \alpha} = 2.3$$

For the presentation of the damage development the N_s- and K_D-values were calculated for different damage ratios, see table 5.12. In figure 5.22 the damage ratios for the displaced units, are presented for the different reference areas.

| Damage ratio	0%	1%	3%	5%	10%	15%
N_s	-	1.64	1.99	2.26	2.54	-
K_D	-	2.9	5.24	7.7	10.9	-

Table 5.12: N_s- and K_D-values for different damage ratios (D_t)
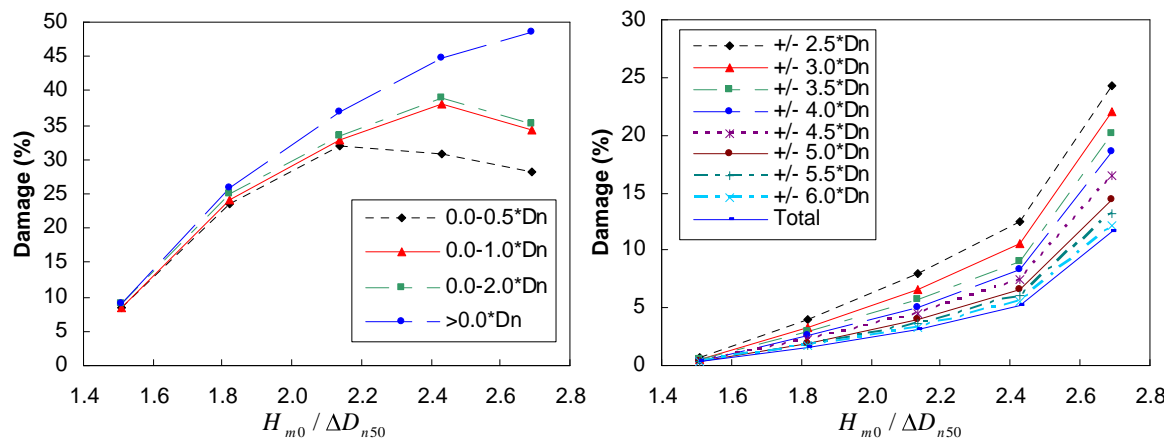
Figure 5.21: Damage for different movements   Figure 5.22: Damage for different reference areas
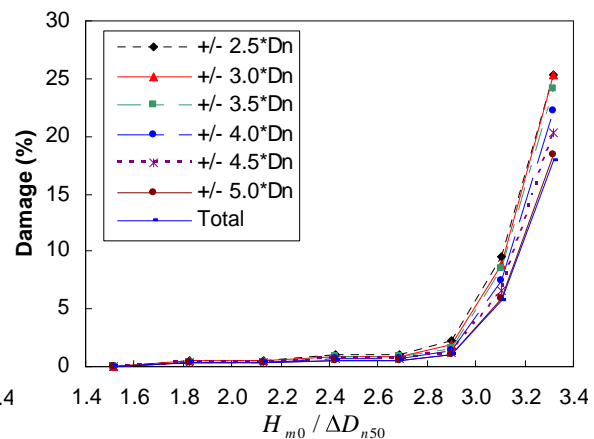
5.7 Experiment 5

The Antifer-blocks are irregular placed per layer. First the complete first layer is placed from the left corner at the bottom up to the upper corner at the right. Hereafter the second layer is placed in the same way, mainly filling up the holes of the first layer. No pattern and strict position is required, see figure 5.23 and 5.24. The blocks were dropped individually from a few centimetres above the slope and an attempt is made to get a porous layer. The properties of the layer are presented in table 5.13. The layer thickness is determined from the photo by drawing a line at the average height of the layer, see figure 5.25. The test results are presented in table 5.14.

Figure 5.23: Photo of experiment 5
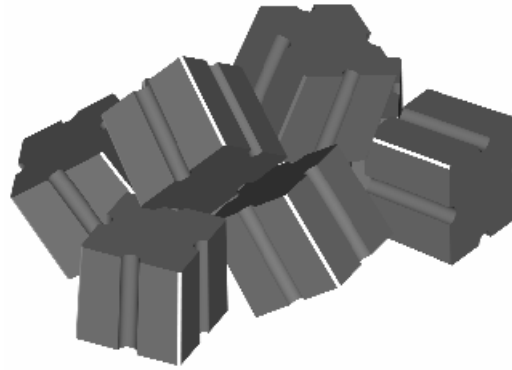
Figure 5.24: 3D drawing of experiment 5

Packing density, ψ_S	61.1%
Layer thickness, t	8.3cm
Layer thickness coefficient, k_Δ	1.03
Solid density, d	59.2%
Real porosity, P_r	40.8%

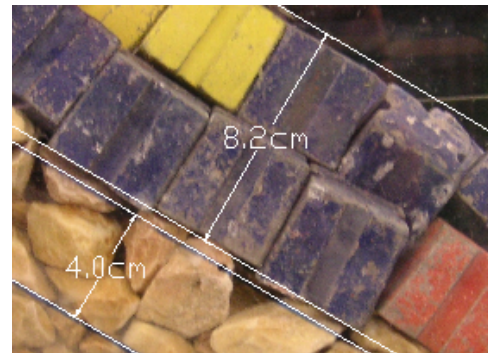Table 5.13: Layer properties
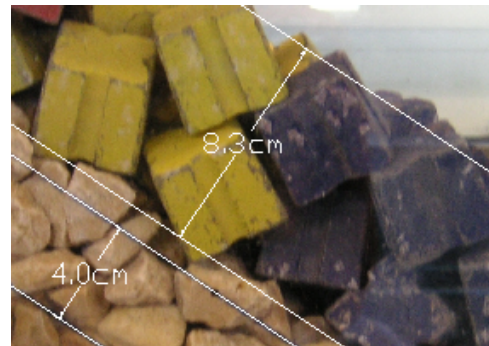
Figure 5.25: Thickness derivation

H_{m0} (cm)	s_p (%)	$s_{m0,1}$ (%)	$s_{m-1,0}$ (%)	C_r (%)	N_s (-)	M_1 (%)	M_2 (%)	M_t (%)	D_1 (%)	D_2 (%)	D_t (%)
9.15	3.03	4.08	3.56	32.7	1.51	1.4	0.0	1.4	0.0	0.0	0.0
11.08	3.04	3.97	3.58	33.0	1.83	10.4	0.6	11.0	0.0	0.3	0.3
12.87	3.02	3.87	3.62	33.8	2.13	22.3	0.6	22.8	0.0	0.3	0.3
14.70	3.11	3.90	3.66	36.4	2.43	35.2	1.1	36.3	0.0	0.6	0.6
16.29	3.06	3.92	3.67	39.7	2.69	40.6	3.4	43.9	0.0	0.6	0.6
17.56	2.83	3.94	3.61	42.9	2.90	35.2	9.3	44.5	0.0	1.1	1.1
18.78	2.81	4.03	3.66	45.7	3.10	23.1	16.6	39.7	0.3	5.6	5.9
20.09	2.70	4.37	3.59	46.7	3.32	16.9	11.8	28.7	0.0	18.3	18.3

Table 5.14: Test results within the reference area SWL ±20cm

During the tests there was a lot of settlement in the middle of the layer which developed to the top. The first displacements occurred during the second wave series around SWL. From here the number of displacements around SWL increased up to the final wave series, when also blocks in the upper part of the layer were displaced. Figure 5.26 shows the behaviour of the layer. Because of the settlement and displacements the part below SWL (around 10cm) became very densely packed and above SWL (around 10cm) very loose. The overtopping started at $H_{m0} = 17.56$cm. The stability-value for this irregular method is calculated from the stability parameter where the first displacements occurred (below 5%). This was for $N_s = 1.83$, where the damage ratio is 0.3%. From this follows:

$$K_{DH} = \frac{N_s^3}{\cot \alpha} = 4.1$$

The stability value before failure, which makes the irregular method comparable to the regular methods, is calculated with $N_s = 2.90$, where the damage ratio is 1.1%. From this follows:

$$K_{DI} = \frac{N_s^3}{\cot \alpha} = 16.3$$

For the presentation of the damage development the N_s- and K_D-values were calculated for different damage ratios, see table 5.15. In figure 5.27 the damage ratios for the displaced units, are presented for the different reference areas.

Damage ratio	0%	1%	3%	5%	10%	15%
N_s	1.51	2.86	2.98	3.06	3.17	3.26
K_D	2.3	15.6	17.6	19.1	21.3	23.1

Table 5.15: N_s- and K_D-values for different damage ratios (D_t)
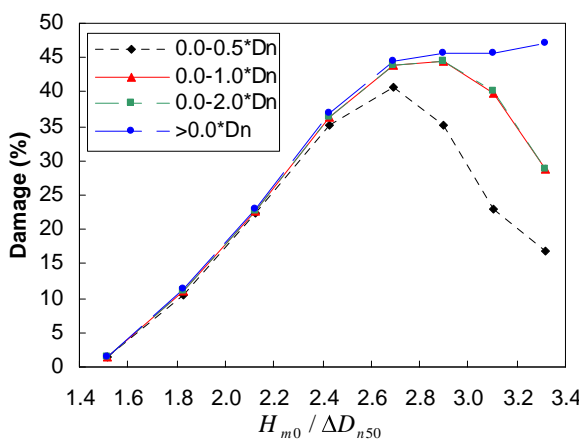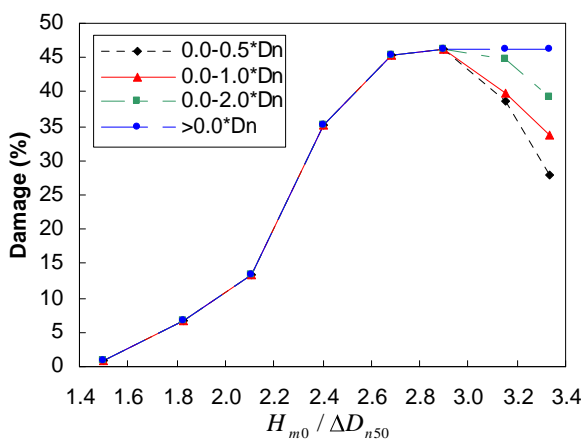
Figure 5.26: Damage for different movements   Figure 5.27: Damage for different reference areas
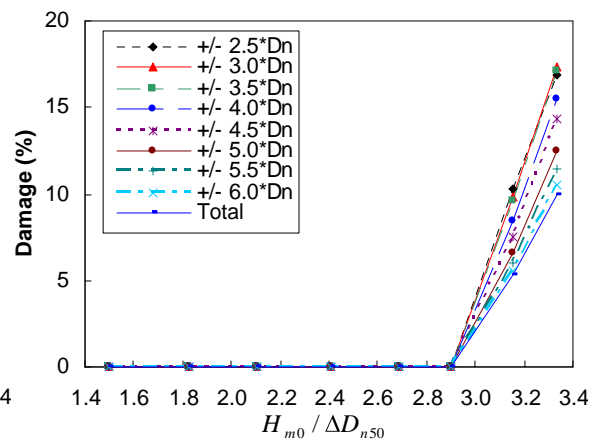
5.8   Experiment 6

From experiment 3 appeared that it was not possible to place the blocks regular with distances between on another over the slope, because the blocks slide down. Therefore the column method was tested with only horizontal spreading to obtain a regular pattern. The blocks were placed row by row and the blocks of the second layer were placed over the gaps of the first layer, see figure 5.28 and 5.29. The layer thickness is equal to two times the block height. The properties of the layer are presented in table 5.16 and figure 5.30 and the test results in table 5.17.
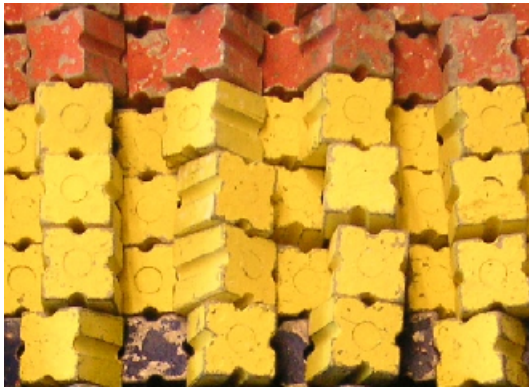
Figure 5.28: Photo of experiment 6
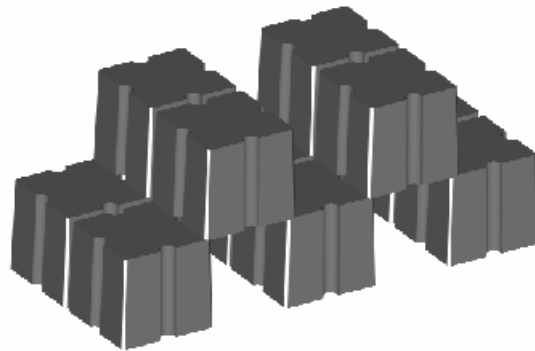
Figure 5.29: 3D drawing of experiment 6

Hor. spreading ratio, X / D_n	1.88
Diag. spreading ratio, Y / D_n	1.08
Packing density, ψ_S	49.1%
Layer thickness, t	8.2cm
Layer thickness coefficient, k_Δ	1.02
Solid density, d	48.1%
Real porosity, P_r	51.9%

Table 5.16: Layer properties

Figure 5.30: Thickness derivation

H_{m0} (cm)	s_p (%)	$s_{m0,1}$ (%)	$s_{m-1,0}$ (%)	C_r (%)	N_s (-)	M_1 (%)	M_2 (%)	M_t (%)	D_1 (%)	D_2 (%)	D_t (%)
9.06	3.00	3.98	3.49	36.0	1.50	0.7	0.0	0.7	0.0	0.0	0.0
11.07	3.10	3.95	3.57	37.3	1.83	6.6	0.0	6.6	0.0	0.0	0.0
12.77	3.00	3.85	3.61	38.5	2.11	13.2	0.0	13.2	0.0	0.0	0.0
14.56	3.08	3.70	3.60	38.7	2.40	35.3	0.0	35.3	0.0	0.0	0.0
16.27	3.05	3.86	3.67	42.8	2.69	45.2	0.0	45.2	0.0	0.0	0.0
17.57	2.83	3.87	3.61	46.0	2.90	46.3	0.0	46.3	0.0	0.0	0.0
19.11	2.79	4.17	3.69	50.4	3.16	38.6	1.1	39.7	5.1	1.5	6.6
20.19	2.71	4.33	3.61	51.7	3.34	27.9	5.9	33.8	5.5	7.0	12.5

Table 5.17: Test results within the reference area SWL ±20cm

The blocks in the columns showed all little movements before the initial damage. During wave series H_{m0}=19.11cm a few blocks around 10cm below SWL were pressed upwards out of the column. This caused a great part of the column to slide down. The blocks of the first layer also moved because of the high pressures on them, especially when the above lying column did slide down. The movements in the first layer gave the opportunity for blocks in the second layer to dislocate. Graphs for the behaviour of the layer are drawn in figure 5.31. The stability is obtained by the high pressures within the columns. These high pressures also cause the failure of the layer (block pressed out of column) and can lead to problems at the toe. During the tests there was a lot of overtopping, which started at H_{m0}= 12.77cm. This is because the columns work as canals which lead the water to the top without any blockage. Another possible disadvantage is the wave direction. Because this is a 2-dimensional wave test, the waves attack the layer perpendicular. Oblique incoming waves can possibly press the blocks easier out of the column, because the blocks are not supported from the side. This experiment, however, turned out to be more stable than experiment 3, which was denser packed. Because of the attempt to spread the blocks over the slope, in experiment 3, the blocks did slide down and displaced earlier than in this experiment. The stability-value for this regular method is calculated from the last stability parameter where no displacements occurred, $N_s = 2.90$. From this follows:

$$K_{D0} = \frac{N_s^3}{\cot \alpha} = 16.3$$

For the presentation of the damage development the N_s - and K_D -values were calculated for different damage ratios, see table 5.18. In figure 5.32 the damage ratios for the displaced units, are presented for the different reference areas.

Damage ratio	0%	1%	3%	5%	10%	15%
N_s	2.90	2.94	3.02	3.10	3.26	-
K_D	16.3	16.9	18.3	19.8	23.2	-

Table 5.18: N_s - and K_D -values for different damage ratios (D_t)

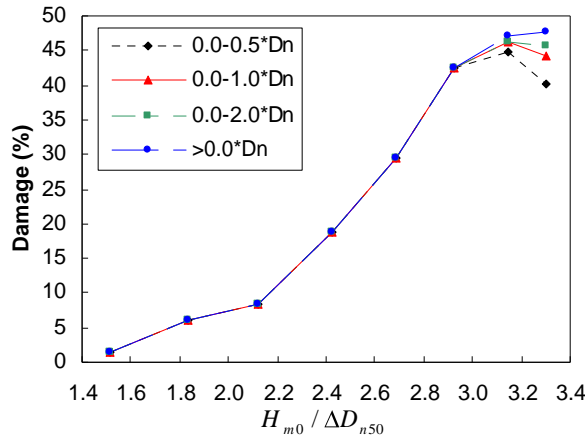
Figure 5.31: Damage for different movements   Figure 5.32: Damage for different reference areas
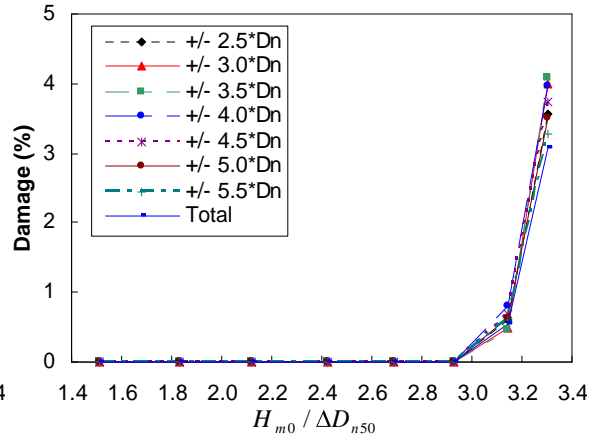
5.9   Experiment 7

For experiment 7 the first layer is placed by the pyramid method. In this experiment also an attempt was made for spreading the rows over the slope. Again the blocks did slide down which made the first layer less regular. The blocks were originally placed with a vertical spreading ratio of 1.17, but after sliding this ratio became 1.09. During the placement it turned out that a smooth under layer is very important for this placement method. This is because the blocks obtain there stability from both sides resting on the blocks of the preceding row. If this is not obtained they turn with there corner between the preceding blocks, which makes the placing of a stable next row impossible. After every four rows of the first layer the blocks of the second layer are placed in a similar way (pyramid method), with equal packing density. Therefore this method is called the double pyramid placing method, see figure 5.33 and 5.34. The second layer was shifted horizontal compared to the first layer, so the blocks of the second layer are placed over the gaps of the first layer. Because of the settlement holes directly to the under layer appeared. For this experiment the second layer turned out to be placed staggered over the slope around a quarter nominal diameter ($\frac{1}{4} \cdot D_n$) compared to the first layer. There are also blocks in the second layer which rest, beside the sides of the underlying two blocks of the second layer, also on the top edge of the underlying block of the first layer. The layer thickness is equal to two times the block height. The properties for the tested layer are presented in table 5.19 and figure 5.35 and the test results in table 5.20.

Figure 5.33: Photo of experiment 7
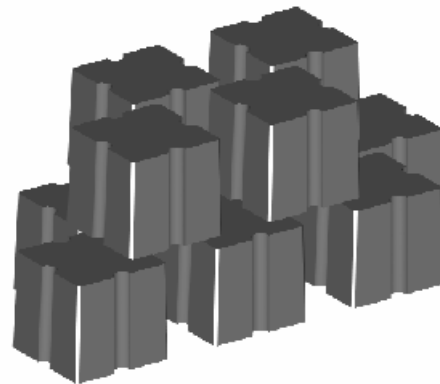
Figure 5.34: 3D drawing of experiment 7

Hor. spreading ratio, X / D_n	1.57
Diag. spreading ratio, Y / D_n	1.09
Packing density, ψ_S	58.5%
Layer thickness, t	8.2cm
Layer thickness coefficient, k_Δ	1.02
Solid density, d	57.3%
Real porosity, P_r	42.7%

Table 5.19: Layer properties
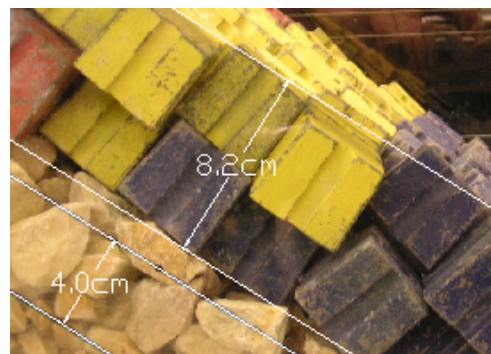
Figure 5.35: Thickness derivation

H_{m0} (cm)	s_p (%)	$s_{m0,1}$ (%)	$s_{m-1,0}$ (%)	C_r (%)	N_s (-)	M_1 (%)	M_2 (%)	M_t (%)	D_1 (%)	D_2 (%)	D_t (%)
9.16	3.04	4.05	3.55	30.7	1.51	1.6	0.0	1.6	0.0	0.0	0.0
11.10	3.04	3.93	3.58	32.3	1.83	6.0	0.0	6.0	0.0	0.0	0.0
12.85	3.02	3.90	3.63	34.5	2.12	8.3	0.0	8.3	0.0	0.0	0.0
14.67	3.04	3.84	3.65	37.2	2.42	18.7	0.0	18.7	0.0	0.0	0.0
16.25	2.98	3.87	3.66	41.3	2.68	29.5	0.0	29.5	0.0	0.0	0.0
17.71	2.86	4.10	3.73	46.7	2.92	42.5	0.0	42.5	0.0	0.0	0.0
19.05	2.78	4.25	3.65	50.2	3.15	44.8	1.6	46.3	0.0	0.6	0.6
20.00	2.68	4.40	3.60	52.3	3.30	40.3	3.8	44.1	1.6	1.9	3.5

Table 5.20: Test results within the reference area SWL ±20cm

During the first six wave series the blocks moved a little and in the upper part some blocks started to turn. These movements were especially observed for blocks which slide down during construction and did not have a stable connection to the underlying blocks of the second layer. When H_{m0} was 9.05cm the first blocks, mainly in the upper part of the slope, were displaced and the blocks around SWL turned. This initial damage can be subscribed to two types of damage mechanisms. The blocks in the upper part of the layer are less stable, because they are less pressurised (clamped) by the above lying blocks. They are easier lifted out the layer by high wave forces. The blocks in the middle obtain higher block pressures, but also higher wave pressures. When they are moved a little, they can loose one of the two side connections to the underlying block and they tend to turn in between the underlying blocks. When this happens the above lying blocks also loose a connection, turn and move down. This cumulative turning and subsequent settling causes instability (displacements). Because the layer becomes instable when blocks are moved to the side and loose their connection with one of the underlying blocks, it is important not to neglect the possible influence of oblique incoming waves. These can move the blocks easier to the side than the waves from the performed perpendicular 2D-tests. Graphs for the behaviour of the layer are drawn in figure 5.36. The reflection and overtopping for this method were low compared to previous tests. For repair of a dislocated unit the blocks of the above rows have to be removed. This is unwanted, because it can mean that almost half the armour layer has to be removed. Therefore the stability-value for this regular method is calculated from the last stability parameter where no displacements occurred, $N_s = 2.92$. From this follows:

$$K_{D0} = \frac{N_s^3}{\cot \alpha} = 16.7$$

For the presentation of the damage development the N_s- and K_D-values were calculated for different damage ratios, see table 5.21. In figure 5.37 the damage ratios for the displaced units, are presented for the different reference areas.

Damage ratio	0%	1%	3%	5%	10%	15%
N_s	2.92	3.17	3.27	-	-	-
K_D	16.7	21.3	23.4	-	-	-

Table 5.21: N_s- and K_D-values for different damage ratios (D_t)
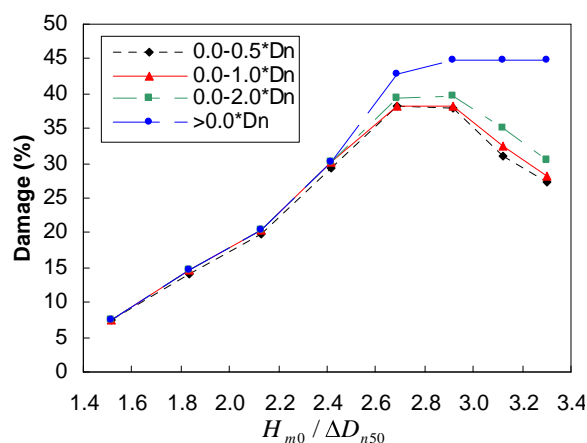
Figure 5.36: Damage for different movements

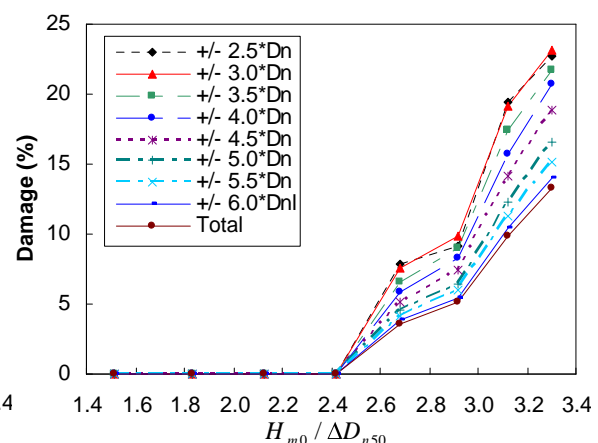Figure 5.37: Damage for different reference areas

5.10   Experiment 8

In experiment 8 the column method, as in experiment 6, is tested only now under an arbitrary chosen angle of 18 degrees, see figure 5.38 and 5.39. The question rose what the influence of oblique waves should be on the column method. Because it is impossible to do a 3-dimensional breakwater test in a wave flume the columns were placed under an angle. In this way the contact surface between the blocks is less, and bending of the columns is easier. The layer thickness is equal to two times the block height. The properties of the layer are presented in table 5.22 and figure 5.40 and the test results in table 5.23.
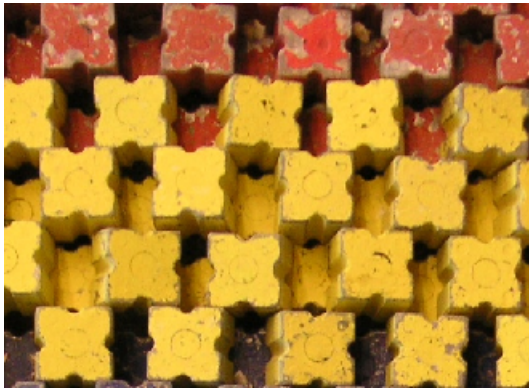

Figure 5.38: Photo of experiment 8
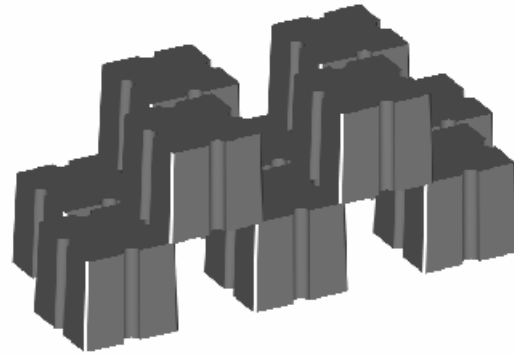
Figure 5.39: 3D drawing of experiment 8

Hor. spreading ratio, X / D_n	1.88
Diag. spreading ratio, Y / D_n	1.06
Packing density, ψ_S	50.0%
Layer thickness, t	8.2cm
Layer thickness coefficient, k_Δ	1.02
Solid density, d	49.0%
Real porosity, P_r	51.0%

Table 5.22: Layer properties
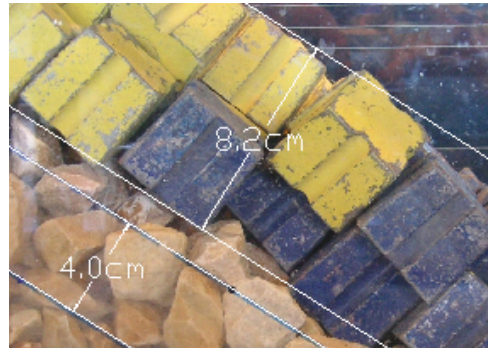
Figure 5.40: Thickness calculation

H_{m0} (cm)	s_p (%)	$s_{m0,1}$ (%)	$s_{m-1,0}$ (%)	C_r (%)	N_s (-)	M_1 (%)	M_2 (%)	M_t (%)	D_1 (%)	D_2 (%)	D_t (%)
9.19	3.12	4.16	3.60	35.7	1.52	7.5	0.0	7.5	0.0	0.0	0.0
11.11	3.04	3.94	3.59	36.2	1.83	14.0	0.6	14.6	0.0	0.0	0.0
12.90	3.10	3.84	3.64	37.1	2.13	19.8	0.6	20.5	0.0	0.0	0.0
14.63	3.10	3.86	3.67	39.2	2.42	29.2	1.0	30.2	0.0	0.0	0.0
16.25	3.04	3.89	3.66	41.2	2.68	38.3	0.0	38.3	1.0	3.6	4.5
17.68	2.91	4.14	3.73	46.0	2.92	38.0	0.3	38.3	1.3	5.2	6.5
18.90	2.76	4.17	3.66	47.5	3.12	31.2	1.3	32.5	2.6	9.7	12.3
19.97	2.62	4.33	3.56	49.9	3.30	27.3	1.0	28.2	2.3	14.3	16.6

Table 5.23: Test results within the reference area SWL ±20cm

The layer behaved quite similar as the layer from experiment 6. Most blocks moved a little before a couple of blocks, positioned between minus 10 cm SWL and SWL, were pressed out the column during wave series H_{m0}=16.25cm. In this experiment they were pressed out to the side, instead of upwards (experiment 6), which resulted in the bending of the column. These displacements caused a great part of the above lying column to slide down. Graphs for the behaviour of the layer are drawn in figure 5.41. During the sliding down of the column more blocks were completely displaced from the layer, which lead to open gutters in the first layer. Because of this also the blocks of the first layer showed great movements downwards, which made other columns fail. The initial damage occurred two wave series earlier than in experiment 6. However the column angle was arbitrary chosen and it was only a rough estimation of oblique wave attack, it can be concluded that oblique wave attack has a negative influence on the stability. The reflection coefficient and overtopping were similar to experiment 6 very high. Because of the angle of the columns the overtopping was mostly directed to the right. The stability-value for this regular method is calculated from the last stability parameter where no displacements occurred, N_s = 2.42. From this follows:

$$K_{D0} = \frac{N_s^3}{\cot \alpha} = 9.4$$

For the presentation of the damage development the N_s- and K_D-values were calculated for different damage ratios, see table 5.24. In figure 5.42 the damage ratios for the displaced units, are presented for the different reference areas.

| Damage ratio	0%	1%	3%	5%	10%	15%
N_s	2.42	2.48	2.59	2.74	3.04	3.23
K_D	9.4	10.1	11.6	13.7	18.7	22.5

Table 5.24: N_s- and K_D-values for different damage ratios (D_t)

Figure 5.41: Damage for different movements Figure 5.42: Damage for different reference areas
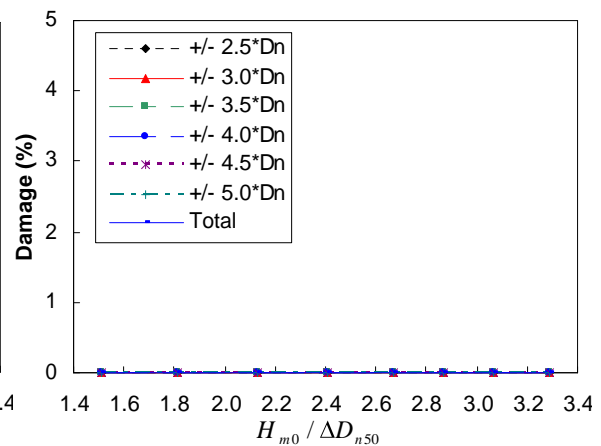
5.11 Experiment 9

From experiment 3 and 7 it can be concluded that diagonal spreading (over the slope) leads to sliding down and irregularity of the first layer. Therefore the placing method of experiment 7 is repeated with the same packing density only obtained by horizontal spreading, see figure 5.43 and 5.44. Both layers were placed directly on each other, so the staggering is minimal and gaps to the under layer are very small. The layer thickness is equal to two times the block height. The properties of the layer are presented in table 5.25 and figure 5.45 and the test results in table 5.26.
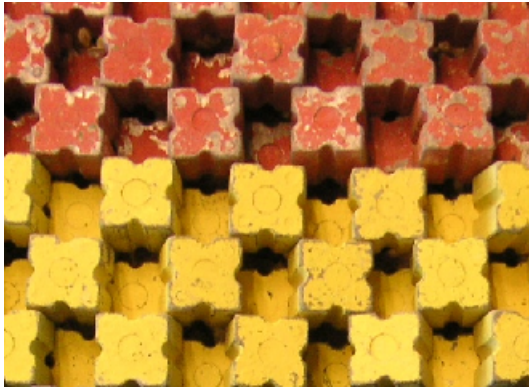

Figure 5.43: Photo of experiment 9
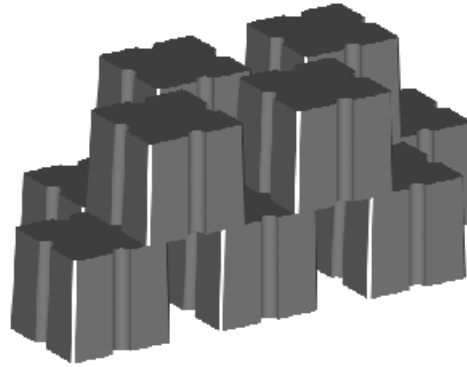
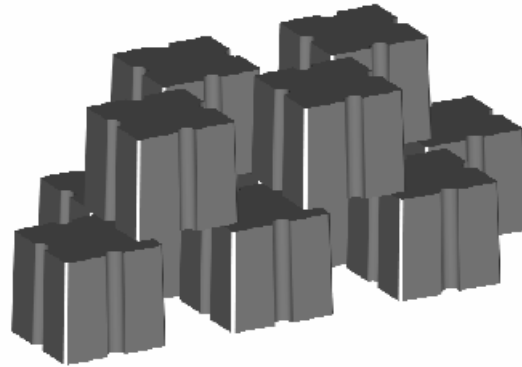Figure 5.44: 3D drawing of experiment 9

|	
Hor. spreading ratio, X/D_n	1.57
Diag. spreading ratio, Y/D_n	1.09
Packing density, ψ_S	58.5%
Layer thickness, t	8.2cm
Layer thickness coefficient, k_Δ	1.02
Solid density, d	57.3%
Real porosity, P_r	42.7%

Table 5.25: Layer properties
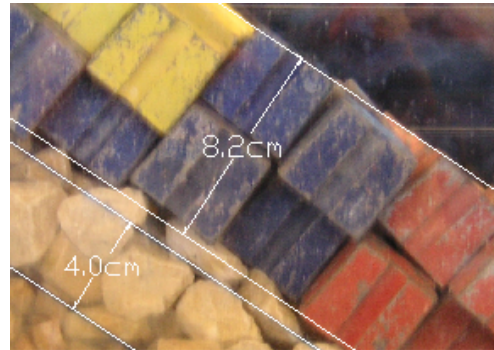
Figure 5.45: Thickness derivation

H_{m0} (cm)	s_p (%)	$s_{m0,1}$ (%)	$s_{m-1,0}$ (%)	C_r (%)	N_s (-)	M_1 (%)	M_2 (%)	M_t (%)	D_1 (%)	D_2 (%)	D_t (%)
9.15	3.11	4.09	3.56	32.8	1.51	0.3	0.0	0.3	0.0	0.0	0.0
11.00	3.09	3.91	3.56	33.6	1.82	0.3	0.0	0.3	0.0	0.0	0.0
12.91	3.03	3.89	3.65	35.6	2.13	1.5	0.0	1.5	0.0	0.0	0.0
14.60	3.09	3.83	3.64	38.0	2.41	2.5	0.0	2.5	0.0	0.0	0.0
16.15	2.89	3.82	3.60	41.4	2.67	15.6	0.0	15.6	0.0	0.0	0.0
17.39	2.86	3.91	3.56	45.9	2.87	23.3	0.0	23.3	0.0	0.0	0.0
18.59	2.85	3.96	3.60	49.7	3.07	27.9	0.3	28.2	0.0	0.0	0.0
19.92	2.67	4.41	3.58	53.1	3.29	39.0	0.3	39.3	0.0	0.0	0.0

Table 5.26: Test results within the reference area SWL ±20cm

The layer turned out to be extremely stable. Even for the highest wave series no displacements were observed. Only in the upper part of the layer and just beneath SWL a couple of blocks started to turn. This is due to the damage mechanisms as described for experiment 7. Graphs for the behaviour of the layer are drawn in figure 5.46. Since this experiment was more stable than experiment 7, with the same packing density, no more attempts will be made for spreading the blocks over the slope for this method. It can be concluded that the attempt for vertical spreading will not enlarge the stability (in contrary) for this placing method. The stability-value for this regular placing method is calculated from the last measured stability parameter, $N_s = 3.29$. The real stability-coefficient with zero damage can even turn out higher. From this follows:

$$K_{D0} = \frac{N_s^3}{\cot \alpha} = 23.7$$

For the presentation of the damage development the N_s- and K_D-values were calculated for different damage ratios, see table 5.27. In figure 5.47 the damage ratios for the displaced units, are presented for the different reference areas.

Damage ratio	0%	1%	3%	5%	10%	15%
N_s	3.29	-	-	-	-	-
K_D	23.7	-	-	-	-	-

Table 5.27: N_s- and K_D-values for different damage ratios (D_t)
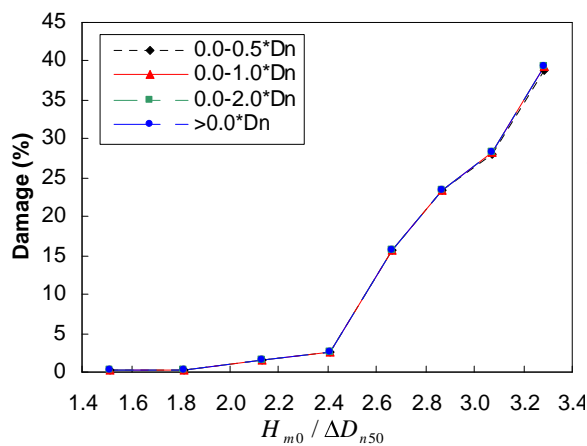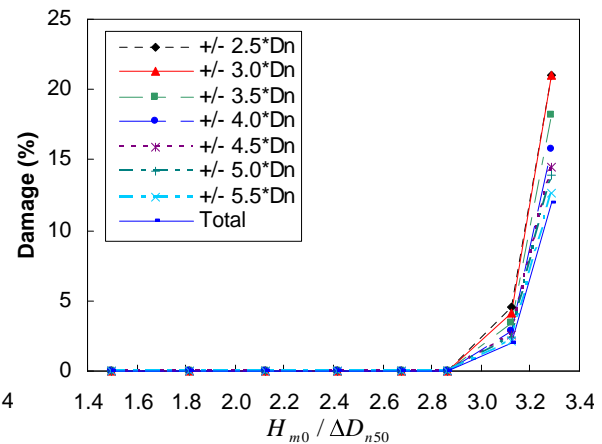

Figure 5.46: Damage for different movements   Figure 5.47: Damage for different reference areas

5.12   Experiment 10

Because no damage occurred for experiment 9 the double pyramid method was again applied for this experiment, only with a lower packing density. In the lower part of the slope the blocks of the second layer were stabilized by the two underlying blocks of the second layer and by the top edge of the underlying block of the first layer. The placement of the second layer on the first layer turned out a little staggered, in the order of ? -¼·D_n, see figure 5.48 and 5.49. The layer thickness is equal to two times the block height. The properties for the tested layer are presented in table 5.28 and figure 5.50 and the test results in table 5.29.
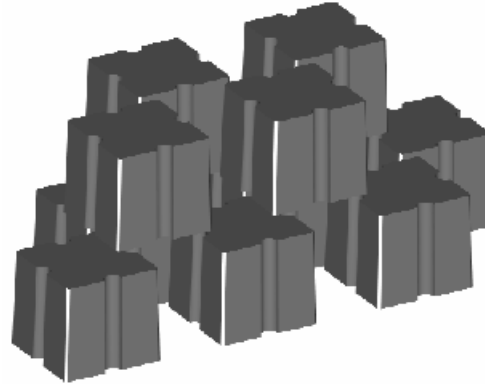

Figure 5.48: Photo of experiment 10

Figure 5.49: 3D drawing of experiment 10

|	
Hor. spreading ratio, X / D_n	1.71
Diag. spreading ratio, Y / D_n	1.10
Packing density, ψ_S	53.2%
Layer thickness, t	8.2cm
Layer thickness coefficient, k_Δ	1.02
Solid density, d	52.1%
Real porosity, P_r	47.9%

Table 5.28: Layer properties
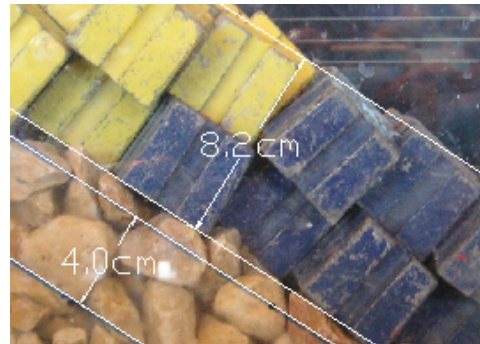
Figure 5.50: Thickness derivation

H_{m0} (cm)	s_p (%)	$s_{m0,1}$ (%)	$s_{m-1,0}$ (%)	C_r (%)	N_s (-)	M_1 (%)	M_2 (%)	M_t (%)	D_1 (%)	D_2 (%)	D_t (%)
9.08	3.02	4.05	3.53	31.2	1.50	0.0	0.0	0.0	0.0	0.0	0.0
11.00	3.02	3.98	3.57	32.3	1.82	0.3	0.0	0.3	0.0	0.0	0.0
12.84	3.02	3.89	3.61	34.0	2.12	0.7	0.0	0.7	0.0	0.0	0.0
14.65	3.04	3.93	3.68	36.9	2.42	3.1	0.0	3.1	0.0	0.0	0.0
16.21	2.97	3.89	3.65	40.1	2.68	7.5	0.0	7.5	0.0	0.0	0.0
17.35	2.85	3.91	3.58	44.3	2.86	30.8	0.0	30.8	0.0	0.0	0.0
18.91	2.90	4.23	3.67	49.2	3.12	45.1	3.1	48.1	2.4	0.0	2.4
19.92	2.67	4.36	3.57	50.6	3.29	30.2	7.8	38.0	6.8	7.1	13.9

Table 5.29: Test results within the reference area SWL ±20cm

During the first 5 wave series very little movements were observed. Hereafter the stones between minus 10cm SWL and SWL started to turn, which leaded to the first displacements (blocks turning and sliding down) during wave series $H_{m0} = 18.91$cm. It was also observed that blocks of the second layer intruded between the blocks of the first layer, which moved sideways and therefore made the neighbouring blocks from the second layer, resting on them, move. The overtopping started during wave series $H_{m0} = 16.21$cm. Graphs for the behaviour of the layer are drawn in figure 5.51. The stability-value for this regular method is calculated from the last stability parameter where no displacements occurred, $N_s = 2.86$. From this follows:

$$K_{D0} = \frac{N_s^3}{\cot \alpha} = 15.7$$

For the presentation of the damage development the N_s- and K_D-values were calculated for different damage ratios, see table 5.30. In figure 5.52 the damage ratios for the displaced units, are presented for the different reference areas.

Damage ratio	0%	1%	3%	5%	10%	15%
N_s	2.86	2.97	3.13	3.16	3.23	-
K_D	15.7	17.4	20.4	21.0	22.5	-

Table 5.30: N_s- and K_D-values for different damage ratios (D_t)
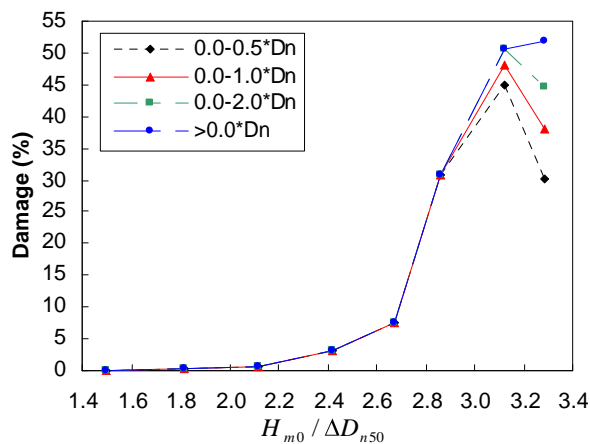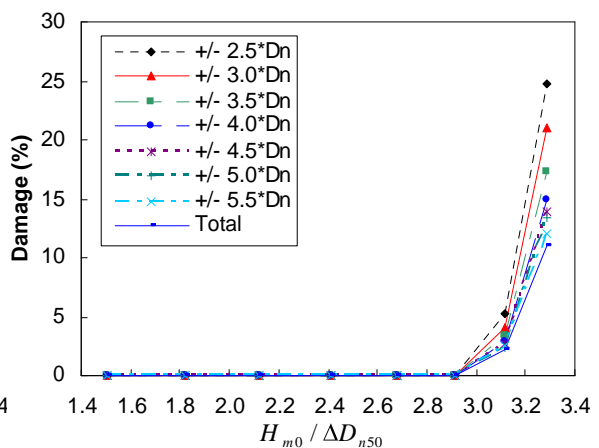

Figure 5.51: Damage for different movements   Figure 5.52: Damage for different reference areas

5.13 Experiment 11

Experiment 11 is built with the same placing method (double pyramid) and almost the same packing density as experiment 10. The only difference is that for this experiment the second layer is placed around ½ · D_n staggered on the first layer, see figure 5.53 and 5.54. The properties of the layer are presented in table 5.31 and figure 5.55 and the test results in table 5.32.
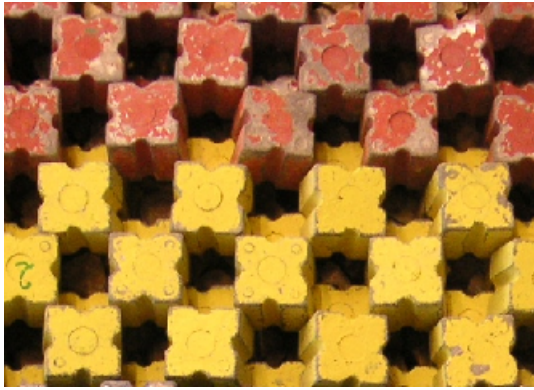
Figure 5.53: Photo of experiment 11

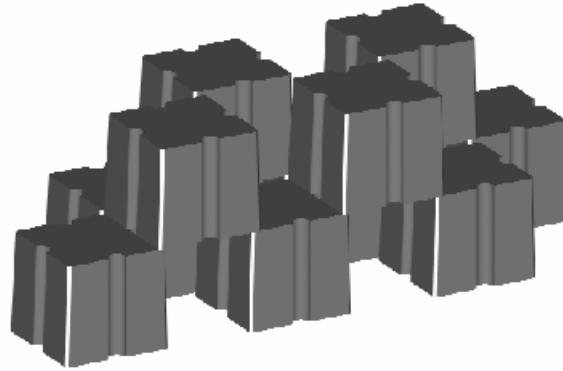
Figure 5.54: 3D drawing of experiment 11

|	
Hor. spreading ratio, X / D_n	1.71
Diag. spreading ratio, Y / D_n	1.08
Packing density, ψ_S	54.3%
Layer thickness, t	8.2cm
Layer thickness coefficient, k_Δ	1.02
Solid density, d	53.2%
Real porosity, P_r	46.8%

Table 5.31: Layer properties
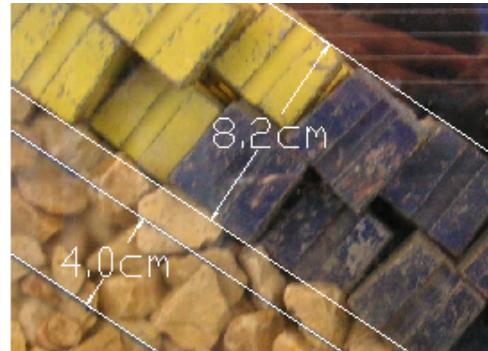
Figure 5.55: Thickness derivation

H_{m0} (cm)	s_p (%)	$s_{m0,1}$ (%)	$s_{m-1,0}$ (%)	C_r (%)	N_s (-)	M_1 (%)	M_2 (%)	M_t (%)	D_1 (%)	D_2 (%)	D_t (%)
9.12	3.09	4.07	3.55	28.6	1.51	0.4	0.0	0.4	0.0	0.0	0.0
11.01	3.09	3.97	3.57	29.7	1.82	1.1	0.0	1.1	0.0	0.0	0.0
12.83	3.01	3.91	3.61	31.5	2.12	1.4	0.0	1.4	0.0	0.0	0.0
14.61	3.09	3.87	3.65	33.5	2.41	4.6	0.0	4.6	0.0	0.0	0.0
16.22	2.97	3.92	3.64	37.8	2.68	8.1	0.0	8.1	0.0	0.0	0.0
17.62	2.84	4.13	3.71	43.6	2.91	9.5	0.0	9.5	0.0	0.0	0.0
18.89	2.76	4.25	3.65	47.4	3.12	28.8	13.7	42.5	2.5	0.0	2.5
19.92	2.67	4.43	3.57	50.2	3.29	14.7	23.5	38.2	8.4	4.9	13.3

Table 5.32: Test results within the reference area SWL ±20cm

Small turnings and movements were observed between minus 10cm SWL and SWL. During wave series H_{m0} = 18.89cm the first displacements occurred. Also during that wave series the blocks of the upper part of the second layer did slide down less than half a nominal diameter, where they stabilized on the top edges of the first layer (as described for the lower part of the slope of experiment 10). This is a disadvantage of the here used stagger. There is no integration between the first and second layer and therefore there is much pressure on the toe, which has to be very strong.

During the run-up of the waves a lot more and bigger bubbles were observed than for previous experiments. The reflection and overtopping were also both low compared to the other experiments. From this can be concluded that the energy dissipation of this layer is relatively high. Graphs for the behaviour of the layer are drawn in figure 5.56. The stability-value for this regular method is calculated from the last stability parameter where no displacements occurred, N_s = 2.91. From this follows:

$$K_{D0} = \frac{N_s^3}{\cot \alpha} = 16.4$$

For the presentation of the damage development the N_s- and K_D-values were calculated for different damage ratios, see table 5.33. In figure 5.57 the damage ratios for the displaced units, are presented for the different reference areas.

Damage ratio	0%	1%	3%	5%	10%	15%
N_s	2.91	2.99	3.13	3.16	3.24	-
K_D	16.4	17.9	20.4	21.0	22.6	-

Table 5.33: N_s- and K_D-values for different damage ratios (D_t)
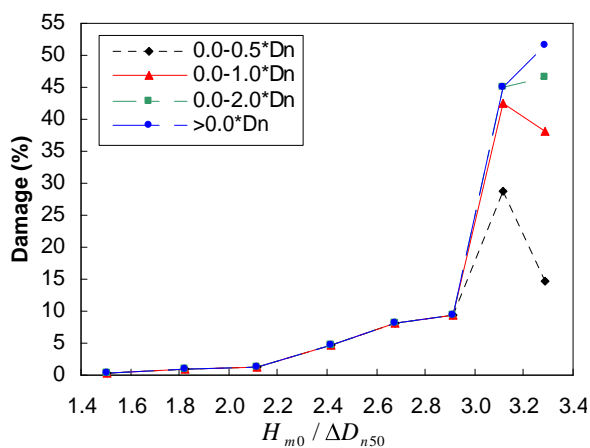
Figure 5.56: Damage for different movements   Figure 5.57: Damage for different reference areas
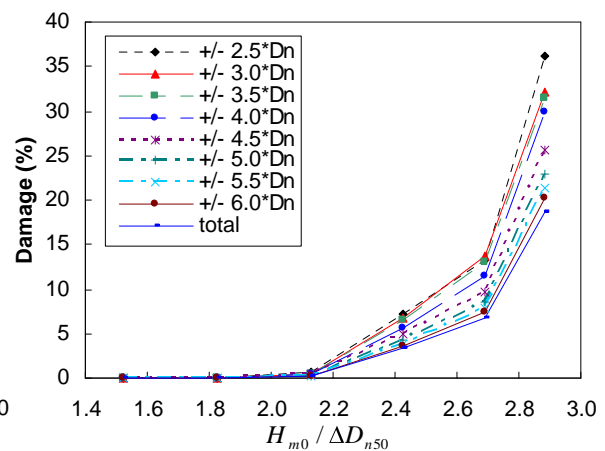
5.14 Experiment 12

For experiment 12 the same placement method (double pyramid, minimal staggered) as in experiment 9 and 10 is applied, see figure 5.58 and 5.59. The packing density is again decreased to obtain its influence on the stability. The properties of the layer are presented in table 5.34 and figure 5.60 and the test results in table 5.35.
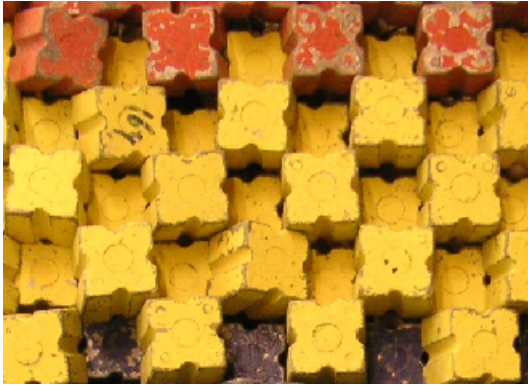
Figure 5.58: Photo of experiment 12

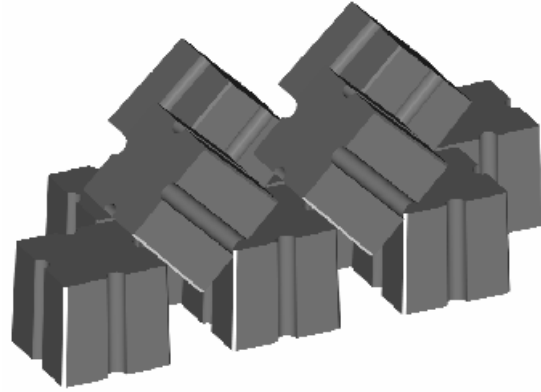Figure 5.59: 3D drawing of experiment 12

|	
Hor. spreading ratio, X / D_n	1.88
Diag. spreading ratio, Y / D_n	1.08
Packing density, ψ_S	49.1%
Layer thickness, t	8.2cm
Layer thickness coefficient, k_Δ	1.02
Solid density, d	48.1%
Real porosity, P_r	51.9%

Table 5.34: Layer properties
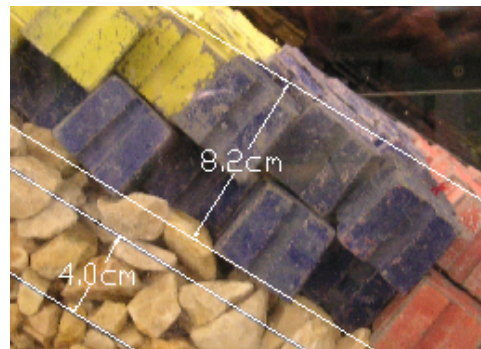
Figure 5.60: Thickness derivation

H_{m0} (cm)	s_p (%)	$s_{m0,1}$ (%)	$s_{m-1,0}$ (%)	C_r (%)	N_s (-)	M_1 (%)	M_2 (%)	M_t (%)	D_1 (%)	D_2 (%)	D_t (%)
9.21	3.13	4.20	3.62	30.6	1.52	8.2	0.0	8.2	0.0	0.0	0.0
11.05	3.17	3.99	3.60	32.2	1.82	16.4	0.0	16.4	0.0	0.0	0.0
12.91	3.03	3.91	3.64	34.5	2.13	25.0	0.0	25.0	0.0	0.3	0.3
14.69	3.04	3.86	3.66	35.9	2.43	36.2	1.6	37.8	2.0	2.3	4.3
16.29	2.92	3.92	3.67	38.5	2.69	31.3	5.6	36.8	3.0	5.6	8.6
17.47	2.88	3.93	3.60	39.3	2.88	13.2	9.5	22.7	0.3	22.7	23.0
18.95	2.76	4.25	3.70	42.7	3.13	-	-	-	-	-	-
19.98	2.68	4.38	3.59	45.0	3.30	-	-	-	-	-	-

Table 5.35: Test results within the reference area SWL ±20cm

During the third wave series the first block was displaced 10cm under SWL and around SWL some blocks started to turn. The following wave series more blocks were displaced and the damage area expanded upwards the slope. Because of the lower packing density the connecting surface between the blocks and therefore the stability of the layer was less compared to experiment 9 and 10. Graphs for the behaviour of the layer are drawn in figure 5.61. The stability-value for this regular method is calculated from the last stability parameter where no displacements occurred, $N_s = 1.82$. From this follows:

$$K_{D0} = \frac{N_s^3}{\cot \alpha} = 4.0$$

For the presentation of the damage development the N_s- and K_D-values were calculated for different damage ratios, see table 5.36. In figure 5.62 the damage ratios for the displaced units, are presented for the different reference areas.

Damage ratio	0%	1%	3%	5%	10%	15%
N_s	1.82	2.18	2.33	2.47	2.71	2.77
K_D	4.0	6.9	8.5	10.1	13.2	14.2

Table 5.36: N_s- and K_D-values for different damage ratios (D_t)
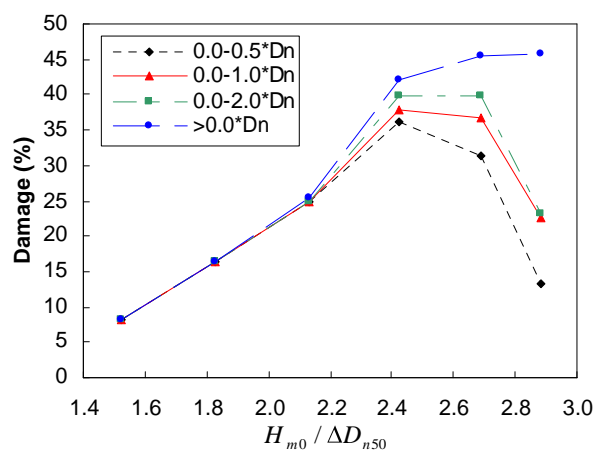
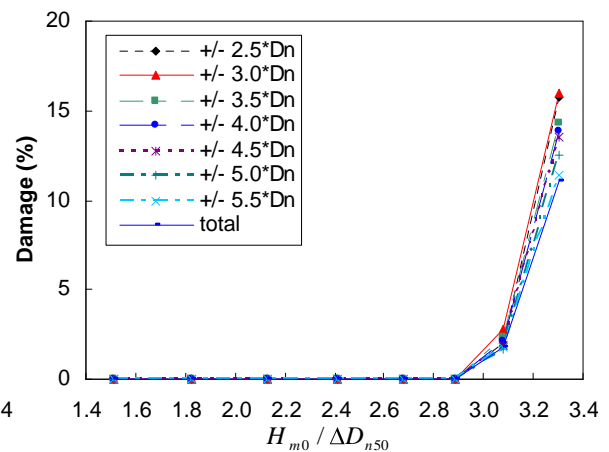Figure 5.61: Damage for different movements   Figure 5.62: Damage for different reference areas

5.15 Experiment 13

In experiment 13 the closed pyramid method is tested with a higher packing density than for experiment 1, see figure 5.63 and 5.64. In this way the stability versus the packing density can be evaluated for this method. It makes this experiment also comparable to experiment 10 and 11 (because of the same packing density). The properties of the layer are presented in table 5.37 and figure 5.65 (measurements in cm) and the test results in table 5.38.
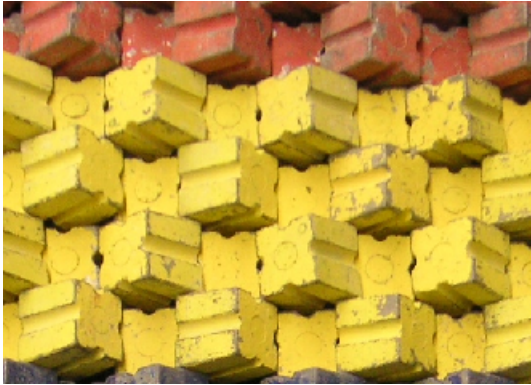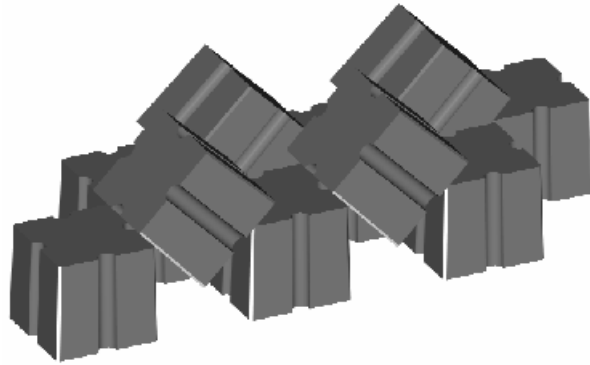

Figure 5.63: Photo of experiment 13

Figure 5.64: 3D drawing of experiment 13

Hor. spreading ratio, X / D_n	1.71
Diag. spreading ratio, Y / D_n	1.08
Packing density, ψ_S	54.3%
Layer thickness, t	8.7cm
Layer thickness coefficient, k_Δ	1.08
Solid density, d	50.2%
Real porosity, P_r	49.8%

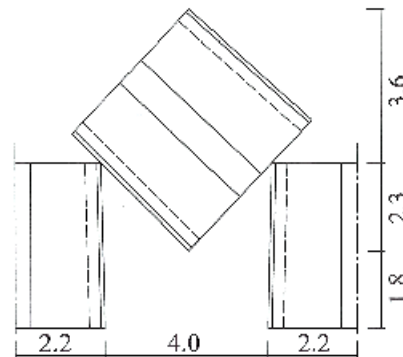Table 5.37: Layer properties
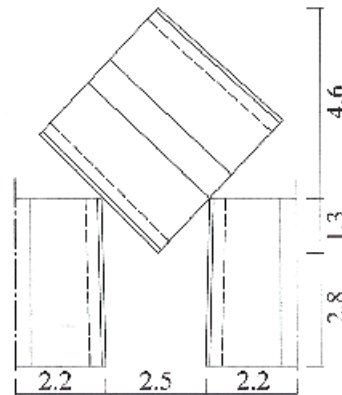
Figure 5.65: Thickness derivation

H_{m0} (cm)	s_p (%)	$s_{m0,1}$ (%)	$s_{m-1,0}$ (%)	C_r (%)	N_s (-)	M_1 (%)	M_2 (%)	M_t (%)	D_1 (%)	D_2 (%)	D_t (%)
9.17	3.11	4.13	3.57	34.7	1.51	0.0	0.0	0.0	0.0	0.0	0.0
11.04	3.16	3.97	3.58	35.8	1.82	0.0	0.0	0.0	0.0	0.0	0.0
12.90	3.03	3.88	3.64	37.6	2.13	1.0	0.0	1.0	0.0	0.0	0.0
14.58	3.08	3.73	3.60	38.5	2.41	3.6	0.0	3.6	0.0	0.0	0.0
16.22	2.91	3.84	3.65	43.4	2.68	13.2	0.0	13.2	0.0	0.0	0.0
17.45	2.81	3.90	3.61	47.5	2.88	25.0	0.0	25.0	0.0	0.0	0.0
18.66	2.86	3.95	3.49	51.2	3.08	36.5	0.0	36.5	0.0	1.6	1.6
20.00	2.68	4.38	3.57	52.5	3.30	31.9	0.7	32.6	0.7	11.8	12.5

Table 5.38: Test results within the reference area SWL ±20cm

On several places in the layer blocks moved. During $H_{m0} = 18.66$cm the first displacements occurred between minus 10cm SWL and SWL. The damage expanded straight upwards and spread out a little. Graphs for the behaviour of the layer are drawn in figure 5.66. The layer derives its stability from clamping of the blocks of the second layer by the first layer. Also the extending bottoms of the blocks from the second layer clamp to one another and form columns. The stability-value for this regular method is calculated from the last stability parameter where no displacements occurred, $N_s = 2.88$. From this follows:

$$K_{D0} = \frac{N_s^3}{\cot \alpha} = 16.0$$

For the presentation of the damage development the N_s - and K_D -values were calculated for different damage ratios, see table 5.39. In figure 5.67 the damage ratios for the displaced units, are presented for the different reference areas.

Damage ratio	0%	1%	3%	5%	10%	15%
N_s	2.88	3.01	3.11	3.15	3.25	-
K_D	16.0	18.1	20.0	20.8	22.9	-

Table 5.39: N_s - and K_D -values for different damage ratios (D_t)
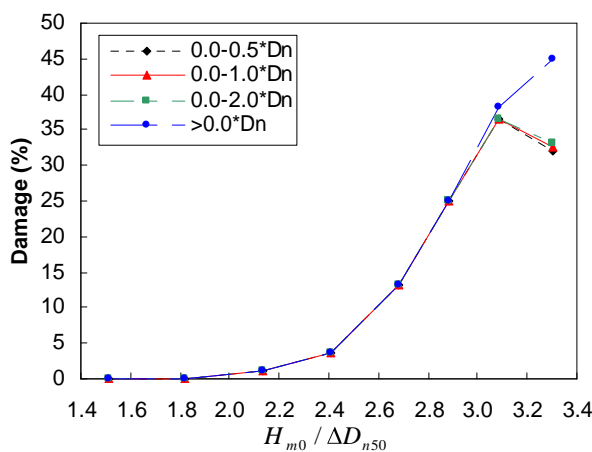
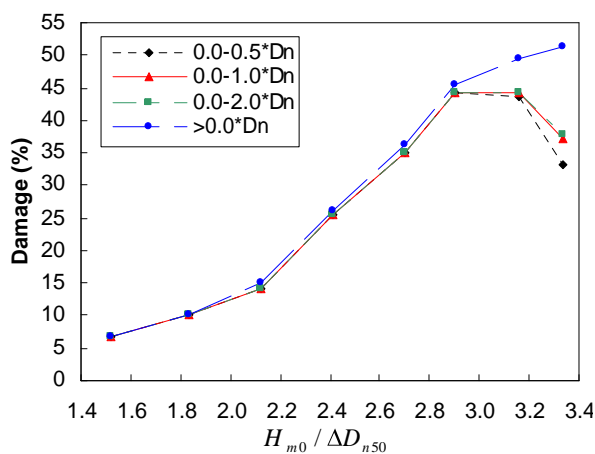
Figure 5.66: Damage for different movements   Figure 5.67: Damage for different reference areas

5.16 Experiment 14

For experiment 14 again the closed pyramid method is tested, however, now with a lower packing density than experiment 1 and 13, see figure 5.68 and 5.69. The packing density for this experiment is so low that it is almost a single layer. The properties of the layer are presented in table 5.40 and figure 5.70 (measurements in cm) and the test results in table 5.41.

Figure 5.68: Photo of experiment 14

Figure 5.69: 3D drawing of experiment 14

|	
Hor. spreading ratio, X / D_n	2.09
Diag. spreading ratio, Y / D_n	1.07
Packing density, ψ_S	44.8%
Layer thickness, t	7.7cm
Layer thickness coefficient, k_Δ	0.96
Solid density, d	46.8%
Real porosity, P_r	53.3%

Table 5.40: Layer properties

Figure 5.70: Thickness derivation

H_{m0} (cm)	s_p (%)	$s_{m0,1}$ (%)	$s_{m-1,0}$ (%)	C_r (%)	N_s (-)	M_1 (%)	M_2 (%)	M_t (%)	D_1 (%)	D_2 (%)	D_t (%)
9.21	3.13	4.19	3.60	34.4	1.52	6.7	0.0	6.7	0.0	0.0	0.0
11.11	3.18	3.99	3.61	35.8	1.83	10.0	0.0	10.0	0.0	0.0	0.0
12.85	3.02	3.91	3.64	37.4	2.12	14.2	0.0	14.2	0.0	0.8	0.8
14.62	3.09	3.74	3.63	38.1	2.41	25.4	0.0	25.4	0.0	0.8	0.8
16.34	3.00	3.87	3.67	42.8	2.70	35.0	0.0	35.0	0.0	1.3	1.3
17.59	2.83	3.90	3.62	46.4	2.90	44.2	0.0	44.2	0.0	1.3	1.3
19.11	2.79	4.18	3.71	50.7	3.16	43.8	0.4	44.2	0.0	5.4	5.4
20.18	2.71	4.33	3.62	51.8	3.33	33.3	3.8	37.1	0.8	13.3	14.2

Table 5.41: Test results within the reference area SWL ±20cm

At the third wave series the first displacements appeared at both sides of the layer a few centimetres under SWL. The damage developed straight upwards. Graphs for the behaviour of the layer are drawn in figure 5.71. The layer obtains its stability from the clamping of the blocks of the second layer by the first layer. Because of the low packing density the bottoms of the blocks of the second layer do not connect well with each other to form stable columns (like in experiment 13). When a block of the second layer presses the two under lying blocks of the first layer to the side a neighbouring block is pressed upwards (out of the layer). After the displacement of a couple of blocks the armour looked like a single layer. The stability-value for this regular method is calculated from the last stability parameter where no displacements occurred, $N_s = 1.83$. From this follows:

$$K_{D0} = \frac{N_s^3}{\cot \alpha} = 4.1$$

For the presentation of the damage development the N_s- and K_D-values were calculated for different damage ratios, see table 5.42. In figure 5.72 the damage ratios for the displaced units, are presented for the different reference areas.

Damage ratio	0%	1%	3%	5%	10%	15%
N_s	1.83	2.53	3.07	3.13	3.24	-
K_D	4.1	10.7	19.3	20.5	22.9	-

Table 5.42: N_s- and K_D-values for different damage ratios (D_t)
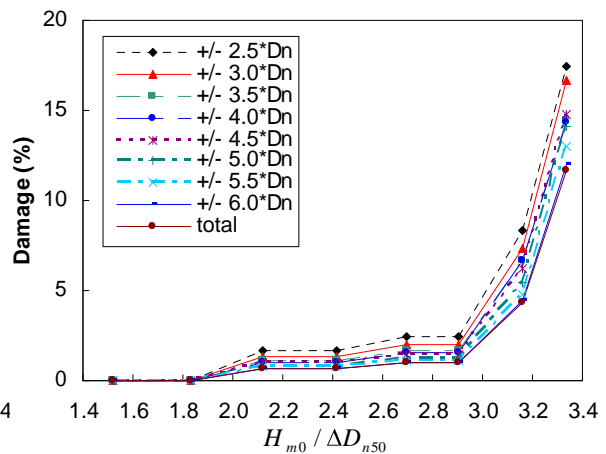
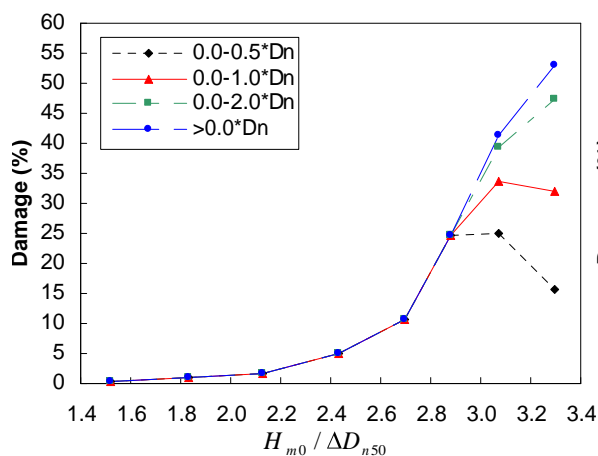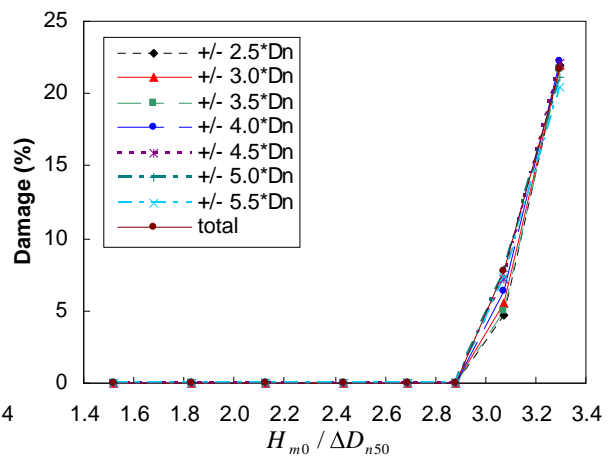
Figure 5.71: Damage for different movements   Figure 5.72: Damage for different reference areas

5.17 Experiment 15

In experiment 15 the double pyramid method is tested. The second layer is placed about $\frac{3}{4} \cdot D_n$ staggered on the first layer, see figure 5.73 and 5.74. With this experiment, together with the experiments 10 and 11, the influence of the staggering can be evaluated. The properties of the layer are presented in table 5.43 and figure 5.75 and the test results in table 5.44.
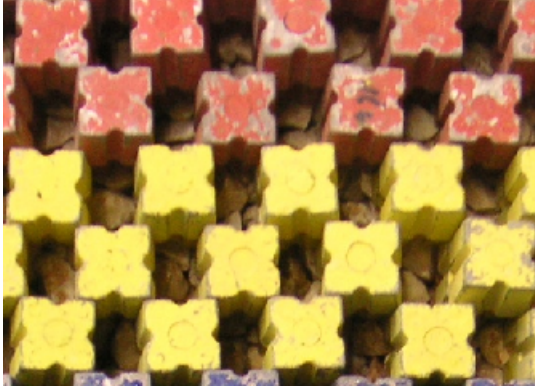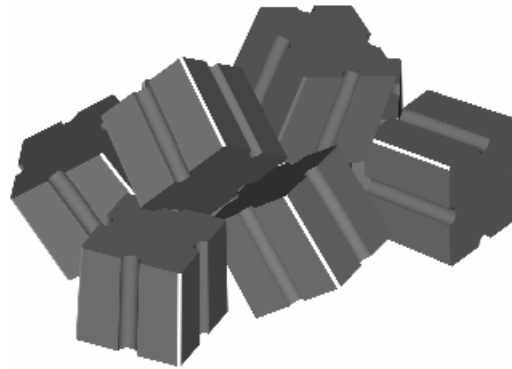

Figure 5.73: Photo of experiment 15
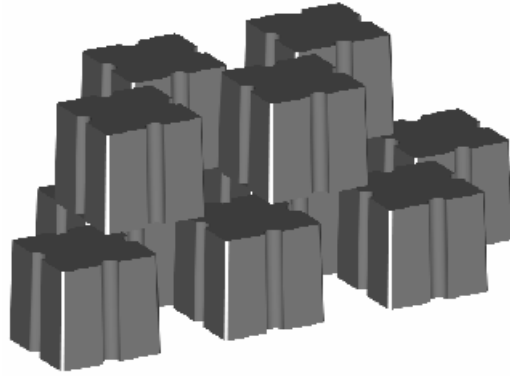
Figure 5.74: 3D drawing of experiment 15

|	
Hor. spreading ratio, X / D_n	1.71
Diag. spreading ratio, Y / D_n	1.08
Packing density, ψ_S	53.9%
Layer thickness, t	8.2cm
Layer thickness coefficient, k_Δ	1.02
Solid density, d	52.8%
Real porosity, P_r	47.2%

Table 5.43: Layer properties
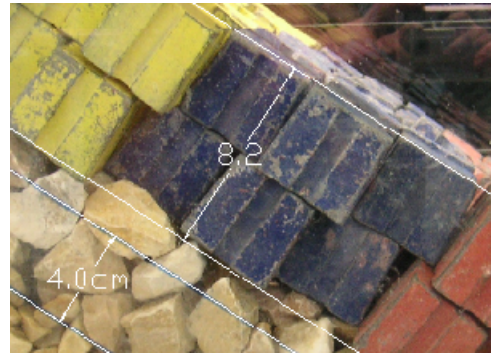
Figure 5.75: Thickness derivation

H_{m0} (cm)	s_p (%)	$s_{m0,1}$ (%)	$s_{m-1,0}$ (%)	C_r (%)	N_s (-)	M_1 (%)	M_2 (%)	M_t (%)	D_1 (%)	D_2 (%)	D_t (%)
9.22	3.13	4.19	3.61	31.3	1.52	0.3	0.0	0.3	0.0	0.0	0.0
11.11	3.04	3.98	3.60	32.8	1.83	0.9	0.0	0.9	0.0	0.0	0.0
12.88	3.03	3.85	3.62	34.9	2.13	1.5	0.0	1.5	0.0	0.0	0.0
14.73	3.05	3.86	3.68	37.2	2.43	4.9	0.0	4.9	0.0	0.0	0.0
16.31	2.92	3.90	3.66	41.5	2.69	10.7	0.0	10.7	0.0	0.0	0.0
17.44	2.81	3.93	3.58	45.5	2.88	24.5	0.0	24.5	0.0	0.0	0.0
18.60	2.72	3.97	3.49	49.6	3.07	24.8	8.9	33.7	5.5	2.1	7.7
19.97	2.68	4.42	3.59	53.1	3.30	15.6	16.3	31.9	15.3	5.8	21.2

Table 5.44: Test results within the reference area SWL ±20cm

During the sixth wave series some blocks in the right upper part of the layer turned and settled between the two blocks below. These blocks were pressed sideways, turned and a chain-reaction was started in downward direction. After a couple of turned and settled rows the movement of the higher blocks is around one nominal diameter. The first displacements appeared during the wave series with $H_{m0} = 18.60$ cm. Graphs for the behaviour of the layer are drawn in figure 5.76. The stability-value for this regular method is calculated from the last stability parameter where no displacements occurred, $N_s = 2.88$. From this follows:

$$K_{D0} = \frac{N_s^3}{\cot \alpha} = 15.9$$

For the presentation of the damage development the N_s- and K_D-values were calculated for different damage ratios, see table 5.45. In figure 5.77 the damage ratios for the displaced units, are presented for the different reference areas.

Damage ratio	0%	1%	3%	5%	10%	15%
N_s	2.88	2.90	2.95	3.00	3.11	3.19
K_D	15.9	16.3	17.2	18.1	20.0	21.7

Table 5.45: N_s- and K_D-values for different damage ratios (D_t)

Figure 5.76: Damage for different movements   Figure 5.77: Damage for different reference areas

5.18 Experiment 16

The armour for experiment 16 is irregular placed per layer, see figure 5.78 and 5.79. This experiment was done for the reproducibility of experiment 5. For this experiment the blocks are positioned mostly with their top directing upwards, which differs a little from the more irregular positioning of experiment 5. Also the obtained packing density is a couple of percents lower. The properties of the layer are presented in table 5.46 and figure 5.80 and the test results in table 5.47.

Figure 5.78: Photo of experiment 16
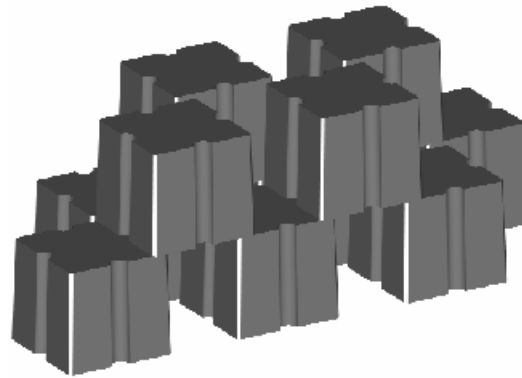

Figure 5.79: 3D drawing of experiment 16

| Packing density, ψ_S	57.4%
Layer thickness, t	8.8cm
Layer thickness coefficient, k_Δ	1.10
Solid density, d	52.4%
Real porosity, P_r	47.6%

Table 5.46: Layer properties
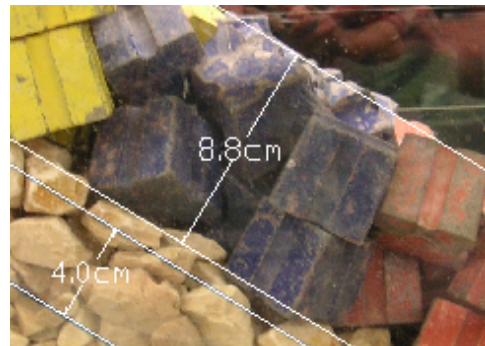
Figure 5.80: Thickness derivation

H_{m0} (cm)	s_p (%)	$s_{m0,1}$ (%)	$s_{m-1,0}$ (%)	C_r (%)	N_s (-)	M_1 (%)	M_2 (%)	M_t (%)	D_1 (%)	D_2 (%)	D_t (%)
9.24	3.14	4.18	4.14	28.8	1.53	21.9	0.0	21.9	0.0	0.0	0.0
11.12	3.12	3.98	4.03	29.8	1.84	39.3	0.0	39.3	0.0	0.0	0.0
12.96	3.05	3.93	3.94	32.1	2.14	47.0	1.8	48.8	0.0	0.0	0.0
14.78	3.06	3.98	3.87	35.2	2.44	41.4	8.9	50.3	0.0	0.6	0.6
16.30	3.06	3.91	3.80	39.0	2.69	24.0	15.7	39.6	9.2	3.3	12.4
17.85	2.88	4.15	3.81	44.7	2.95	-	-	-	-	-	-
19.12	2.93	4.28	3.76	47.7	3.16	-	-	-	-	-	-
20.06	2.69	4.44	3.59	49.7	3.31	-	-	-	-	-	-

Table 5.47: Test results within the reference area SWL ±20cm

The movements started in the centre of the layer. From here on the whole layer settled. The first displacements appeared 10 cm below SWL during the fourth wave series. One wave series later the complete left side of the second layer has settled more than one nominal diameter. It is possible to repair this settling by placing blocks in the upper part of the layer. Graphs for the behaviour of the layer are drawn in figure 5.81. The stability-value for this irregular method is calculated from the stability parameter where the first real displacements occurred (below 5%), $N_s = 2.44$, where the damage ratio is 0.6%. The stability value before failure, which makes the irregular method comparable to the regular methods, is for this case equal to the Hudson stability value. From this follows:

$$K_{DH} = K_{D<5\%} = \frac{N_s^3}{\cot \alpha} = 9.7$$

For the presentation of the damage development the N_s- and K_D-values were calculated for different damage ratios, see table 5.48. In figure 5.82 the damage ratios for the displaced units, are presented for the different reference areas.

Damage ratio	0%	1%	3%	5%	10%	15%
N_s	2.14	2.45	2.49	2.53	2.64	-
K_D	6.5	9.8	10.3	10.8	12.3	-

Table 5.48: N_s- and K_D-values for different damage ratios (D_t)
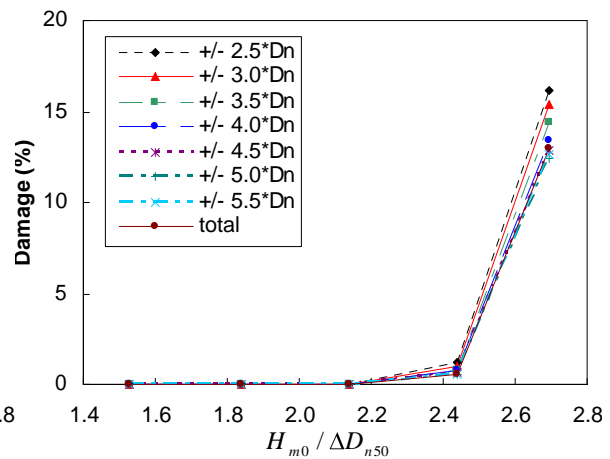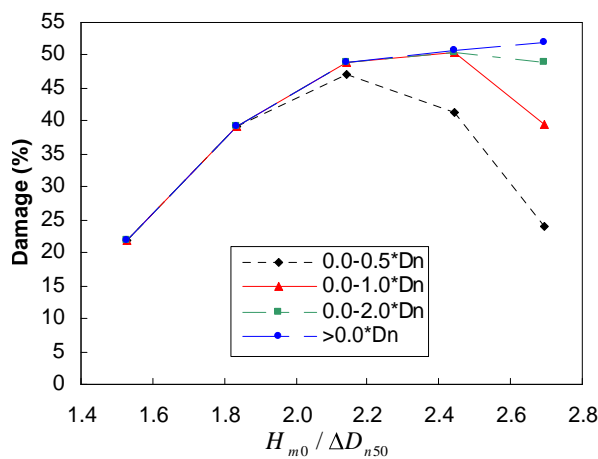
Figure 5.81: Damage for different movements   Figure 5.82: Damage for different reference areas
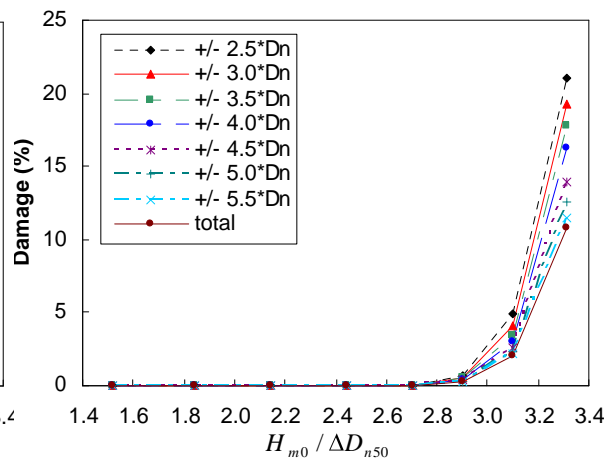
5.19 Experiment 17

Experiment 17 was a reproducibility experiment for the double pyramid method of experiment 10. The difference however is that for this experiment the staggering turned out as planned, namely 0-$? \cdot D_n$, see figure 5.83 and 5.84. With this experiment, together with the experiments 10, 11 and 15, the influence of the staggering can be evaluated. The properties of the layer are presented in table 5.49 and figure 5.85 and the test results in table 5.50.
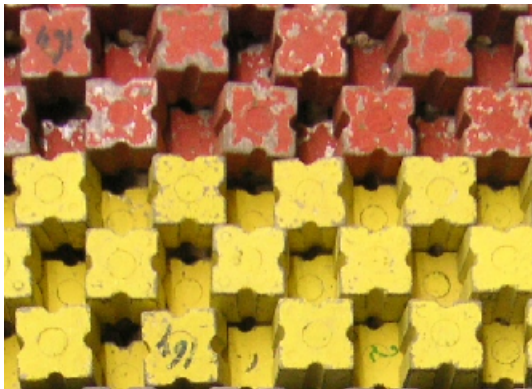
Figure 5.83: Photo of experiment 17

Figure 5.84: 3D drawing of experiment 17

Hor. spreading ratio, X/D_n	1.71
Diag. spreading ratio, Y/D_n	1.09
Packing density, ψ_S	53.5%
Layer thickness, t	8.2cm
Layer thickness coefficient, k_Δ	1.02
Solid density, d	52.4%
Real porosity, P_r	47.6%

Table 5.49: Layer properties
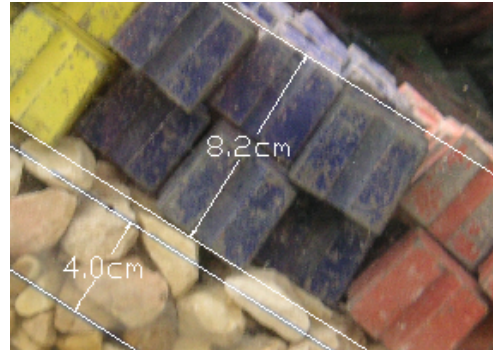
Figure 5.85: Thickness derivation

H_{m0} (cm)	s_p (%)	$s_{m0,1}$ (%)	$s_{m-1,0}$ (%)	C_r (%)	N_s (-)	M_1 (%)	M_2 (%)	M_t (%)	D_1 (%)	D_2 (%)	D_t (%)
9.22	3.06	4.21	3.62	32.3	1.52	0.7	0.0	0.7	0.0	0.0	0.0
11.15	3.06	4.01	3.62	33.1	1.84	3.1	0.0	3.1	0.0	0.0	0.0
12.96	3.11	3.92	3.65	35.0	2.14	6.4	0.0	6.4	0.0	0.0	0.0
14.78	3.06	3.89	3.69	37.1	2.44	10.8	0.0	10.8	0.0	0.0	0.0
16.39	3.01	3.92	3.67	41.1	2.71	15.9	0.0	15.9	0.0	0.0	0.0
17.55	2.83	3.94	3.59	44.9	2.90	21.7	0.3	22.0	0.3	0.0	0.3
18.77	2.88	3.99	3.63	48.7	3.10	43.7	0.3	44.1	1.4	1.0	2.4
20.05	2.69	4.38	3.59	51.0	3.31	35.9	1.4	37.3	5.4	7.1	12.5

Table 5.50: Test results within the reference area SWL ±20cm

The first displacement appeared during the sixth wave series a few centimetres above SWL. On this place there was a small bump on the under layer. The block on top of the bump was less clammed and therefore easier to displace. A hole in the under layer has less influence than a bump on the movements. When there is a hole in the under layer, the blocks of the second layer at the edge of the hole are less clammed. The extra space because of the irregularity of the under layer is then divided over more blocks then for a bump. After the first displacement there were more displacements around SWL by settling and in the upper part of the slope by lifting. Graphs for the behaviour of the layer are drawn in figure 5.86. The stability-value for this regular method is calculated from the last stability parameter where no displacements occurred, $N_s = 2.71$. From this follows:

$$K_{D0} = \frac{N_s^3}{\cot \alpha} = 13.2$$

For the presentation of the damage development the N_s- and K_D-values were calculated for different damage ratios, see table 5.51. In figure 5.87 the damage ratios for the displaced units, are presented for the different reference areas.

Damage ratio	0%	1%	3%	5%	10%	15%
N_s	2.71	2.97	3.11	3.15	3.26	-
K_D	13.2	17.4	20.1	20.9	23.1	-

Table 5.51: N_s- and K_D-values for different damage ratios (D_t)
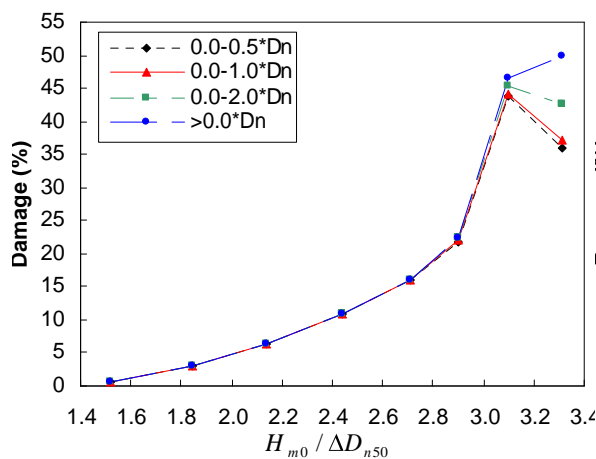
Figure 5.86: Damage for different movements   Figure 5.87: Damage for different reference areas

6   Evaluation experiments

The stability values with accompanying packing densities for the different placement methods, obtained in the previous chapter, are presented in figure 6.1. For the irregular method the $K_{D<5\%}$ - values and for the regular methods the K_{D0} -values are used. It has to be noted that for experiment 3 and 7 an attempt was made to place the blocks with distances in between over the slope. This resulted in a less regular positioning of the blocks. For experiment 8 the columns were placed under an angle and the experiments 10, 11, 15 and 17 were performed with different openings to the under layer.
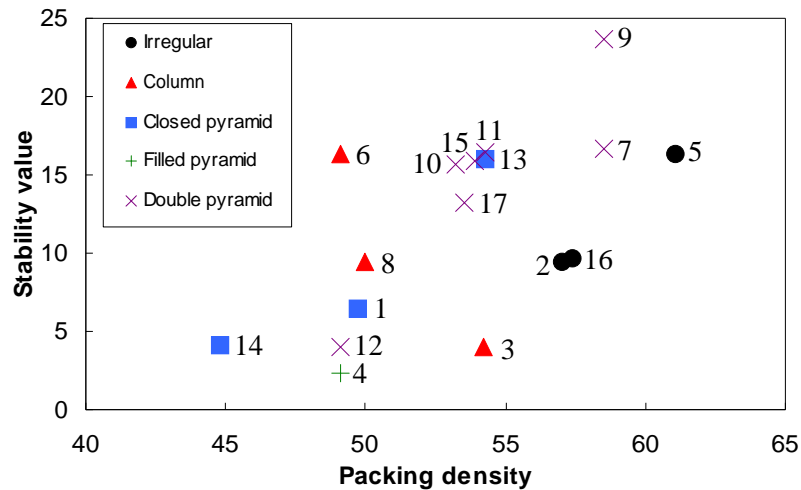
Figure 6.1: Packing density and stability for all performed experiments

In this chapter the results from the experiments will be evaluated by comparing them with one another. In the first paragraph the method of evaluation will be discussed. In the second paragraph the different experiments will be evaluated per method and in the third paragraph they will be evaluated per packing density. In the last paragraph the obtained results, which are useful for the design of an Antifer-block armour layer, will be presented.

6.1 Evaluation method

The experiments are compared and evaluated with three criteria which determine the suitability of the placement method. These criteria are the stability behaviour, the reflection and overtopping and the practical applicability. In this chapter the costs are qualitatively described within the practical applicability. They will be further discussed in the next chapter.

6.1.1 Stability behaviour

For the different methods is described in which way the stability is obtained and how the method fails (damage mechanism). The ratios for the moved blocks (movement less than a nominal diameter) and for the displaced blocks (movement more than a nominal diameter) are presented in two figures. Also a table is given wherein the N_s- and K_D-values for the different damage ratios are presented. With this information the start of damage and the damage development is compared. In paragraph 4.3.3 the importance of the reference area was mentioned. The stability analysis is done within the reference area SWL ±20cm (or SWL $\pm 5 \cdot D_n$). To indicate the importance of the reference area the damage spreading ratio, S_d, is introduced. This ratio indicates the spreading over the slope of the displaced units and is calculated by dividing the damage ratio for the reference area SWL ±10cm by the damage ratio for the reference area SWL ±20cm.

$$S_d = \frac{D_{t,SWL\pm10cm}}{D_{t,SWL\pm20cm}} \tag{6.1}$$

When this spreading ratio is 2 all displacements occurred in the smallest reference area around SWL. When the ratio decreases rapidly the damage spreads out rapidly. For a damage spreading ratio of 1 the damage is equal divided over the slope.

6.1.2 Reflection and overtopping

The reflection coefficient, C_r, is the ratio between the reflected and the incident wave and follows from the wave characteristics. In some breakwater designs a low wave reflection is required, because of passing vessels. The reflection is also connected to the overtopping. For some breakwaters low overtopping is required, because of the accessibility of the breakwater. When a wave attacks the structure part of its energy will dissipate and the other part will overtop or reflect. When overtopping is not possible, because of the height of the structure, all the energy which is not dissipated will be reflected. A higher reflection indicates less dissipation and will therefore result in more overtopping. The use of the obtained reflection coefficients is only suitable when the structure is still in tact and no overtopping has occurred, because when the overtopping starts this will decrease the reflection coefficient. The amount of overtopped water is estimated from the deformation of the leeside of the structure. This deformation was in the form of a berm at SWL. The length of this berm was measured after each experiment and these lengths can be used for a qualitative comparison of the overtopping. The lengths can also be applied as a check for the reflection theory as described above. Because overtopping was beyond the original scope of this research the length of the berm was only measured at the end of the experiment, and not after each wave series. When a placement method is damaged, the overtopping is not longer influenced by the original placement. This is why no hard conclusions can be drawn from these results.

6.1.3 Practical applicability

For the practical applicability of a method a qualitative description is given of the suitability of the method for real construction. The suitability depends on the environmental conditions of the site where the breakwater has to be constructed and on the costs of the construction of the layer. The criteria for this suitability are the incoming wave direction, the irregularity of the under layer and toe, the stability of the toe and the accuracy of block positioning. The costs also depend on the required block volume (type of crane), the required volume of concrete and the required number of blocks, which are determined by the packing density and accompanying stability value of a placement method. These volumes and numbers give also more insight in the obtained stability data and are therefore graphically presented for different significant wave heights for the irregular, the closed pyramid and the double pyramid placement methods. For these methods the similar placement was performed with different packing densities which led to different stability values. The ratios between the obtained values are also calculated. For these calculations concrete with a density of 2400 kg/m³ and salt water with a density of 1035 kg/m³ is used. In the next chapter a more detailed analysis of the costs is presented.

The block volume, V_b, is calculated with the Hudson formula, see equation 6.2. The ratio between the required block volumes, R_{Vb}, for placing method x and y, can be calculated with equation 6.3.

$$V_b = \frac{H_s^3}{K_D \cdot \cot\alpha \cdot \left(\dfrac{\rho_s}{\rho_w} - 1\right)^3} \quad [\text{m}^3] \tag{6.2}$$

$$R_{Vb} = \frac{V_{bx}}{V_{by}} = \frac{K_{Dy}}{K_{Dx}} \tag{6.3}$$

For a breakwater design the total required volume of concrete per surface unit, V_t, can be calculated by multiplying the packing density (surface-occupation) with the number of layers and the required nominal block diameter, which follows from the damage coefficient, see equation 6.4. The ratio between the required volume of concrete, R_{Vt}, for placing method x and y, can be calculated with equation 6.5.

$$V_t = \psi_S \cdot n \cdot \sqrt[3]{V_b} \quad [\text{m}^3/\text{m}^2] \tag{6.4}$$

$$R_{Vt} = \frac{V_{tx}}{V_{ty}} = \frac{\psi_{sx}}{\psi_{sy}} \cdot \sqrt[3]{\frac{K_{Dy}}{K_{Dx}}} \tag{6.5}$$

The required number of Antifer-blocks per surface, N_t, is calculated by dividing the required volume of concrete per surface unit by the required block volume, see equation 6.6. The ratio between the required number of blocks, R_{Nt}, for placing method x and y, can be calculated with equation 6.7.

$$N_t = \frac{V_t}{V_b} = \frac{\psi_S \cdot n}{V_b^{2/3}} \quad [\text{-}/\text{m}^2] \tag{6.6}$$

$$R_{Nt} = \frac{N_{tx}}{N_{ty}} = \frac{V_{tx}/V_{ty}}{V_{bx}/V_{by}} = \frac{\psi_{sx}}{\psi_{sy}} \cdot \left(\frac{K_{Dx}}{K_{Dy}}\right)^{2/3} \tag{6.7}$$

6.2 Evaluation per placement method

In this paragraph the obtained results from the irregular, column, closed pyramid and double pyramid placement methods are compared. The double pyramid placement method was optimised by placing the second layer higher on the first layer. This is evaluated in paragraph 6.2.5. The filled pyramid method (experiment 4) is not evaluated in this paragraph, because only one experiment was performed with this method. These results can be found in paragraph 5.6.

6.2.1   Irregular placement method

Three experiments are performed with an irregular placement. For experiment 2 the Antifer-blocks were placed row by row and for experiment 5 and 16 they were placed layer by layer. It was perceived that it is very difficult to obtain a low packing density, because the blocks tend to slide down and settle. This phenomenon was also found in previous research and in practice, see paragraph 2.4.3. Experiment 2 and 16 were placed with the focus on a low packing density. For experiment 5 the blocks were placed with the focus on stability (more mutual connections) which resulted in a higher packing density. The ratios for the moved blocks and for the displaced blocks are presented in figure 6.2 and 6.3 respectively. In the legend of these figures the experiment number is given first followed by its packing density. The stability parameters for the different experiments are presented in table 6.1.
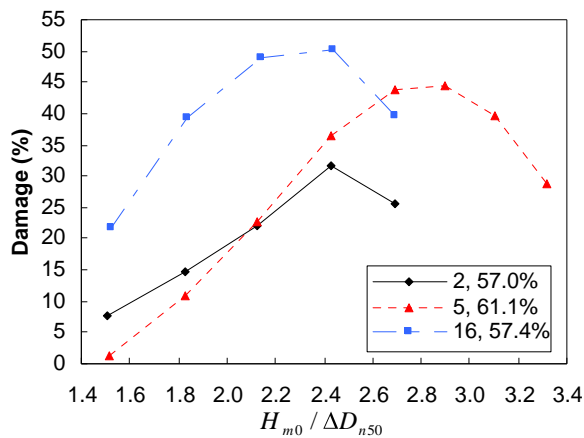
Figure 6.2: Movement ratio
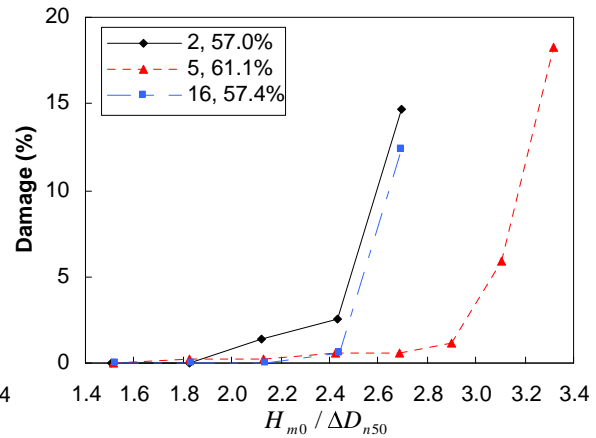
Figure 6.3: Displacement ratio

		Hudson	<5%						
Experiment 2 $\psi_s = 57.0\%$	Damage ratio	1.4%	2.5%	0%	1%	3%	5%	10%	15%
	N_s	2.13	2.43	1.83	2.04	2.44	2.49	2.60	-
	K_D	6.4	9.4	4.1	5.7	9.7	10.2	11.7	-
Experiment 5 $\psi_s = 61.1\%$	Damage ratio	0.3%	1.1%	0%	1%	3%	5%	10%	15%
	N_s	1.83	2.90	1.51	2.86	2.98	3.06	3.17	3.26
	K_D	4.1	16.3	2.3	15.6	17.6	19.1	21.3	23.1
Experiment 16 $\psi_s = 57.4\%$	Damage ratio	0.6%	0.6%	0%	1%	3%	5%	10%	15%
	N_s	2.44	2.44	2.14	2.45	2.49	2.53	2.64	-
	K_D	9.7	9.7	6.5	9.8	10.3	10.8	12.3	-

Table 6.1: Comparison of stability parameters

From figure 6.2 follows that the movement ratios for experiment 16 are higher than for experiment 2 and 5. Experiment 16 settles more than the other experiments because of the lower integration between the layers compared to experiment 2 (placed per row) and the lower packing density compared to experiment 5 (both placed per layer). The first displacements (by extraction) all occurred just below SWL. The stability value from Hudson, K_{DH}, is based on the first displacement. From this analysis follows that experiment 5 is the least stable, see table 6.1. However figure 6.3 shows that after the first displacement the layer stays stable for a period and the displacement ratio rapidly increases 2 wave series later than for the other experiments. For all experiments the damage ratio suddenly increases far above the 5 percent, which results in severe damage where repair is necessary (in practice). Therefore the stability value, $K_{D<5\%}$, is used to compare the different experiments. This stability value makes it also possible to compare the stability from the irregular methods with the regular methods as described in paragraph 4.3.3. With this stability value it can be concluded that, for similar packing densities, both placements (per row or per layer) are almost equally stable (experiment 2 versus 16), see table 6.1. For the row by row placement, however, the damage ratio is higher for the calculated stability value and the first displacements appear earlier (lower Hudson stability value). The difference between the placements is that the row by row placement has less settlement because of the higher integration between the layers, but blocks are earlier extracted from the structure. Because the settlement is less the stability within the second layer is lower. When the packing density increases (also by settlement) the stability increases (experiment 16 versus 5). Therefore the layer by layer placement is preferred.

The damage spreading ratio is presented in figure 6.4. From this figure follows that the ratio is 2 during the first displacements, which means that all displacements occur around SWL (within the smaller reference area). If this damage area was chosen for the stability analysis the ratios would turn out twice as high. This stresses the importance of the choice of the reference area for stability tests. The figure also shows that after the N_s-values, which were taken for the calculation of $K_{D<5\%}$, are reached the spreading ratio decreases and displacements are also counted within the larger reference area. It can be concluded that when the layer fails, blocks are displaced in a larger area around SWL and that the used N_s-values are correct.
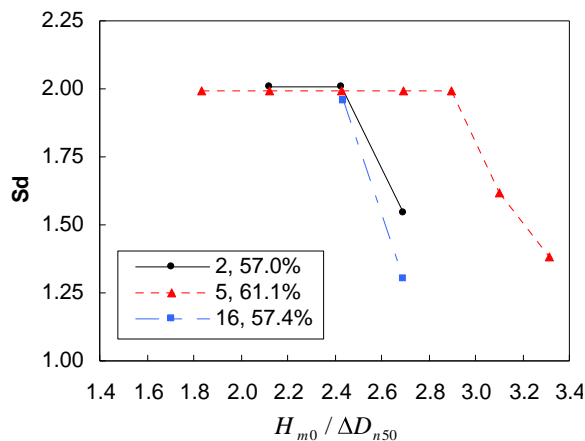
Figure 6.4: Damage spreading ratio   Figure 6.5: Reflection coefficients
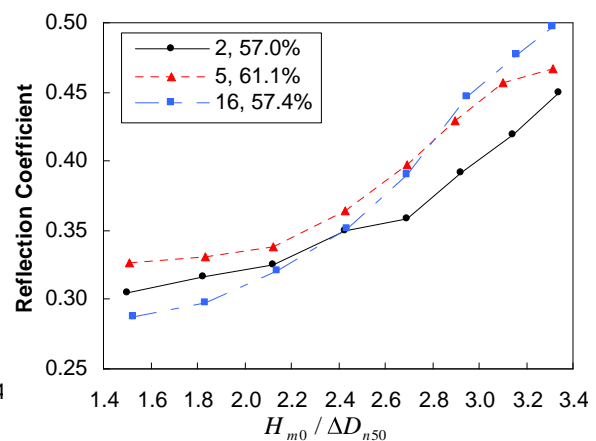
In figure 6.5 the reflection coefficients for the different experiments are presented. From this figure follows that experiment 16 has the lowest reflection coefficient at the start of the tests. With increasing wave heights the reflection coefficient for experiment 16 increases more than for the other experiments. This is caused by the higher settlement of experiment 16, figure 6.2, which results in a lower porosity. The effect of the lower porosity is acknowledged by the reflection coefficients of experiment 5 (with the lowest porosity) which were the highest at the start of the tests. Around the fourth wave series the overtopping started and from here experiments 2 and 16 failed. The reflection coefficients from this point are influenced and are therefore not analysed.

Maquet (1985) also described the effect of the porosity on the armour layer. He indicated a value above which there was insufficient stability and below which there occurred a 'paving' action that reinforced the reflection. The same is found in this investigation, a higher packing density (lower porosity) leads to more stability and higher reflection coefficients.

From this evaluation it can be concluded that the irregular placement method placed per layer is more stable and has less reflection than the row by row placement. Therefore only this method will be further evaluated. The required block volume, the required concrete volume per surface and the required number of blocks per surface for different wave heights are presented in figure 6.6, 6.7 and 6.8 respectively. The values are calculated with the $K_{D<5\%}$ -value. For the higher packing density (experiment 5) smaller blocks (factor 0.6) and less concrete (factor 0.9) is required. However more blocks (factor 1.5) have to be placed. When an armour layer is designed with a packing density of 57.4%, but during placement the packing density turns out to become 61.1%, because of the settling, then 6.4% extra blocks have to be added.
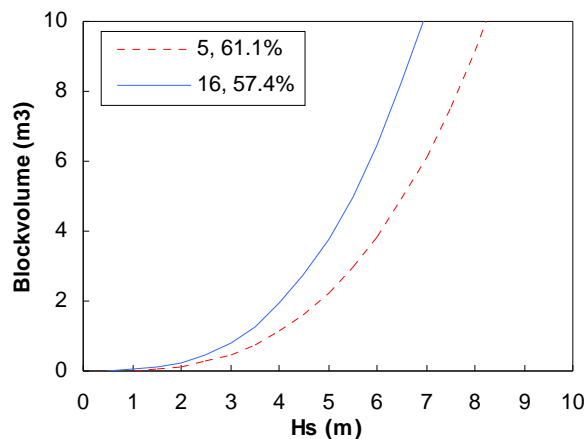
Figure 6.6: Block volume
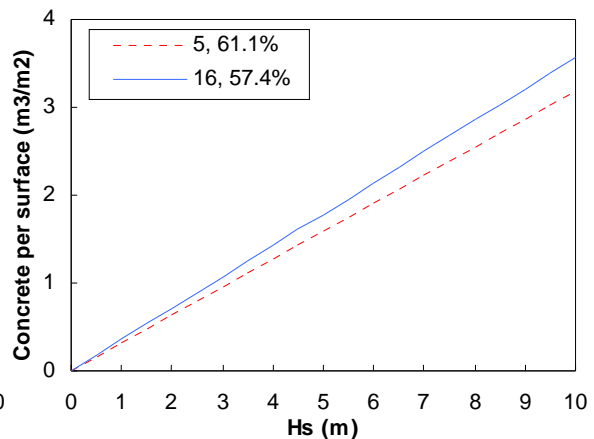
Figure 6.7: Concrete volume per surface
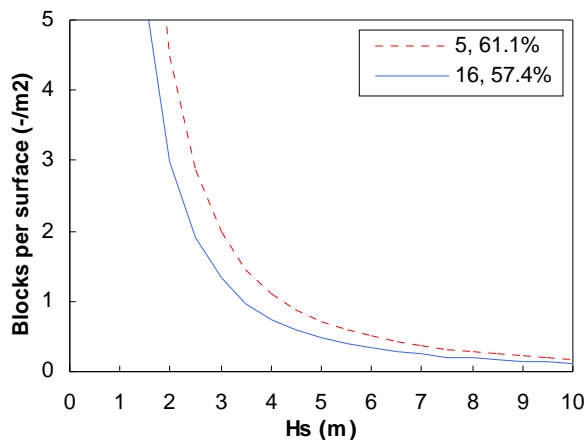
Figure 6.8: Number of blocks

6.2.2   Column placement method

Experiment 3 was placed with a spreading over the slope, which resulted in the sliding down of the blocks and therefore a more irregular positioning of the blocks. This acknowledges the theory that the blocks can not be placed within a square grid. For experiment 6 the blocks were placed in straight columns and for experiment 8 these columns were placed under an angle of 18 degrees. The ratios for the moved blocks and for the displaced blocks are presented in figure 6.9 and 6.10 respectively. The stability parameters for the different experiments are presented in table 6.2.
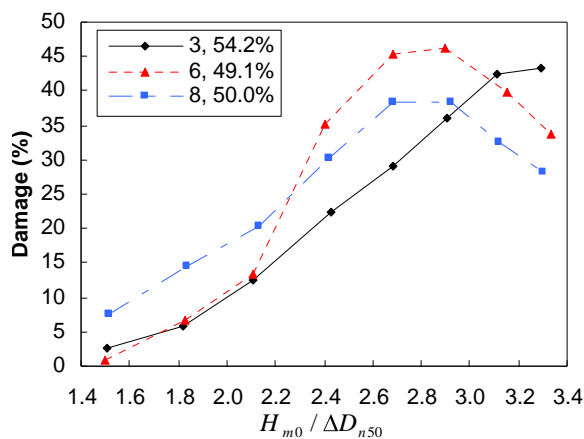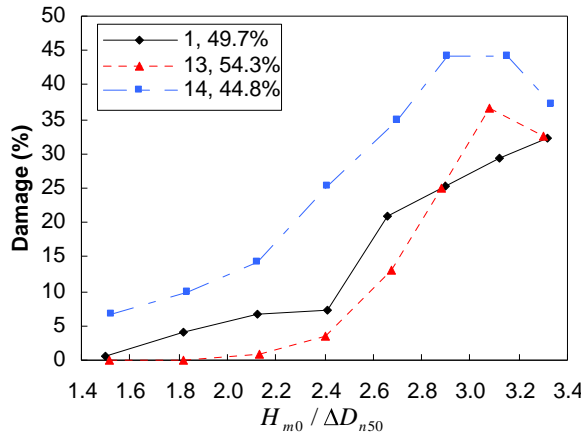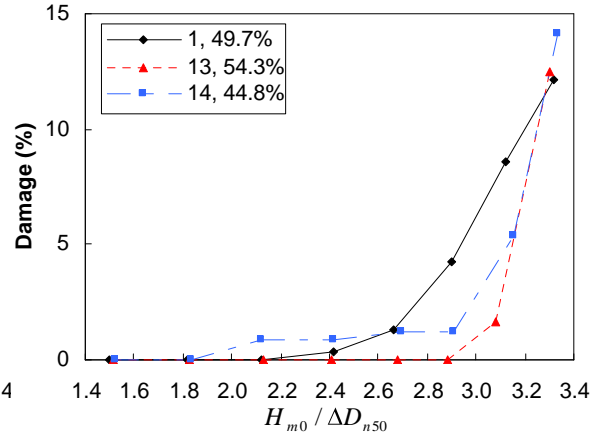

Figure 6.9: Movement ratio
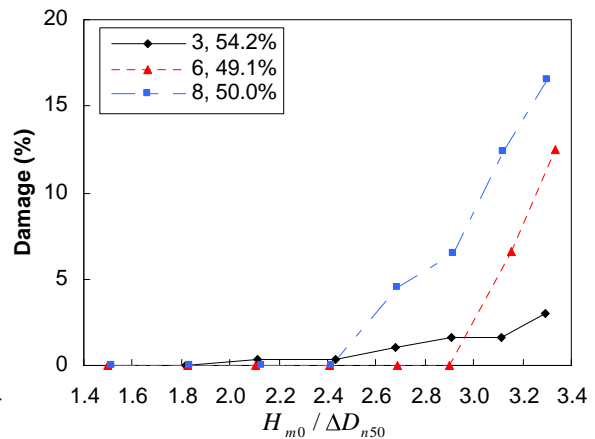
Figure 6.10: Displacement ratio

	Damage ratio	0%	1%	3%	5%	10%	15%
Experiment 3 $\psi_s = 54.2\%$	N_s	1.82	2.68	3.29	-	-	-
	K_D	4.0	12.8	23.7	-	-	-
Experiment 6 $\psi_s = 49.1\%$	N_s	2.90	2.94	3.02	3.10	3.26	-
	K_D	16.3	16.9	18.3	19.8	23.2	-
Experiment 8 $\psi_s = 50.0\%$	N_s	2.42	2.48	2.59	2.74	3.04	3.23
	K_D	9.4	10.1	11.6	13.7	18.7	22.5

Table 6.2: Comparison of stability parameters

For all experiments the first displacements were found between minus 10 cm SWL and SWL. The blocks were pressed out of the column in this area. For experiment 3 and 6 they were pressed upwards out of the column and in experiment 8 they were pressed to the side. The stability is obtained by the pressure built up within the column. This however is also the reason of failure and causes great pressures on the toe. For experiment 3 the first displacements occurred in an earlier stage compared to experiment 6, where the blocks were positioned regular and where the packing density is lower, see figure 6.10. However, the damage development is very different, for experiment 6 the first displacements led to a chain-reaction and the columns slid down. The irregular positioning of experiment 3 led to a higher integration between the layers, which resulted in a slower damage development and more irregular behaviour. In experiment 3 both columns at the sides completely failed in an early stage, but because of the wall effect they were not counted. This implies that the columns are sensitive for oblique incoming waves. The experiments were performed in a wave flume, in which it is only possible to test perpendicular incoming waves (2D). To approach the effect of oblique incoming waves experiment 6 was also performed with the columns placed under a small angle (experiment 8). This resulted in a lower stability, which acknowledges the assumption that oblique incoming waves have a great influence on this method.

From figure 6.11 it follows that for the irregular positioned blocks the damage starts around SWL and spreads out during later wave series. For the experiment 6 and 8 the first displacements are directly followed by the sliding down of the above lying blocks. This results in a higher spreading of displacements over the slope (lower damage spreading ratio). When the irregular placed column method is used for the design of a breakwater armour layer, where small damage is allowed, the agreed height of the reference area is very important.
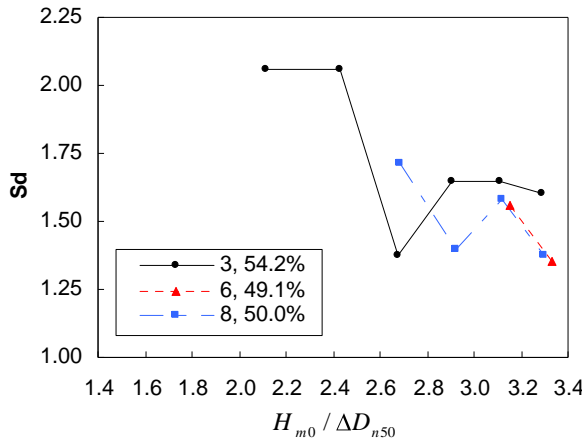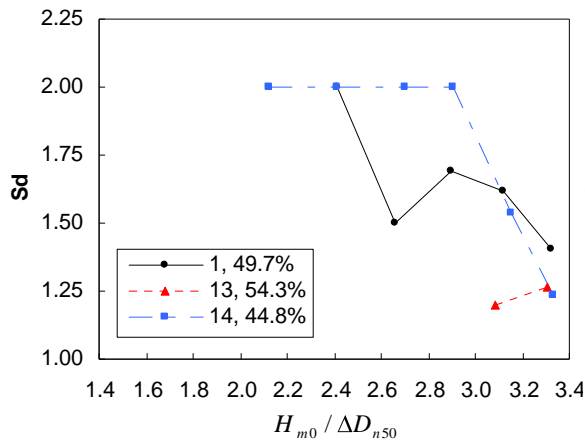

Figure 6.11: Damage spreading ratio   Figure 6.12: Reflection coefficients
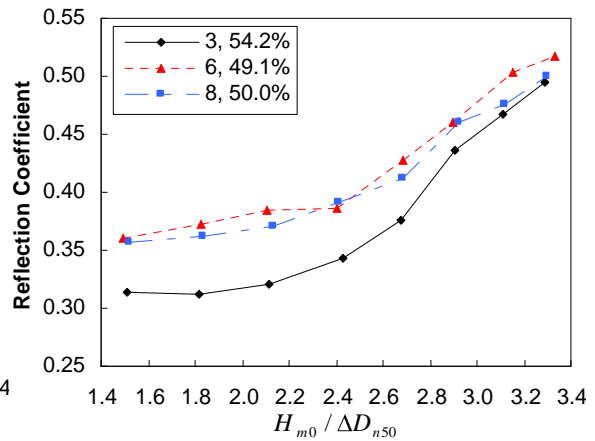
In figure 6.12 the reflection coefficients for the different experiments are presented. The reflection coefficients of the irregular positioned column method are lower than for the regular placed methods. Because of the regular placement there are no holes were the water can intrude to loose its energy. The overtopping was also far higher for this method, due to the smooth surface and to the columns which work as canals and lead the water to the top without any blockage. The measured berm length on the leeside was for experiment 3 around 10cm and for experiment 6 around 24cm, see figures 6.13 and 6.14. This acknowledges the theory as described in paragraph 6.1, that a higher reflection coefficient is an indication for higher overtopping.

Figure 6.13: Leeside experiment 3   Figure 6.14: Leeside experiment 6

From this evaluation it can be concluded that the regular positioned column method is very stable, but has high overtopping. For the irregular positioned column method (with higher packing density) the blocks slide down, which makes it necessary to add extra blocks. The instability starts in an early stage around SWL, but the damage development is very slow. For the design of a breakwater with this method, where small damage is allowed, the agreed reference area is therefore very important. For both methods oblique incoming waves have a negative influence on the stability and the high pressure on the toe should not be underestimated.

6.2.3   Closed pyramid placement method

Experiments 1, 13 and 14 are all performed with the closed pyramid method, but with different packing densities. The packing density of experiment 14 was 44.8%, which approaches a single layer placement. The packing density of experiment 1 was 49.7% and the packing density of experiment 13 was 54.3%. The ratios for the moved blocks and for the displaced blocks are presented in figure 6.15 and 6.16 respectively. The stability parameters for the different experiments are presented in table 6.3.

Figure 6.15: Movement ratio   Figure 6.16: Displacement ratio

	Damage ratio	0%	1%	3%	5%	10%	15%
Experiment 1 $\psi_s = 49.7\%$	N_s	2.13	2.59	2.80	2.94	3.20	-
	K_D	6.4	11.6	14.6	16.9	21.8	-
Experiment 13 $\psi_s = 54.3\%$	N_s	2.88	3.01	3.11	3.15	3.25	-
	K_D	16.0	18.1	20.0	20.8	22.9	-
Experiment 14 $\psi_s = 44.8\%$	N_s	1.83	2.53	3.07	3.13	3.24	-
	K_D	4.1	10.7	19.3	20.5	22.9	-

Table 6.3: Comparison of stability parameters

From figure 6.15 follows that the movement ratio is higher when the packing density is lower. From figure 6.16 can be concluded that when the packing density is higher the layer is also more stable, because the first displacements for higher packing densities occur during later wave-series. The damage development of experiment 14 is notable. After the first displacements the damage develops very slowly and crosses the 5% damage line between the other two experiments (both with higher packing densities) and approaches the damage development of the highest packing density. This can be explained by the way the layer obtains its stability. For the lowest packing density (experiment 14) the blocks are the most integrated with the first layer, which clamps them. For the highest packing density (experiment 13) the stability is obtained by the clamping between the blocks of the first layer, but the side of the bottom of a block is also clamped between the side of the bottom of the under and above lying block. In this way a kind of column is formed which integrates the second layer. For experiment 1 the clamping within the first layer is less than for experiment 14 and also the clamping within the second layer is minimal. During the tests for experiment 14 in an early stage some blocks around SWL pressed the two underlying blocks to the side and sunk in between. The blocks in the first layer again pressed some blocks from the second layer upwards, which were displaced. After this resettling around SWL the layer became stable again for a while.

For all the three experiments the damage started just below SWL. For experiment 13 the damage developed very rapidly upwards. For experiment 14 the damage developed very slowly and spread also much slower. This is acknowledged by the graphs in figure 6.17.
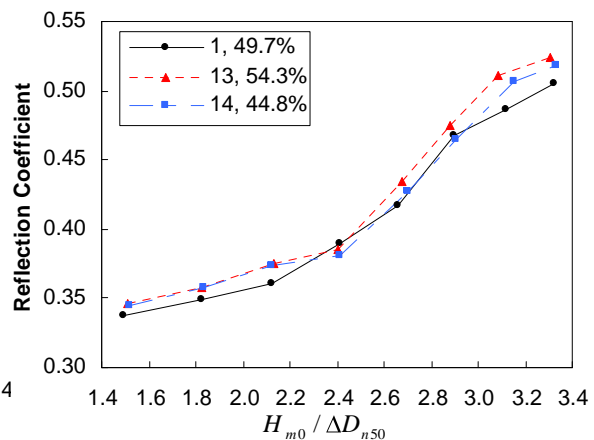

Figure 6.17: Damage spreading ratio

Figure 6.18: Reflection coefficients

From figure 6.18 follows that the reflection coefficients are high for all three experiments. This is because the surfaces are quite similar and there are no significant holes in the layer which lead to the under layer.

The required block volume, the required concrete volume per surface and the required number of blocks per surface for different wave heights are presented in figure 6.19, 6.20 and 6.21 respectively. The values are calculated with the K_{D0}-value. The ratios between the volumes and number of blocks are presented in table 6.4.
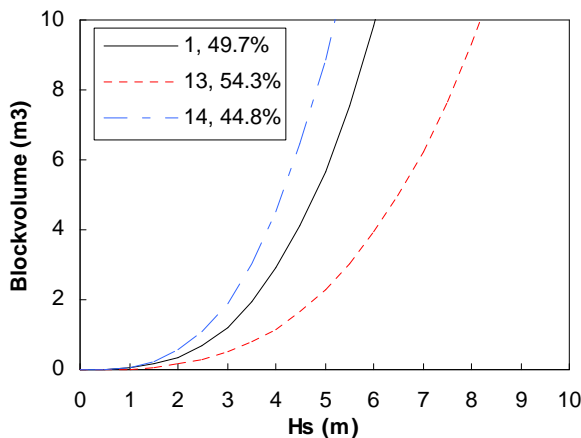
Figure 6.19: Block volume
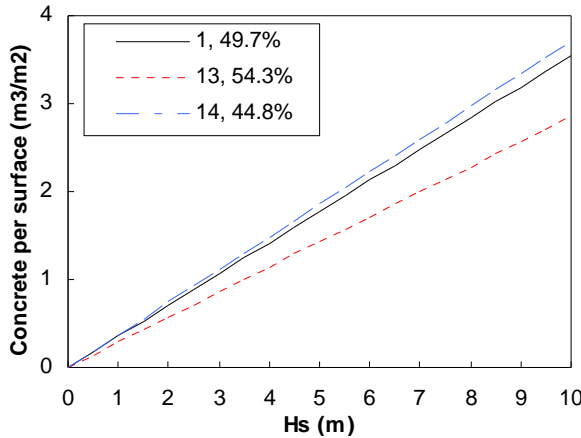
Figure 6.20: Concrete volume per surface
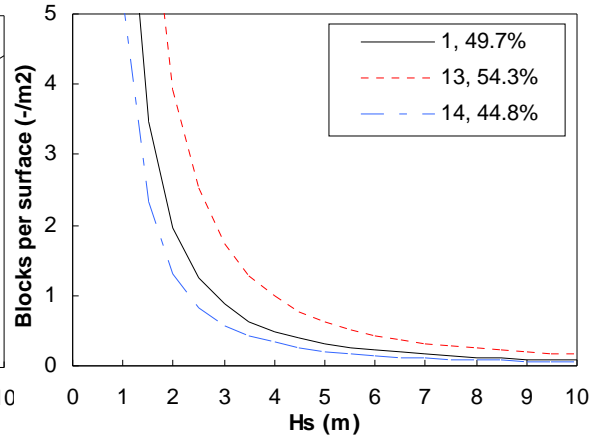
Figure 6.21: Number of blocks

	1:13	1:14	13:14
R_{Vb} (Block volume)	2.50	0.64	0.26
R_{Vt} (Concrete volume)	1.24	0.96	0.77
R_{Nt} (Number of blocks)	0.50	1.49	3.00

Table 6.4: Determining ratios

6.2.4   Double pyramid placement method

Experiment 7 was placed with a spreading over the slope, which resulted in the sliding down of the blocks and therefore a more irregular positioning of the blocks. The other experiments were regular positioned without an attempt to spread the blocks over the slope. Experiment 9 has the same packing density as experiment 7 (58.5%). The packing density of experiment 10 was lower (53.2%) and the packing density of experiment 12 was the lowest (49.1%). The ratios for the moved blocks and for the displaced blocks are presented in figure 6.22 and 6.23 respectively. The stability parameters for the different experiments are presented in table 6.5.
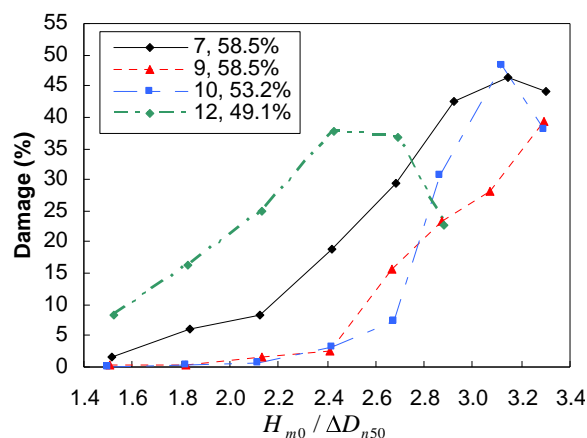
Figure 6.22: Movement ratio
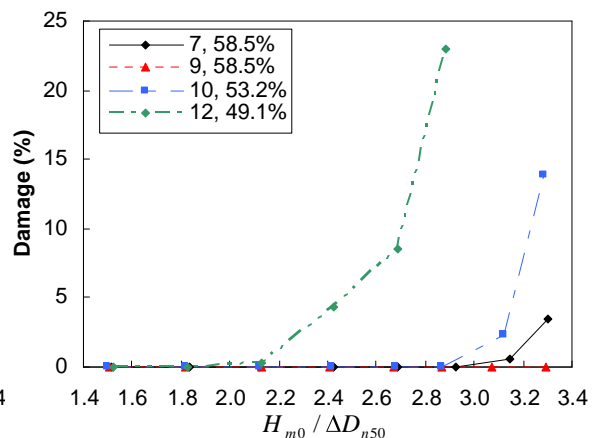
Figure 6.23: Displacement ratio

93

	Damage ratio	0%	1%	3%	5%	10%	15%
Experiment 7 $\psi_s = 58.5\%$	N_s	2.92	3.17	3.27	-	-	-
	K_D	16.7	21.3	23.4	-	-	-
Experiment 9 $\psi_s = 58.5\%$	N_s	3.29	-	-	-	-	-
	K_D	23.7	-	-	-	-	-
Experiment 10 $\psi_s = 53.2\%$	N_s	2.86	2.97	3.13	3.16	3.23	-
	K_D	15.7	17.4	20.4	21.0	22.5	-
Experiment 12 $\psi_s = 49.1\%$	N_s	1.82	2.18	2.33	2.47	2.71	2.77
	K_D	4.0	6.9	8.5	10.1	13.2	14.2

Table 6.5: Comparison of stability parameters

From figure 6.22 and 6.23 follows that for the same packing density (experiment 7 and 9) the regular positioned double pyramid method is more stable. The movement ratio is less and in contrary to experiment 7 there were no blocks displaced. Because of the regular positioning the under layer has to be smoother for good stability. Because of the better stability the other experiments were also performed with the regular positioning. From the experiments followed that the higher the packing density was the more stable the layer behaved. The layer obtains its stability from the downward pressures within the layer. The blocks are clamped between the 2 above- and the 2 underlying blocks. There is minimal integration with the first layer. Only at some places the blocks rest on the edge of the top of the first layer. The first displacements occurred between minus 10 cm SWL and SWL. In this area the blocks turned and moved down when they lost an underlying side connection because of movement. When this happened the above lying blocks also lost a connection, turned and moved down. This cumulative turning and subsequent moving down caused instability (displacements). When the packing density is higher the connection surface is bigger and the layer is more stable. It was also seen, especially for the irregular positioned placement, that blocks in the upper part of the layer are lifted out by higher waves because they are less pressurised (clamped) by the above lying blocks. It is important not to neglect the possible influence of oblique incoming waves. They can move the blocks easier to the side than the waves from these perpendicular 2D-tests.

For experiment 7 both types of failure were observed. For the regular positioned blocks the initial damage started just below SWL. This also follows from figure 6.24.
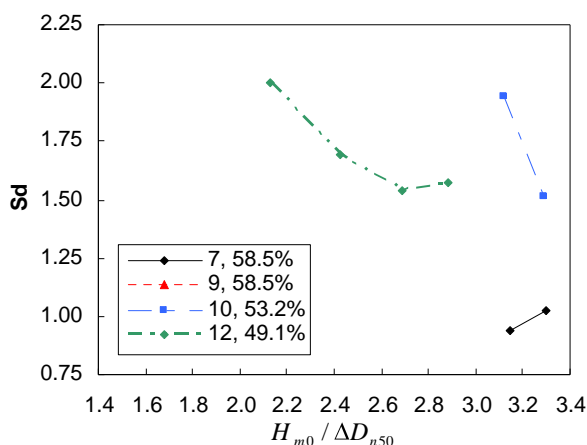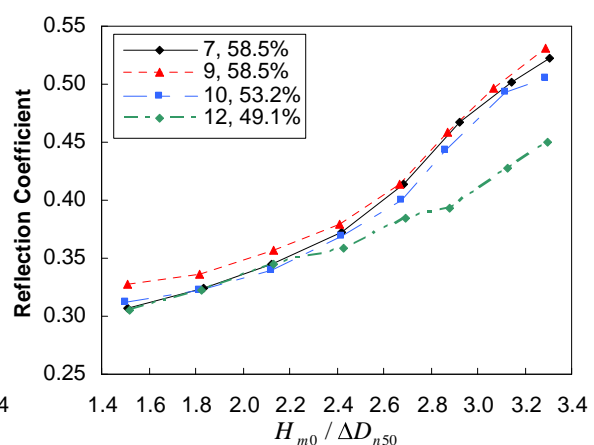

Figure 6.24: Damage spreading ratio

Figure 6.25: Reflection coefficients

From figure 6.25 follows that for the regular positioned blocks the reflection coefficient (before failure and overtopping) is higher for higher packing densities. The reflection coefficient for the irregular positioned placement with high packing density also turned out to be on the low side. This is caused by the placement of the second layer which was placed a little shifted on the first layer. This led to small openings to the under layer where the wave energy could dissipate. The measured berm length on the leeside was also the smallest for experiment 7 (13cm). Experiment 12 had the most overtopping, after the displacements during wave series 3 the slope became smoother and the overtopping high (berm length was 19cm). The reflection coefficients for later wave series are very low compared to the other experiments because most of the water was overtopped in stead of reflected or dissipated. This subscribes why only the reflection coefficients before failure or overtopping are useful. Because of the low reflection coefficients from experiment 7, experiment 10 was optimised by placing the second layer shifted on the first layer. This will be discussed in the next paragraph.

The required block volume, the required concrete volume per surface and the required number of blocks per surface for different wave heights are presented in figure 6.26, 6.27 and 6.28 respectively. The values are calculated with the K_{D0}-value. The ratios between the volumes and number of blocks are presented in table 6.6.
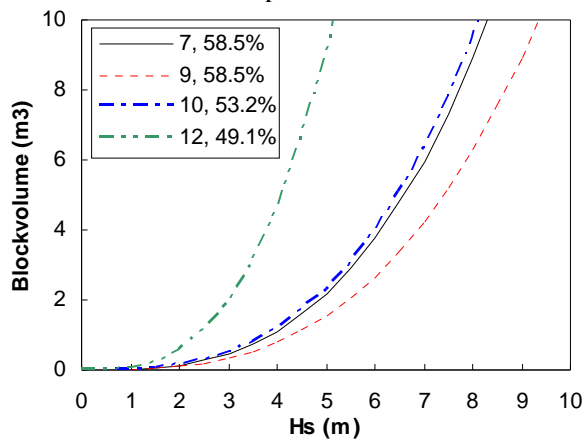
Figure 6.26: Block volume
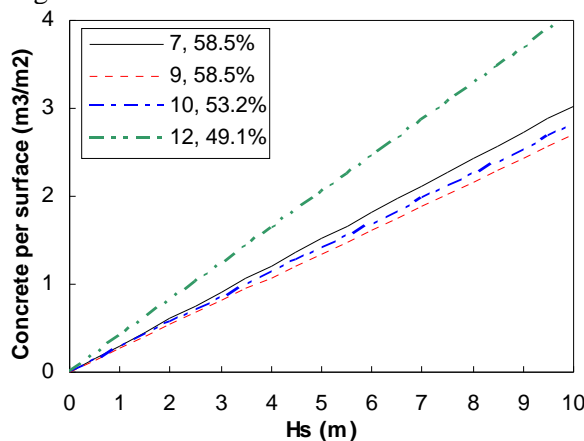
Figure 6.27: Concrete volume per surface
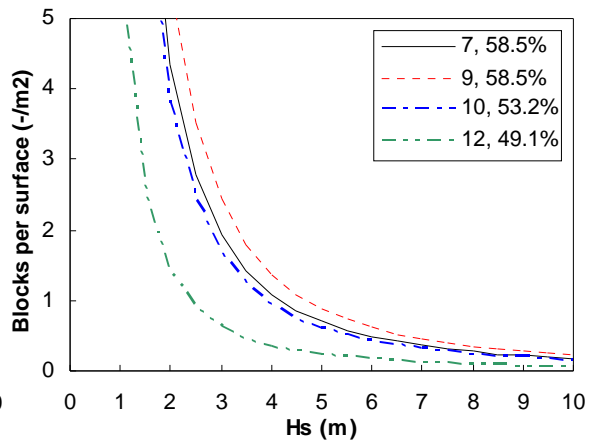
Figure 6.28: Number of blocks

	7:9	7:10	7:12	9:10	9:12	10:12
R_{Vb} (Block volume)	1,42	0,94	0,24	0,66	0,17	0,25
R_{Vt} (Concrete volume)	1,12	1,08	0,74	0,96	0,66	0,69
R_{Nt} (Number of blocks)	0,79	1,15	3,09	1,45	3,90	2,70

Table 6.6: Determining ratios

6.2.5 Optimisation of the double pyramid placement method

The double pyramid placement method from experiment 10 is repeated with the second layer placed higher on the first layer. Because of this the holes to the under layer are larger. These experiments were performed to determine the influence of the shifted placement (larger holes) on the stability and the reflection. Also the reproducibility of the placement method is tested. The opening to the under layer for experiment 10 turned out to be $?-\frac{1}{4}\cdot D_n$ over the slope, for experiment 11 around $\frac{1}{2}\cdot D_n$ and for experiment 15 around $\frac{3}{4}\cdot D_n$. For experiment 17 the placing of experiment 10 was reproduced. The openings turned out be a little lower namely $0-?\cdot D_n$. The ratios for the moved blocks and for the displaced blocks are presented in figure 6.29 and 6.30 respectively. The stability parameters for the different experiments are presented in table 6.7.
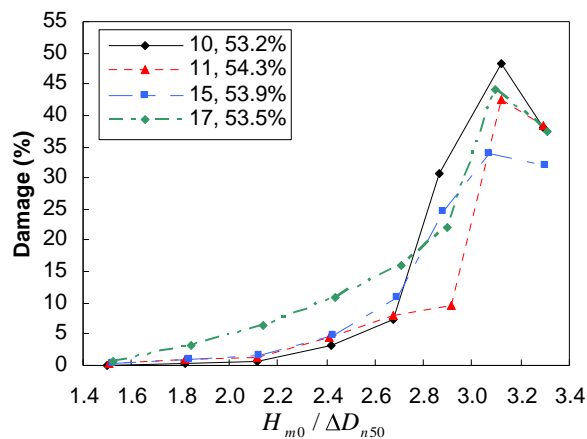
Figure 6.29: Movement ratio
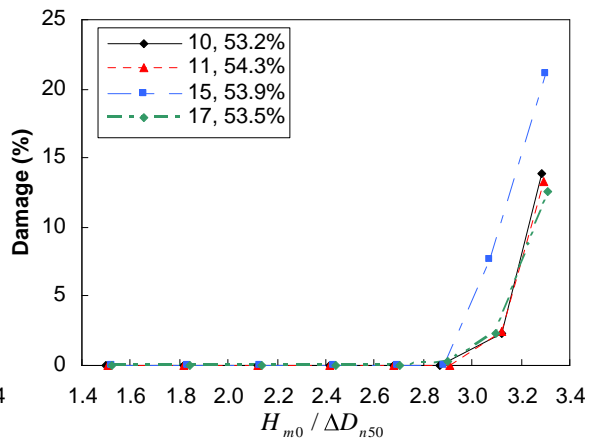
Figure 6.30: Displacement ratio

	Damage ratio	0%	1%	3%	5%	10%	15%
Experiment 10 $?-\frac{1}{4}\cdot D_n$	N_s	2.86	2.97	3.13	3.16	3.23	-
	K_D	15.7	17.4	20.4	21.0	22.5	-
Experiment 11 $\frac{1}{2}\cdot D_n$	N_s	2.91	2.99	3.13	3.16	3.24	-
	K_D	16.4	17.9	20.4	21.0	22.6	-
Experiment 15 $\frac{3}{4}\cdot D_n$	N_s	2.88	2.90	2.95	3.00	3.11	3.19
	K_D	15.9	16.3	17.2	18.1	20.0	21.7
Experiment 17 $0-?\cdot D_n$	N_s	2.71	2.97	3.11	3.15	3.26	-
	K_D	13.2	17.4	20.1	20.9	23.1	-

Table 6.7: Comparison of stability parameters

There was little difference in the stability for the different placements. For experiment 17 one block was displaced during the sixth wave series in contrary to the other experiments where no displacements occurred during this wave series. This happened because there was a small bump on the under layer. The block on top of this bump was less clammed and therefore easier displaced. This stresses the necessity for a smooth under layer for this placement. The displacement ratio for experiment 15 developed different than for the other experiments. This is because the damage for experiment 15 started in the right upper part of the layer and spread downwards. Because of the large openings there was no integration between the layers which made this failure possible. For the other methods the first displacements were observed around SWL. This also follows from figure 6.31.
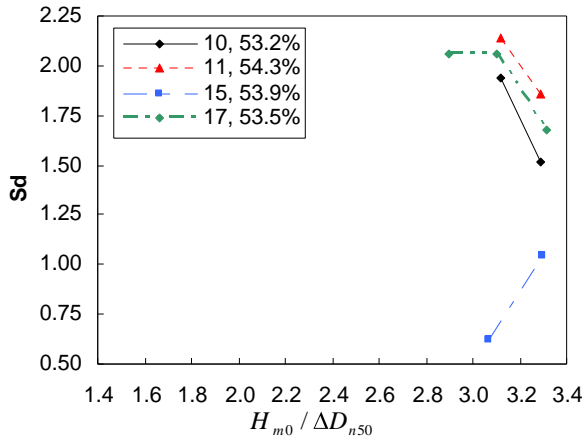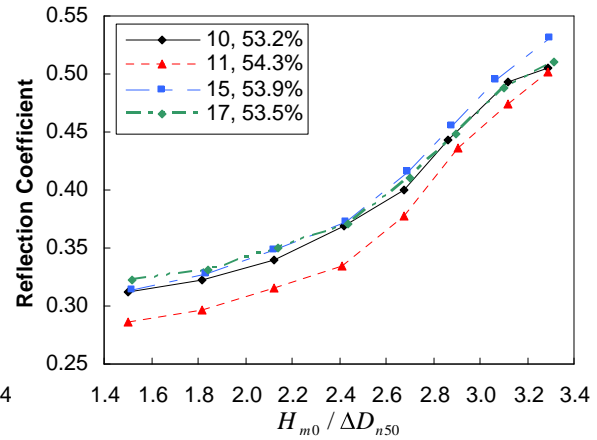
Figure 6.31: Damage spreading ratio

Figure 6.32: Reflection coefficients

From figure 6.32 follows that for openings of $\frac{1}{2} \cdot D_n$ the reflection coefficient turned out to be the lowest. Therefore in the following evaluation only experiment 11 will be used for this packing density. For the smallest opening, $0\text{-?} \cdot D_n$ (experiment 17), the reflection coefficient was the highest. When the porosity of the first layer is very exposed as in experiment 10 (openings of $\frac{3}{4} \cdot D_n$) the reflection coefficient is high again.

From the results from the double pyramid method can be concluded that there are two factors which determine the reflection: the packing density and the exposure of the pores of the first layer, see figure 6.33. When the packing density is higher (the pores are smaller) the reflection coefficient is higher. For the exposure of the porosity the reflection coefficient turned out to be minimal for $\frac{1}{2} \cdot D_n$. The theory behind these differences is that a wave looses its energy when the water intrudes and extrudes the pores of the first layer. When the opening (over the slope) to these pores is very small only a little water can intrude and extrude during a wave, but when the opening is large it takes less energy to intrude and extrude. It was found that an optimum of energy loss is found when the opening is half the nominal diameter. When the packing density is lower, the pores are wider so more water can intrude and extrude which leads to a lower reflection coefficient. The lowest reflection will therefore be obtained with a low packing density and openings of $\frac{1}{2} \cdot D_n$. This low packing density also results in a lower stability.
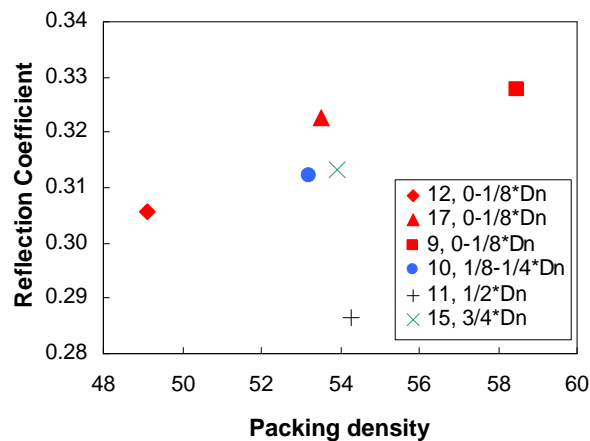
Figure 6.33: Reflection coefficients for first wave series

6.3   Evaluation per packing density

In this paragraph the obtained results by the performed experiments are compared for corresponding packing densities. Four packing densities with a bandwidth of 5 percent are chosen for this comparison, namely: packing densities around 45% (42.5 - 47.5%), 50% (47.5 - 52.5%), 55% (52.5 - 57.5%) and 60% (57.5 - 62.5%). The experiments 2, 10, 15 and 17 were left out the comparison because different placements within the same method performed better on stability or reflection. Experiment 8 is left out because it was performed for the approach of oblique incoming waves. In figure 6.34 the stability values with accompanying packing densities obtained in the previous chapter for the different experiments which will be evaluated in this paragraph are presented.
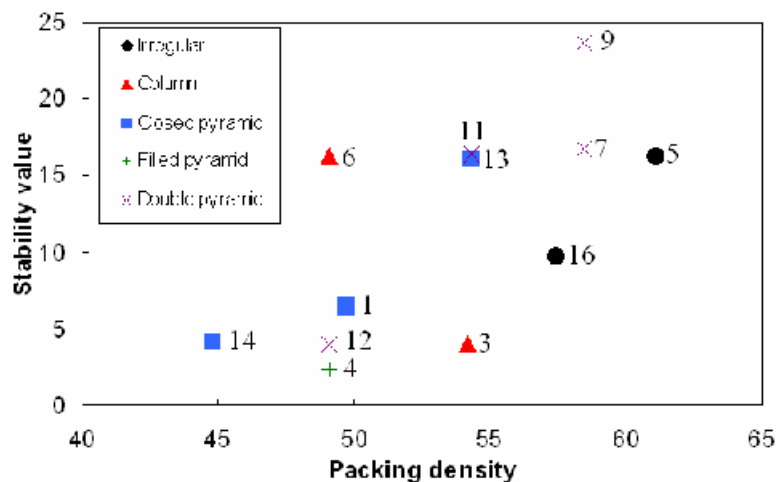
Figure 6.34: Packing density and stability

6.3.1   Packing densities around 45%

A layer with a packing density around 45% approaches a single layer placement. This packing density was only possibly for the closed pyramid method (experiment 14) and led to a high integration between both layers. The results of this placement can be found in the paragraphs 5.16 and 6.2. For the double and filled pyramid method this packing density is impracticable, because the slightest irregularity in the under layer or the toe makes the placement of a stable row impossible. For the column method the blocks will intrude within the first layer, which destabilises the column. Irregular placement is only possible with a packing density above 55% because of the sliding down and settling of blocks.

6.3.2   Packing densities around 50%

The closed pyramid (experiment 1), the filled pyramid (experiment 4) and the regular positioned column (experiment 6) placement methods were performed with a packing density of 49.1%. The double pyramid (experiment 12) placement method was performed with a packing density of 49.7%. The ratios for the moved blocks and for the displaced blocks are presented in figure 6.35 and 6.36 respectively. The stability parameters for the different experiments are presented in table 6.8.
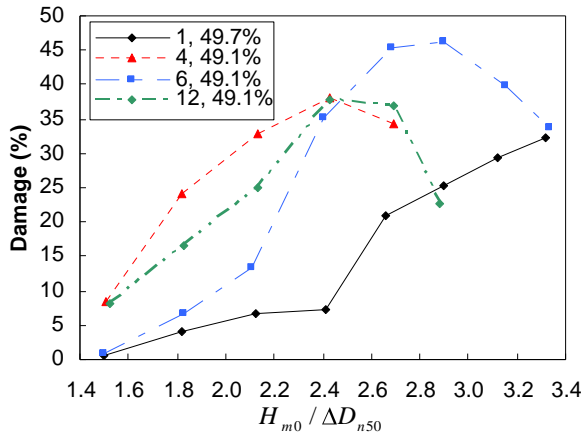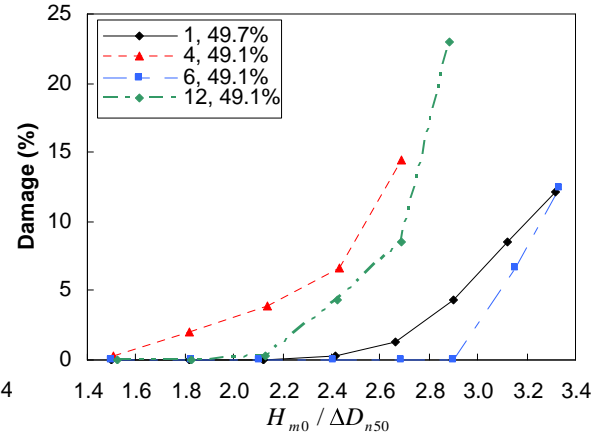
Figure 6.35: Movement ratio

Figure 6.36: Displacement ratio

	Damage ratio	0%	1%	3%	5%	10%	15%
Experiment 1 Closed pyramid	N_s	2.13	2.59	2.80	2.94	3.20	-
	K_D	6.4	11.6	14.6	16.9	21.8	-
Experiment 4 Filled pyramid	N_s	-	1.64	1.99	2.26	2.54	-
	K_D	-	2.9	5.24	7.7	10.9	-
Experiment 6 Column	N_s	2.90	2.94	3.02	3.10	3.26	-
	K_D	16.3	16.9	18.3	19.8	23.2	-
Experiment 12 Double pyramid	N_s	1.82	2.18	2.33	2.47	2.71	2.77
	K_D	4.0	6.9	8.5	10.1	13.2	14.2

Table 6.8: Comparison of damage parameters

The filled pyramid method was the most unstable. The movement ratio was the highest and already during the first wave series a block was displaced. This is because the blocks are placed irregular within the holes of the first layer. Therefore there is no integration within the second layer and the blocks of the second layer are not clamped by the blocks of the first layer. The next unstable method was the double pyramid placement. During the third wave series the first block was displaced, because it lost one of its connections to the underlying blocks of the second layer, turned, moved down and started a chain reaction. For oblique incoming waves the chance for this to happen is even bigger and first displacements are expected earlier. The closed pyramid method and the column method were the most stable. The movement ratio for the column method was higher, but the first displacements occurred during the seventh wave series in contrary to the closed pyramid where they occurred during the fourth wave series. The column method is, however, only very stable for perpendicular incoming waves. Oblique incoming waves will press the columns sideways and bend them in an earlier stage. Another disadvantage of the column method are the high forces on the toe caused by the column.

For all four methods the damage started around SWL. For the column method the damage developed quickly over the slope, because the columns slide down after the first displacements around SWL. Therefore the damage spreading ratio started below 2, see figure 6.37.
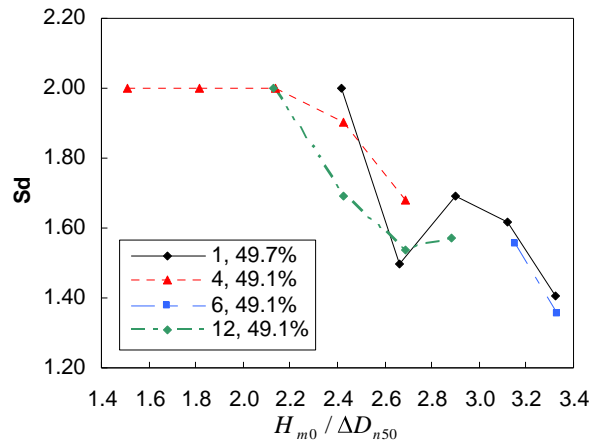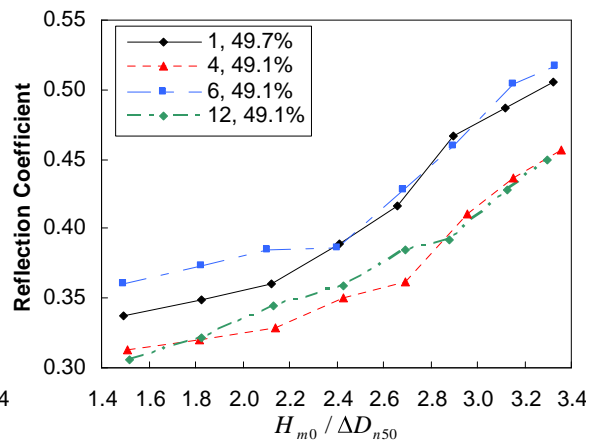
Figure 6.37: Damage spreading ratio

Figure 6.38: Reflection coefficients

From figure 6.38 follows that the reflection coefficients for the filled and double pyramid method were the lowest. Because of the early failure of these methods the overtopping started in an early stage and therefore the reflection coefficient stayed low during later wave series. The reflection coefficient for the column method was the highest. It decreased during wave series 4 because the overtopping started. The berm length caused by the overtopped water was also the longest. Compared to the reflection and overtopping of the column method the closed pyramid method performed better. This can be explained by the behaviour of water, which searches for the path with the least resistance. The columns form canals, which lead the water to the top from where it streams back or overtops. When the water is blocked by a block of the closed pyramid method a part of the energy is dissipated.

For a packing density around 50% and perpendicular incoming waves the regular placed column method behaves the most stable. However, in reality there are in most cases also oblique incoming waves which have a negative effect on the stability. Because of this negative effect of oblique incoming waves on the stability, the high forces on the toe and the high reflection and overtopping the closed pyramid method is preferred over the column method.

6.3.3 Packing densities around 55%

The irregular positioned column placement method (experiment 3) was performed with a packing density of 54.2%. The double pyramid (experiment 11) and closed pyramid (experiment 13) placement methods were performed with a packing density of 54.3% and the layer by layer placed irregular placement method (experiment 16) was performed with a packing density of 57.4%. The ratios for the moved blocks and for the displaced blocks are presented in figure 6.39 and 6.40 respectively. The stability parameters for the different experiments are presented in table 6.9.
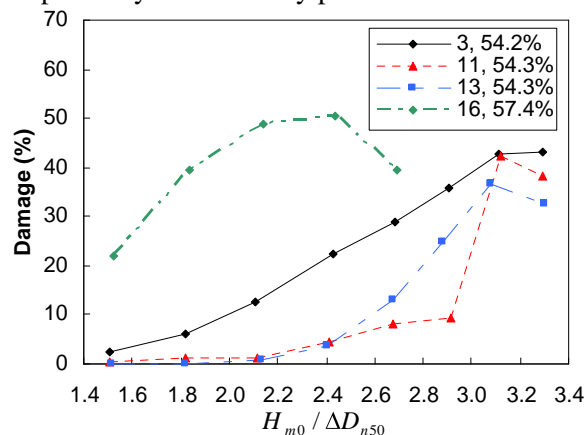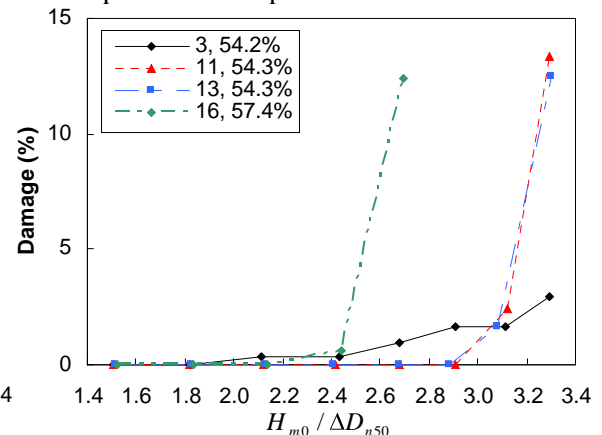

Figure 6.39: Movement ratio

Figure 6.40: Displacement ratio

		Hudson	<5%						
	Damage ratio	0.6%	0.6%	0%	1%	3%	5%	10%	15%
Experiment 3 Column	N_s	-	-	1.82	2.68	3.29	-	-	-
	K_D	-	-	4.0	12.8	23.7	-	-	-
Experiment 11 Double pyramid	N_s	-	-	2.91	2.99	3.13	3.16	3.24	-
	K_D	-	-	16.4	17.9	20.4	21.0	22.6	-
Experiment 13 Closed pyramid	N_s	-	-	2.88	3.01	3.11	3.15	3.25	-
	K_D	-	-	16.0	18.1	20.0	20.8	22.9	-
Experiment 16 Irregular	N_s	2.44	2.44	2.14	2.45	2.49	2.53	2.64	-
	K_D	9.7	9.7	6.5	9.8	10.3	10.8	12.3	-

Table 6.9: Comparison of damage parameters

The first displacements occurred for the irregular positioned column method during wave series 3. Thereafter, during wave series 4 the first blocks were displaced for the irregular method, which has the highest movement ratios and the highest packing density in this comparison. The closed and double pyramid method showed a similar behaviour. For both regular positioned methods the first blocks were displaced during the seventh wave series. The damage for the irregular positioned column method developed very slowly compared to the other three placement methods. For the last wave series the damage ratio was still 3% and lower than the ratios of the closed and double pyramid method. A disadvantage of the irregular positioned methods is that it is difficult to predict the exact packing density, because during the placement blocks tend to settle. This can lead to the necessary placement of extra blocks during construction. When the blocks of the irregular placement settle, in reality, extra blocks can be added, which enforces the stability of the layer. For the irregular positioned column placement the settling is lower and when blocks are displaced the column above can slide down. Another disadvantage is that oblique incoming waves have a negative effect on the stability of the columns. Both pyramid methods show similar stability behaviour, however the stability of the double pyramid method can be influenced by oblique incoming waves. Also the placement is more difficult, because there is no integration between the layers. For both regular positioned methods a smoother under layer and toe, compared to the irregular positioned methods, are required.

For all four placements the damage started around MSL. For the closed pyramid method the damage spread quickly upwards during one wave series. This is why the damage spreading ratio starts below 2, see figure 6.41.
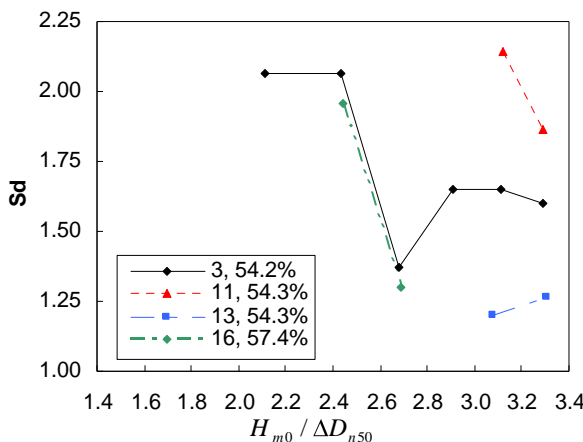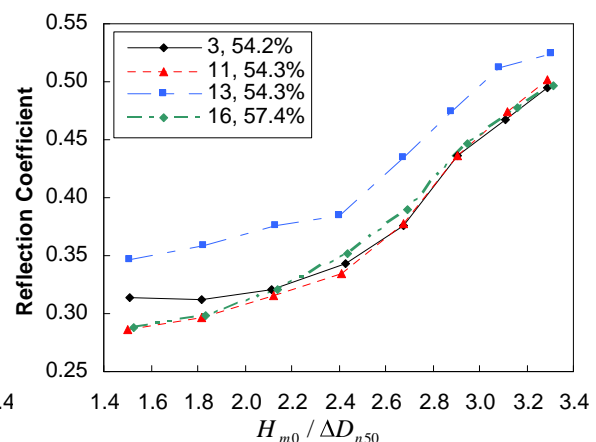

Figure 6.41: Damage spreading ratio

Figure 6.42: Reflection coefficients

From figure 6.42 follows that the reflection coefficients for the irregular and the double pyramid method, with openings of $\frac{1}{2} \cdot D_n$, are both very low. This is because for both methods it is possible for the water to intrude the pores of the first layer with optimal energy loss. The reflection of the irregular positioned column method is a little higher and the reflection for the closed pyramid method is by far the highest.

For a packing density around 55% the closed and double pyramid method behave the most stable. The double pyramid method with openings of $\frac{1}{2} \cdot D_n$ has the lowest reflection, but oblique incoming waves can negatively influence the stability. For both regular methods the under layer and toe have to be smooth and equipment and circumstances for accurate placement are required. If this is not possible or too expensive, than an irregular positioned placement method is recommended. The irregular placed column method is preferred when a small damage ratio is allowed, the reflection is not a determining factor and most waves come in perpendicular to the structure. Otherwise the irregular placement method is advised. Both irregular positioned methods have as disadvantage that the exact packing density is difficult to predict. This can during construction result in higher packing densities, which are more stable, but need more blocks and have higher reflection coefficients.

6.3.4 Packing densities around 60%

For packing densities around 60 percent three experiments were performed: the layer by layer placed irregular placement method (experiment 5) with a packing density of 61.1% and the irregular and regular positioned double pyramid placement method (experiment 7 and 9) both with a packing density of 58.5%. The ratios for the moved blocks and for the displaced blocks are presented in figure 6.43 and 6.44 respectively. The stability parameters for the different experiments are presented in table 6.10.
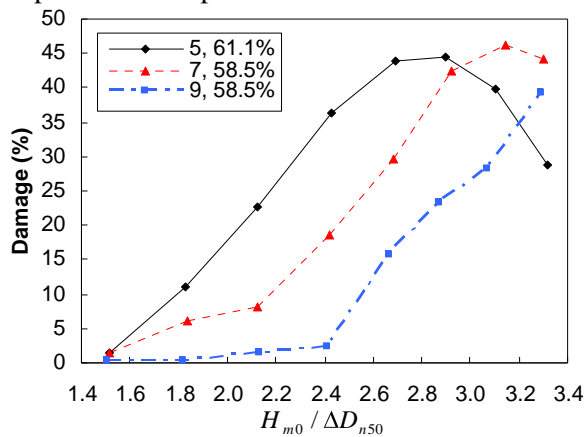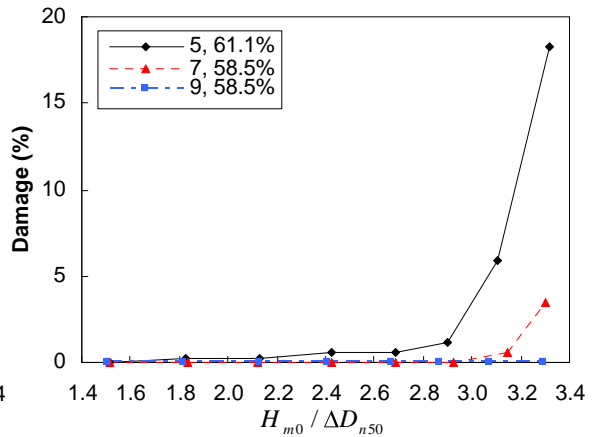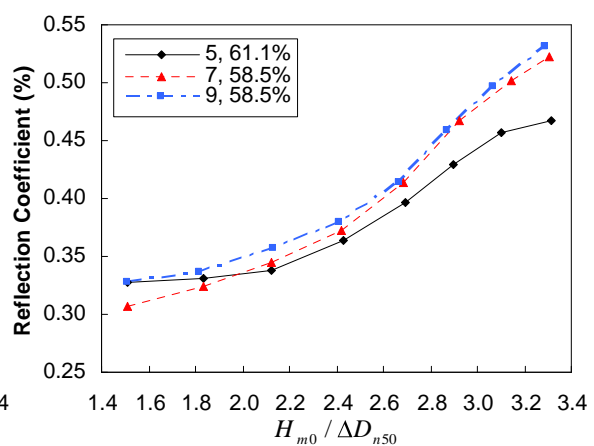

Figure 6.43: Movement ratio   Figure 6.44: Displacement ratio

		Hudson		<5%					
	Damage ratio	0.3%	1.1%	0%	1%	3%	5%	10%	15%
Experiment 5 Irregular	N_s	1.83	2.90	1.51	2.86	2.98	3.06	3.17	3.26
	K_D	4.1	16.3	2.3	15.6	17.6	19.1	21.3	23.1
Experiment 7 Double pyramid (irregular pos.)	N_s	-	-	2.92	3.17	3.27	-	-	-
	K_D	-	-	16.7	21.3	23.4	-	-	-
Experiment 9 Double pyramid (regular pos.)	N_s	-	-	3.29	-	-	-	-	-
	K_D	-	-	23.7	-	-	-	-	-

Table 6.10: Comparison of damage parameters

For the irregular placement method the movement ratios were the highest and the first displacement occurred during the second wave series. The damage developed slowly and the layer stayed very stable up to the sixth wave series. The irregular positioned double pyramid method was more stable. During the seventh wave series the first displacement occurred. The regular placed double pyramid method was the most stable because no displacements occurred during the tests. Oblique incoming waves can have a negative effect on the stability. Other disadvantages of the double pyramid method are that the under layer and the toe have to be smooth and equipment and circumstances for accurate placing are required.

For the irregular placement the damage started around SWL. For the irregular positioned double pyramid placement the damage started in the upper part of the layer, see figure 6.45.
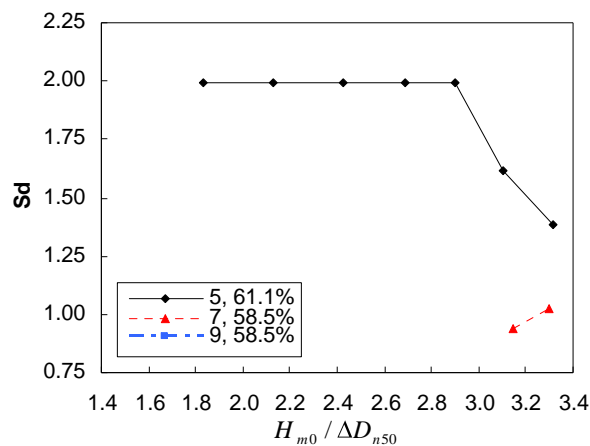
Figure 6.45: Damage spreading ratio   Figure 6.46: Reflection coefficients

From figure 6.46 follows that the reflection coefficient for the irregular positioned double pyramid placement is the lowest. The reflection coefficients for the irregular and the regular positioned double layer placement start similar. When the double pyramid placement is placed with openings to the first layer of $\frac{1}{2} \cdot D_n$ the reflection coefficient will be lower.

For a packing density around 60% the regular positioned double pyramid placement behaves the most stable compared to the irregular positioned double pyramid placement and the irregular placement method. The stability can be negatively affected by oblique incoming waves. Other disadvantages of the double pyramid method are that the under layer and the toe have to be smooth and equipment and circumstances for accurate placing are required. When this is not possible or too expensive the irregular placement is recommended.

6.4 Resulting Antifer-block armour design

From the evaluation of the experiments can be concluded that the regular placement methods behave more stable than the irregular placement methods and higher packing densities lead to higher stabilities. The stability values for the placement methods are based on wave heights before failure (when much repair is necessary). For regular placements this is for zero displaced blocks. For irregular placements a few blocks may be displaced, before the layer fails (displacement ratio increases above 5% for a reference area of SWL $\pm 5 \cdot D_n$).

Within the regular placement methods the closed pyramid and the double pyramid method are preferred. For low packing densities (around 45 and 50 percent), which approach single layer placement, the closed pyramid placement is the most stable. For higher packing densities (around 55 percent) the stability is equal, however the reflection coefficients for the double pyramid placement with openings to the under layer of $\frac{1}{2} \cdot D_n$ are far lower. When the packing density is higher also the stability and the reflection coefficient are higher. For packing densities around 60 percent only the double pyramid method was tested which behaved very stable. It was found that when the double pyramid placement method is placed less accurate (more irregular positioned) the stability decreases. It is recommended to investigate the possible negative influence of oblique incoming waves on the double pyramid placement method.

For situations where the waves come in perpendicular to the structure, the slope is very short (or the toe very stable) and reflection and overtopping are not a determining factor, the regular positioned column method is the most stable solution. The properties for the mentioned regular placement methods are presented in table 6.11, wherein the reflection coefficients are from the first wave series.

A disadvantage of the regular placement methods is that the under layer and the toe have to be smooth (especially for the double pyramid method) and the blocks have to be placed very accurate. This accurate placing depends on the obtainable equipment and the environmental circumstances. When this is not possible or too expensive it is recommended too use the layer by layer placed irregular or the irregular positioned column placement method.

Placement method	Experiment	ψ_s (%)	K_{D0}	C_r
Closed pyramid	14	44.8	4.1	0.34
Closed pyramid	1	49.7	6.4	0.34
Double pyramid ($\frac{1}{2} \cdot D_n$)	11	54.3	16.4	0.29
Double pyramid (0-? $\cdot D_n$)	9	58.5	23.7	0.33
Column	6	49.1	16.3	0.36

Table 6.11: Properties of the regular methods

The layer by layer placed irregular placement method is less stable than the regular placement methods and is only applicable for packing densities above 55 percent. For a packing density around 55 percent the reflection coefficients are similar for the double pyramid placement with openings to the under layer of $\frac{1}{2} \cdot D_n$.

For situations where the waves come in perpendicular to the structure and small damage is allowed (within 5% for a reference area of SWL $\pm 5 \cdot D_n$), the irregular positioned column method behaves more stable than the irregular placement. For this method a stable toe (or short slope) is required. It is possible to obtain packing densities lower than 55 percent with this method. The properties for the mentioned irregular positioned placement methods are presented in table 6.12, wherein the reflection coefficients are from the first wave series. Both irregular positioned methods have as

disadvantage that the blocks will slide and settle after placement. Therefore it is very difficult to obtain a prescribed packing density. Because of this settling it is possible that extra blocks have to be added during construction. The packing density will come out higher, which results in a more stable layer with higher reflection and overtopping.

Placement method	Experiment	ψ_s (%)	K_{D0}	K_{DH}	$K_{D<5\%}$	C_r
Irregular (placed per layer)	16	57.4	6.5	9.7	9.7	0.29
Irregular (placed per layer)	5	61.1	2.3	4.1	16.3	0.33
Irregular positioned column	3	54.2	4.0	-	23.7	0.31

Table 6.12: Properties of the irregular positioned methods

From these results follows that when the layer and the toe are smooth and the blocks can be placed accurate the closed and double pyramid placement methods perform the best. The eventual choice for the packing density depends on the allowed reflection or overtopping and the construction costs. These costs are determined by the required block volume, the required volume of concrete and the required number of blocks, which are determined by the packing density and accompanying stability-value. In the next chapter the costs will be discussed in more detail.

7 Cost analysis

The total costs of a breakwater are determined by the construction costs and the maintenance costs. The maintenance costs contain the costs for monitoring and maintenance of the breakwater. This maintenance can be corrective (after failure) or preventive (before failure). The construction costs can be divided into direct costs and indirect costs. Indirect construction costs are not directly related to the construction of the structure, like offices and staff. The direct construction costs can be divided into constant and variable costs. The constant costs are determined by the material costs, which depend on the required quantity, and the costs for the mobilisation and demobilisation of the plant, equipment and material. The variable costs are time related and contain costs for labour, fuel and equipment.

In the first paragraph the direct construction costs will be discussed. In paragraph 1.2 the costs for the regular placements, which performed the best in the previous chapter, are compared and in paragraph 1.3 the costs for the regular and irregular placements are compared.

7.1 Direct construction costs

For the construction of a breakwater: a core, filter layer(s), toe, scour protection and an armour layer have to be placed. This research focuses on different placement methods of the armour layer and therefore only the influence of the armour layer on the direct construction costs will be discussed. To compare the costs for the different placement methods and packing densities with accompanying stability values the costs are approached by dividing them into production, placement and constant costs, see equation 7.1. These costs are all expressed as costs per square meter of breakwater slope.

$$C_t = V_t \cdot X + N_t \cdot Y + D = \psi_s \cdot n \cdot \sqrt[3]{V_b} \cdot X + \frac{\psi_s \cdot n}{V_b^{2/3}} \cdot Y + D \qquad (7.1)$$

The production costs are expressed as the costs per cubic meter of block per square meter, X, times the required cubic meters of block per square meter, V_t. The production costs consist of the costs for concrete, moulds and the production and hardening of the blocks. The costs for the production plant and storage area are assumed to be constant per project and part of the indirect construction costs and are therefore not included. The production costs are influenced by the concrete, material, labour and equipment prices, the required block volume and the required number of blocks. For the production of bigger blocks; more concrete, a bigger mould, more time (for production and hardening) and more labour are required per block. However, fewer blocks have to be produced. The costs per cubic meter of produced block are therefore rather independent on the block volume and lie around the €200, [VAN DER HOEVEN, 2007].

The placement costs are expressed as costs per block per square meter, Y, times the required number of blocks per square meter, N_t. The placement costs consist of the costs for transport and placing of the blocks. It is assumed that the influence on the placement costs by the transport logistics, possible breakdown of equipment and the environmental conditions (unworkable days) are constant per project. Therefore they are not included in the placement costs. The placement costs are influenced by the labour and equipment prices, the required accuracy of placing, the required block volume and the required number of blocks. For the placement of bigger blocks stronger equipment (more expensive per week) for transport and placing is required with higher mobilisation and demobilisation costs. However, fewer blocks have to be placed, which decreases the total construction time. If the blocks have to be placed very accurately the costs per block rise,

because specialised equipment, more time, and a diving team are required. The costs for small blocks placed from the breakwater (close to the production plant) lie around the €50,- per block. The costs for big blocks placed from the water lie around the €300,- per block [VAN DER HOEVEN, 2007].

The constant costs, D, are the extra costs per square meter, which are directly related to the chosen placement method and packing density with accompanying stability. They can consist of the costs for a smoother under layer and toe, a more stable toe and more under layers or more expensive under layers because of the use of bigger blocks. They are influenced by the size of the blocks and the placement method.

For this cost approach it is assumed that the costs per cubic meter of produced block are constant. Therefore the placement and the constant costs per square meter can be expressed as a ratio of the production costs, see equation 7.2.

$$C_t = \psi_s \cdot n \cdot \sqrt[3]{V_b} \cdot X + \frac{\psi_s \cdot n}{V_b^{2/3}} \cdot Z \cdot X + E \cdot X \tag{7.2}$$

In which Z ($= Y / X$) is the placement costs ratio, which lies between 0.25 and 1.5, and E ($= D / X$) is the constant costs ratio.

7.2 Regular placement

In this paragraph the costs for the four best performing regular pyramid placement methods with different packing densities (experiments 14, 1, 11 and 9) are compared. From the previous paragraph followed that the costs are determined by the required volume of concrete, the required number of blocks (both with accompanying costs) and the constant costs. The required volume of concrete and the required volume of blocks are in their turn determined by the packing density, the number of layers and the block volume. The block volume is calculated with the significant wave height, the stability value, the slope angle and the densities of the concrete and the water.

To visualize the influence of the packing density and accompanying stability value the required block volume, V_b, the required volume of concrete per square meter, V_t, and the required number of blocks per square meter, N_t, for the four pyramid placement methods from the previous chapter, are presented for different wave heights in the figures 7.1, 7.2 and 7.3 respectively. Also the ratios between the different experiments are calculated for these volumes and numbers and are presented in table 7.1. In this table A and B stand for the closed pyramid placement method with packing densities of 44.8% and 49.7% with accompanying K_{D0}-values of 4.1 and 6.4 respectively. C and D stand for the double pyramid placement method with packing densities of 54.3% and 58.5% with accompanying K_{D0}-values of 16.4 and 23.7 respectively. For these calculations concrete with a density of 2400 kg/m³ and salt water with a density of 1035 kg/m³ is used.
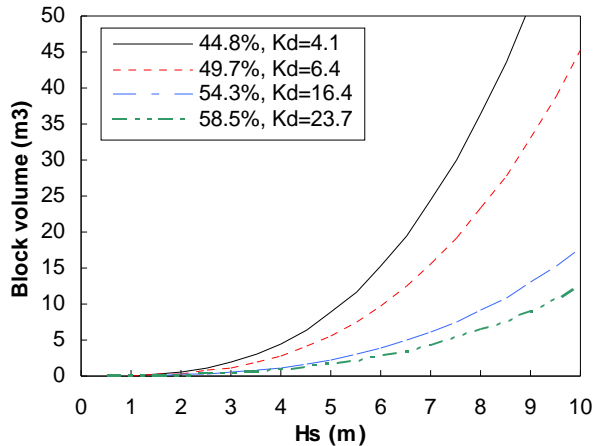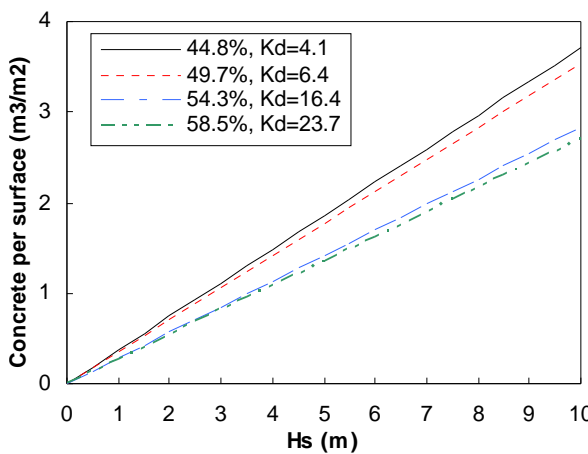
Figure 7.1: Required block volume
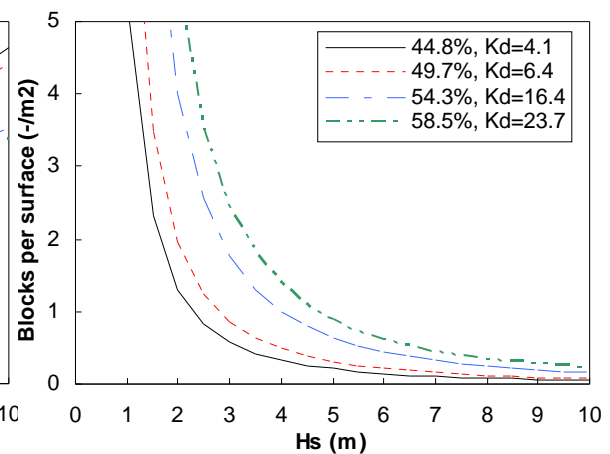

Figure 7.2: Required volume of concrete

Figure 7.3: Required number of blocks

	A:B	A:C	A:D	B:C	B:D	C:D
R_{Vb}	1.56	4.00	5.78	2.56	3.70	1.45
R_{Vt}	1.05	1.31	1.37	1.25	1.31	1.05
R_{Nt}	0.67	0.33	0.24	0.49	0.36	0.73

Table 7.1: Volume and number ratios between the experiments

From these figures and table follows that the lower packing densities with lower accompanying stability values lead to bigger required blocks, more required concrete, but fewer required blocks. Especially the ratios between A and D are striking.

To compare the costs for the different regular placements the constant extra costs are assumed equal per placement and are therefore neglected. In the first comparison the placement costs ratios (Z) are equal for all experiments in the second comparison the placement costs ratios differ per placement.

7.2.1 Cost comparison with equal placement ratios

For this cost comparison the placement costs ratios are assumed to be independent of the block volume and are therefore equal for all experiments ($Z_x = Z_y$). The constant costs are assumed to be equal per placement and are therefore neglected for this comparison. In reality the required block volume would determine the averaged stone weight of the layer and the number of filter layers.

These assumptions result in the following cost equation:

$$C_t = \psi_s \cdot n \cdot \sqrt[3]{V_b} \cdot X + \frac{\psi_s \cdot n}{V_b^{2/3}} \cdot Z \cdot X$$

In which the minimum value for Z is ¼ and the maximum value is 1.5.
In the figures 7.4, 7.5, 7.6 and 7.7 the costs for different placements are presented for the Z-values: 0.25, 0.5, 1.0 and 1.5. The costs are expressed as a ratio of X.
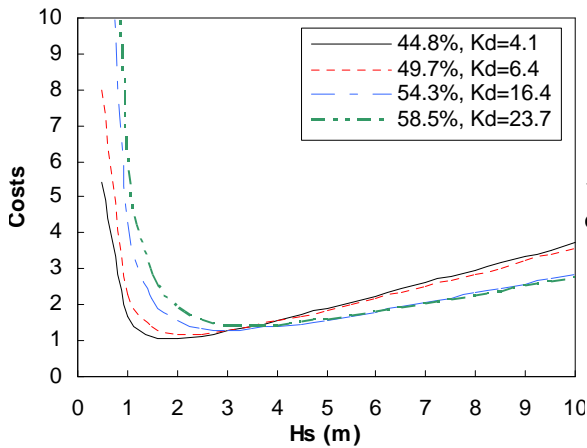
Figure 7.4: Costs for Z =0.25
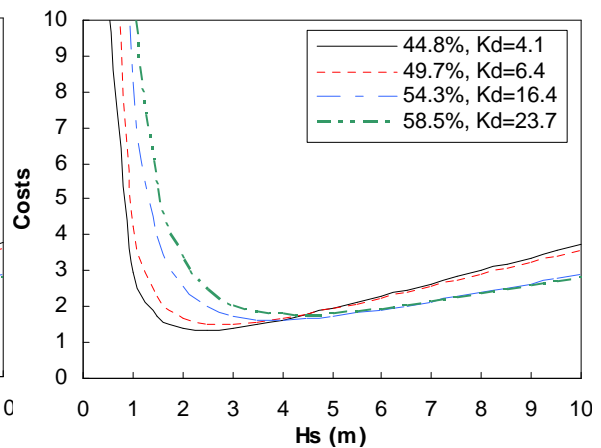
Figure 7.5: Costs for Z =0.5
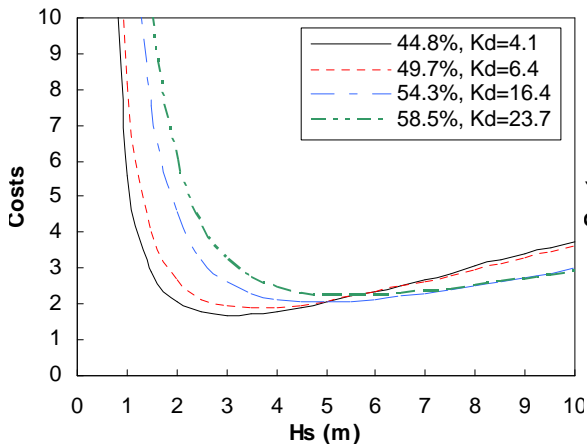
Figure 7.6: Costs for Z =1.0
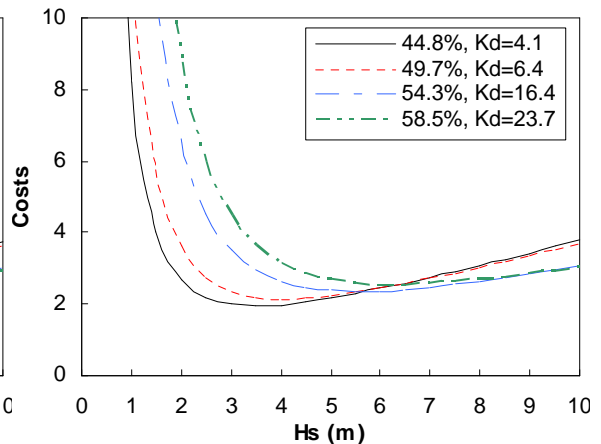
Figure 7.7: Costs for Z =1.5

From these figures it follows that for low design wave heights, where the block volumes are smaller; the costs for the lower packing densities are less than for the higher packing densities. This is because for low wave heights the total costs are mainly determined by the required number of blocks (placement costs), which are lower for lower packing densities. When the placement costs ratio increases the placement costs have more influence on the total costs. Therefore the costs for the lower packing densities stay relatively lower for higher wave heights. The influence of the placement costs on the total costs can also be seen in the figures 7.8 and 7.9. These figures show the percentage of the total costs which is determined by the production costs. In figure 7.8 the influence of the packing density with accompanying stability-value and in figure 7.9 the influence of the placing costs ratio is shown.
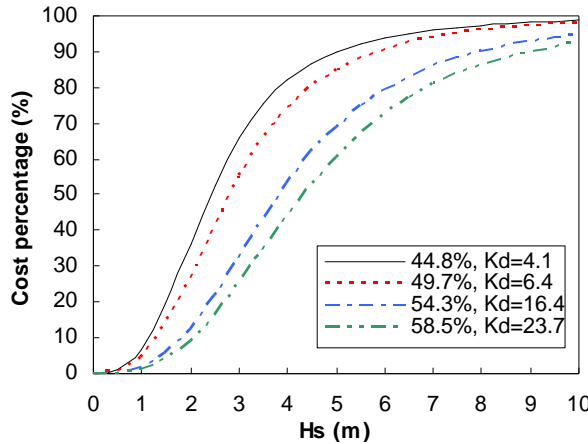
Figure 7.8: Production percentage for $Z=1$ Figure 7.9: Production percentage for method A
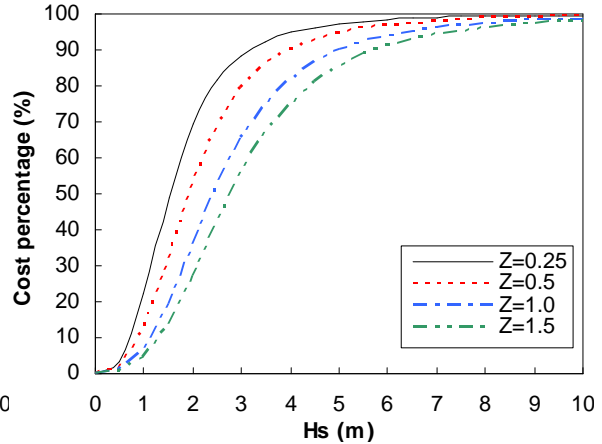
In table 7.2 the minimum costs are presented per placement for different placement costs ratios. The wave heights where the minimum costs are obtained are calculated with equation 7.3:

$$H_s = \left(2 \cdot Z \cdot K_D \cdot \cot \alpha \cdot \Delta^3\right)^{1/3} \tag{7.3}$$

From this table it follows that when the placement costs ratio or the packing density with accompanying stability-value increases the minimum costs also increase and are obtained for higher design wave heights.

		$Z = 0.25$	$Z = 0.5$	$Z = 1.0$	$Z = 1.5$
$\psi_s = 44.8\%$	H_s	1.92	2.42	3.04	3.48
$K_D = 4.1$	C_t	1.07	1.34	1.69	1.94
$\psi_s = 49.7\%$	H_s	2.22	2.80	3.53	4.04
$K_D = 6.4$	C_t	1.18	1.49	1.88	2.15
$\psi_s = 54.3\%$	H_s	3.04	3.84	4.83	5.53
$K_D = 16.4$	C_t	1.29	1.63	2.05	2.35
$\psi_s = 58.5\%$	H_s	3.44	4.34	5.46	6.25
$K_D = 23.7$	C_t	1.39	1.76	2.21	2.53

Table 7.2: Minimum costs for different placements and placement costs ratios

To compare the costs for the different experiments the costs ratios, R_{Ct}, are calculated for the different experiments with equation 7.4.

$$R_{Ct} = \frac{C_{tx}}{C_{ty}} = \frac{\psi_{sx} \cdot V_{bx}^{1/3} + \psi_{sx} \cdot V_{bx}^{-2/3} \cdot Z_x}{\psi_{sy} \cdot V_{by}^{1/3} + \psi_{sy} \cdot V_{by}^{-2/3} \cdot Z_y} \tag{7.4}$$

The ratios are presented for the different placement with $Z=1$ in figure 7.10. In figure 7.11 the cost ratios between experiment A and D are presented for different values of Z.
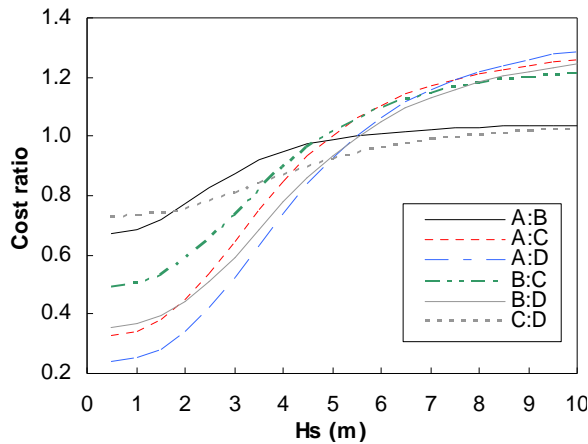
Figure 7.10: Cost ratios for $Z=1$
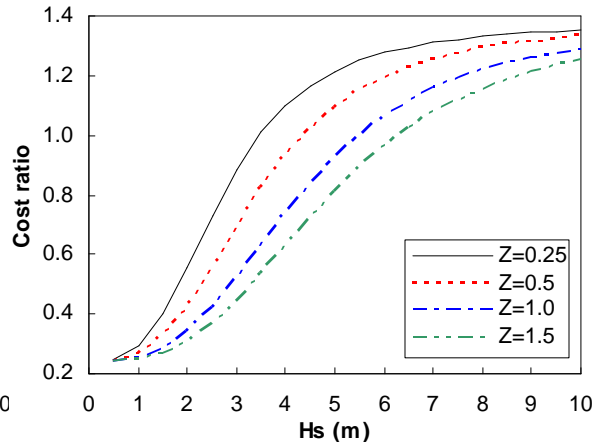
Figure 7.11: Cost ratios for placement A vs. D

When the ratios are below 1 the first experiment (x), with lower packing density, is cheaper. From the figures can be concluded that for the lower wave heights the difference in costs is higher (lower cost ratio) when the packing densities differ more. This is because for the lower wave heights the costs are mostly determined by the number of required blocks, which ratio is large. With increasing wave height the ratios cross 1 (equal costs) and stabilize, because the costs are then mainly determined by the volume of required concrete which ratio is constant and smaller than the ratio for the required number of placed blocks. The ratios for A:B and C:D stabilize around one. The cost differences are therefore minimal for these placements for high design wave heights. From figure 7.11 follows that for increasing Z-values the ratios increase less rapidly. This is because the placement costs have than more influence on the total costs.

When the ratio between the costs is equal to 1 the costs intersect. With equation 7.5 the design wave height for the intersection point can be calculated for different Z-values.

$$H_s = \left(\cot\alpha \cdot \Delta^3 \cdot Z \cdot \frac{\left(\psi_{sy} \cdot K_{Dy}^{2/3} - \psi_{sx} \cdot K_{Dx}^{2/3} \right)}{\left(\psi_{sx} \cdot K_{Dx}^{-1/3} - \psi_{sy} \cdot K_{Dy}^{-1/3} \right)} \right)^{1/3} \tag{7.5}$$

The found intersection wave heights for different Z-values are presented in figure 7.12. Under the line the first experiment (x) is cheaper and above the line the second experiment (y) is cheaper. The intersections are plotted for $Z=1$ in figure 7.13. The intersection points are also presented in table 7.3 for $Z = 0.25$, 0.5, 1.0 and 1.5.
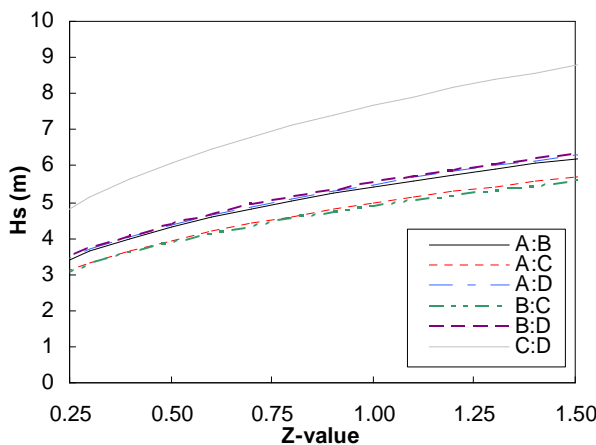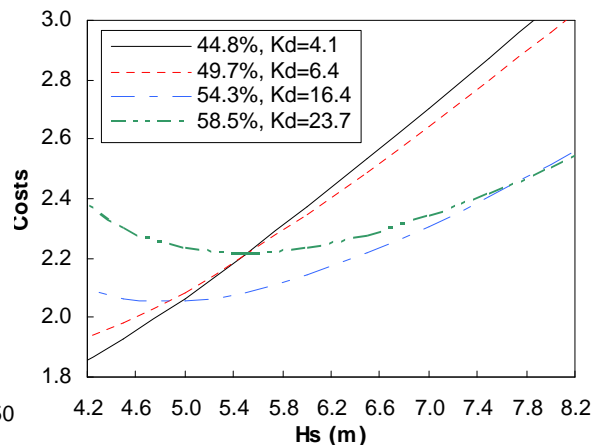

Figure 7.12: Intersection points for diff. Z-values

Figure 7.13: Intersection points for $Z=1$

		A:B	A:C	A:D	B:C	B:D	C:D
$Z = 0.25$	H_s	3.42	3.13	3.46	3.06	3.47	4.83
	C_t	1.38	1.29	1.39	1.29	1.39	1.54
$Z = 0.5$	H_s	4.30	3.94	4.36	3.85	4.37	6.09
	C_t	1.74	1.63	1.76	1.63	1.76	1.94
$Z = 1.0$	H_s	5.42	4.97	5.50	4.85	5.51	7.67
	C_t	2.19	2.05	2.21	2.05	2.21	2.44
$Z = 1.5$	H_s	6.20	5.69	6.29	5.55	6.31	8.78
	C_t	2.50	2.35	2.53	2.35	2.53	2.80

Table 7.3: Intersection of costs for different Z-values

When the design wave height increases the placements with higher packing densities become the cheapest. The design wave heights, where the costs intersect, are higher when the Z-value increases. This means that for higher Z-values the placements with lower packing densities are cheaper for higher wave heights. For design wave heights under 3.13 meter placement A has always the lowest costs (Z=0.25). For design wave heights above 8.78 m. placement D has always the lowest costs (Z=1.5).

For the design of an armour layer the design wave height is known. With equation 7.6 the critical Z-value, where the costs intersect, can be calculated.

$$Z = \frac{H_s^3}{\cot\alpha \cdot \Delta^3} \cdot \frac{\left(\psi_{sx} \cdot K_{Dx}^{-1/3} - \psi_{sy} \cdot K_{Dy}^{-1/3}\right)}{\left(\psi_{sy} \cdot K_{Dy}^{2/3} - \psi_{sx} \cdot K_{Dx}^{2/3}\right)} \tag{7.6}$$

The critical Z-values for different wave heights are presented in figure 7.14. At the left side of the line the first experiment (x) is cheaper and at the right side the second experiment (y) is the cheapest.
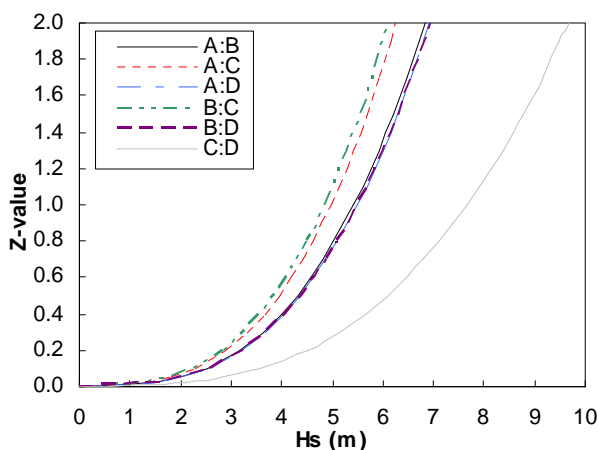
Figure 7.14: Critical Z-values for design wave heights

7.2.2 Cost comparison with different placement ratios

In the previous paragraph was assumed that the Z-value (placement costs ratio) is equal for all placements. However in reality the placing costs are for a part determined by the block size. To approach this the Z-value is calculated with the block volume ratio, R_{Vb}. When is assumed that for the four regular experiments the Z-value is only determined by the block size and the complete bandwidth of Z (0.25-1.5) is used, this will lead to the following values: Z_A=1.5, Z_B=1.1, Z_C=0.6 and Z_D=0.25. With these values the costs are calculated and presented in figure 7.15. From this figure follows that, when the difference in Z-values is very large the placement with the highest packing density and accompanying stability value (smallest Z-value) is the cheapest for all the relevant wave heights.
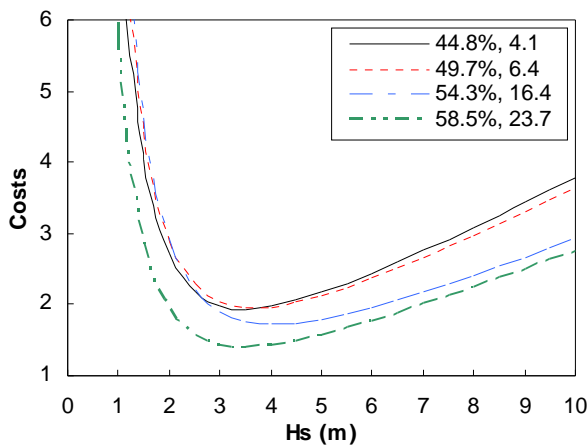
Figure 7.15: Costs for different Z-values

This method, however, is too extreme, because the Z-values are not only determined by the block volume and therefore not the complete bandwidth should be used. The use of the more representative bandwidth (0.6-1.2) leads to the following Z-values: Z_A=1.2, Z_B=1.0, Z_C=0.8 and Z_D=0.6. With these values the costs are calculated and presented in figure 7.16 and 7.17. For wave heights up to 4.1 meter method A is the cheapest, from 4.1 to 4.3 meter method C is the cheapest and for wave heights above 4.3 meters method D, with the highest packing density, is the cheapest.
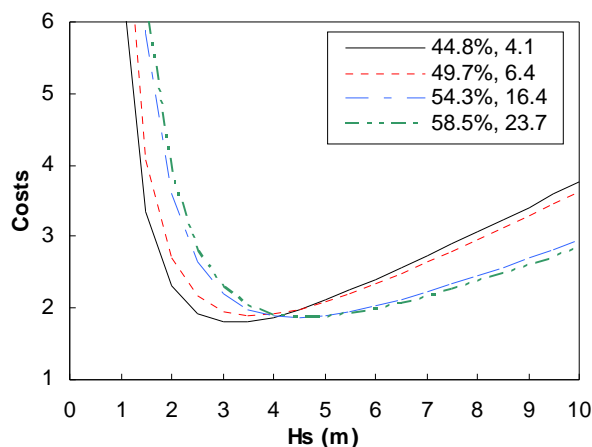
Figure 7.16: Costs for different Z-values   Figure 7.17: Costs for different Z-values
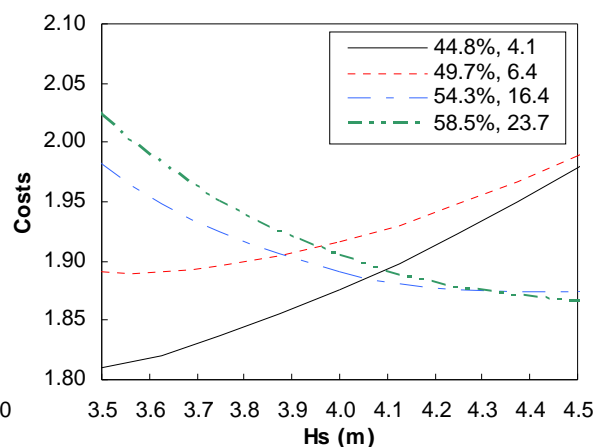
It can be concluded that for a small spreading of Z -values, determined by the ratio of block volumes, the placements with higher packing densities and accompanying stability values are cheaper for higher wave heights. This was also concluded in the previous paragraph. When the spreading width of Z increases, the wave heights where the costs intersect become lower up to the situation wherein the placement with the higher packing density and accompanying stability is the cheapest for all the wave heights.

It is however not completely realistic to determine the Z -values from the block volume ratios, because for small wave heights the blocks are all within the same range of volume. When the wave heights are smaller than 4 meter the required block volumes are for all four methods within 5 cubic meters and therefore the placing costs per block will differ very little. For higher wave heights the difference in absolute block volumes increases exponential. Therefore another approach for the placement costs, depending on the block volume, is presented.

The price for the equipment determines the placement costs. This price depends on the strength of the equipment, which depends on the required block volume. Therefore the placement costs per block are equal when the block sizes are within a fixed range. To illustrate this four ranges are assumed. For the first range the placement costs ratio, Z , is 0.25 when the block volume is less than 1 cubic meter. For block volumes between 1 and 5m³ Z =0.5, for block volumes between 5 and 20m³ Z =1 and for block volumes above 20 m³ Z =1.5. The resulting costs are presented in figure 7.18 and 7.19.
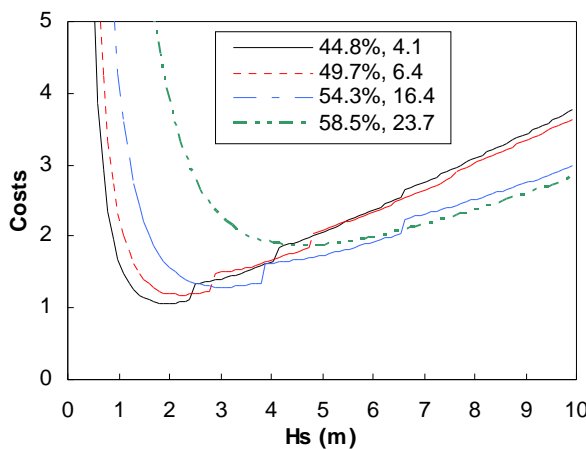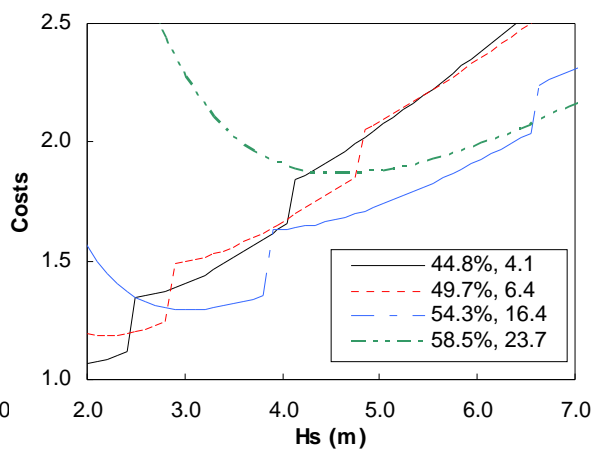

Figure 7.18: Costs per placement   Figure 7.19: Costs per placement

From the figures 7.18 and 7.19 follows again that for higher wave heights the higher packing densities with accompanying stability values are the cheapest.

To calculate the wave height where the costs intersect for 2 placements with different placement costs ratios equation 7.7 is formulated.

$$H_s = \left(\cot \alpha \cdot \Delta^3 \cdot \frac{\left(\psi_{sy} \cdot K_{Dy}^{2/3} \cdot Z_y - \psi_{sx} \cdot K_{Dx}^{2/3} \cdot Z_x \right)}{\left(\psi_{sx} \cdot K_{Dx}^{-1/3} - \psi_{sy} \cdot K_{Dy}^{-1/3} \right)} \right)^{1/3} \qquad (7.7)$$

An armour layer will be designed for a specific design wave height. When two alternatives are chosen the cost ratio of the second placement, where the costs intersect, can be calculated with equation 7.8.

$$Z_y = \frac{\left(\dfrac{H_s^3}{\cot \alpha \cdot \Delta^3}\right) \cdot \left(\psi_{sx} \cdot K_{Dx}^{-1/3} - \psi_{sy} \cdot K_{Dy}^{-1/3}\right) + \psi_{sx} \cdot K_{Dx}^{2/3} \cdot Z_x}{\psi_{sy} \cdot K_{Dy}^{2/3}} \qquad (7.8)$$

The results of this equation for $Z_x = 1$ are presented in figure 7.20. The first experiment (x) is the cheapest when the combination of Z_x and H_s lies above the cost intersection line.
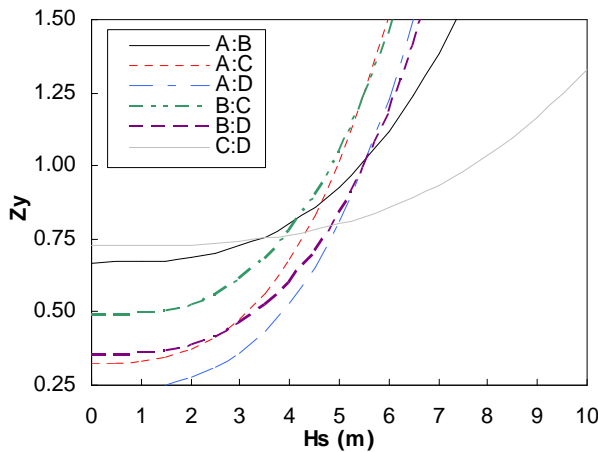
Figure 7.20: Costs intersection lines for $Z_x = 1$

It can be concluded from figure 7.20 that with increasing placement costs for experiment y also the wave height where the costs intersect increases and experiment x is cheaper for higher wave heights. For values below the minimum Z_y-values the second experiment (y) is always the cheapest. When the maximum Z_y-value is 1.5 the wave heights for which the second experiment (y) is always the cheapest can be determined.

7.3 Regular versus irregular placement

From the performed experiments followed that the regular double layered pyramid method (experiment 11) is far more stable than the irregular placement method (experiment 16) for similar packing densities 54.3% and 57.4% respectively. The stability value, K_{D0}, of the regular placed experiment 11 was 16.4 and based on zero displacements. This stability value will possibly be lower for oblique incoming waves. The stability value, $K_{D<5\%}$, of the irregular placed experiment 16 was 9.7 and a few displacements (less than 5%) were allowed. The reflection coefficients were similar and therefore the regular method is preferred, because it is more stable and settles less. However, for the construction of the regular method a smoother under layer and toe are required and the blocks have to be placed more accurately. If this is not possible because of the environmental conditions the irregular placement is preferred. If it is possible it results in extra placing costs per block, for the accurate placing, and in extra costs per square meter, $E \cdot X$, for the smoother under layer and toe.

The costs for the regular placement are expressed with equation 7.9 and the costs for the irregular placement are expressed with equation 7.10.

$$C_{tx} = \psi_{sx} \cdot n_x \cdot \sqrt[3]{V_{bx}} \cdot X + \frac{\psi_{sx} \cdot n_x}{V_{bx}^{2/3}} \cdot Z_x \cdot X + E \cdot X \qquad (7.9)$$

$$C_{ty} = \psi_{sy} \cdot n_y \cdot \sqrt[3]{V_{by}} \cdot X + \frac{\psi_{sy} \cdot n_y}{V_{by}^{2/3}} \cdot Z_y \cdot X \qquad (7.10)$$

In the figures 7.21, 7.22 and 7.23 the required block volume, the required volume of concrete and the required number of blocks are presented respectively to visualize the influence of the different packing densities with accompanying stability values.
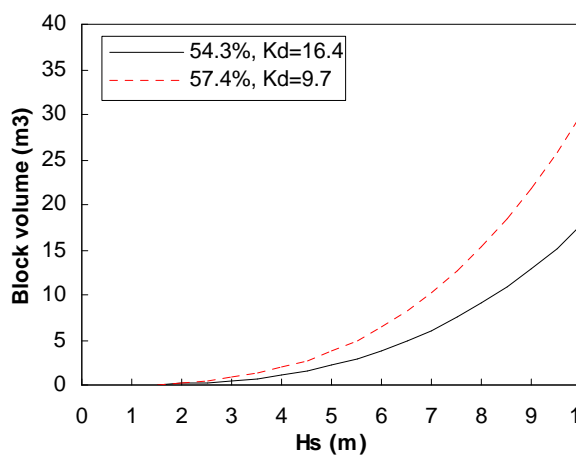
Figure 7.21: Required block volume
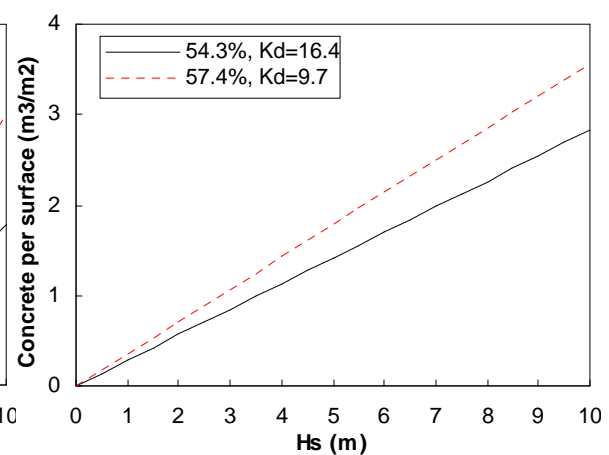
Figure 7.22: Required volume of concrete
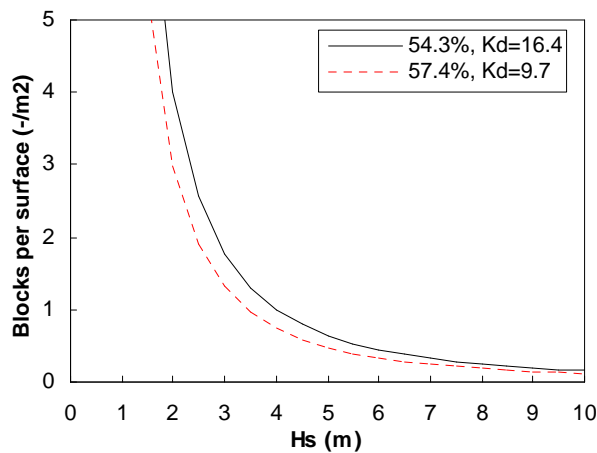
Figure 7.23: Required number of blocks

In figure 7.24 the total costs as ratio of X are presented. For this figure the placement costs ratio was 1 and equal for both methods, $Z = Z_x = Z_y = 1$. The more accurate placement was not taken into account and neither the extra costs for the smoother under layer and toe. When the extra costs were included the line for the regular method would shift upwards. The cost difference between the two methods is presented in figure 7.25.
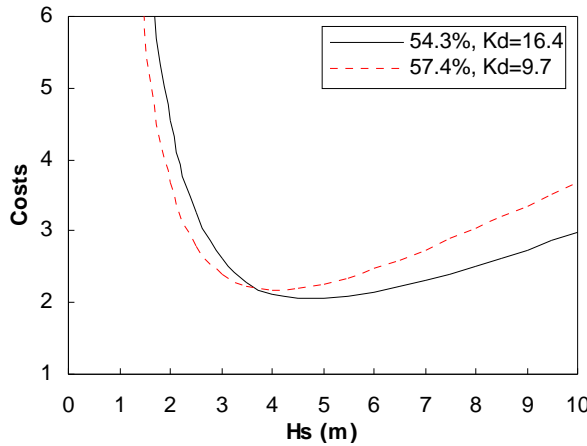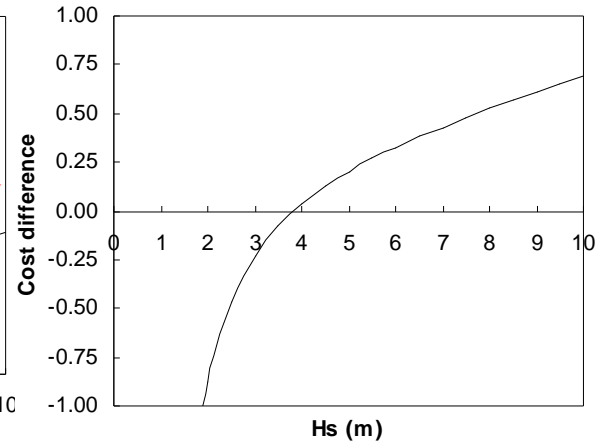
Figure 7.24: Costs for $Z = 1$

Figure 7.25: Cost difference for $Z = 1$

For the calculation of the cost difference the costs for the irregular method were subtracted from the regular method ($\Delta C_t = C_{tx} - C_{ty}$). When this value is negative, for H_s lower than 3.8, the irregular method is cheaper and therefore preferred. When the cost difference is smaller than the extra costs for smoothening the under layer and toe ($\Delta C_t < E$) the irregular method is also preferred.

When the placing costs ratios, for both placements, and the extra costs ratio are known then the total cost ratio can be calculated with equation 7.11.

$$R_{Ct} = \frac{C_{tx}}{C_{ty}} = \frac{\psi_{sx} \cdot V_{bx}^{1/3} + \psi_{sx} \cdot V_{bx}^{-2/3} \cdot Z_x + \dfrac{E}{n}}{\psi_{sy} \cdot V_{by}^{1/3} + \psi_{sy} \cdot V_{by}^{-2/3} \cdot Z_y} \tag{7.11}$$

When this ratio is below one the regular placement is cheaper. The costs are equal when the ratio is one. The Z_y-value for equal costs can be calculated with equation 7.12 if the placing costs ratio and the extra costs ratio are known for the regular method.

$$Z_y = \frac{\left(\dfrac{H_s^3}{\cot\alpha \cdot \Delta^3}\right) \cdot \left(\psi_{sx} \cdot K_{Dx}^{-1/3} - \psi_{sy} \cdot K_{Dy}^{-1/3}\right) + \left(\dfrac{H_s^3}{\cot\alpha \cdot \Delta^3}\right)^{2/3} \cdot \dfrac{E}{n} + \psi_{sx} \cdot K_{Dx}^{2/3} \cdot Z_x}{\psi_{sy} \cdot K_{Dy}^{2/3}} \tag{7.12}$$

The results of this equation, for the regular and irregular placements with $Z_x = 1$, are presented in figure 7.26, for different extra costs ratios. The irregular method is the cheapest when the combination of Z_y and H_s lies under the intersection line.
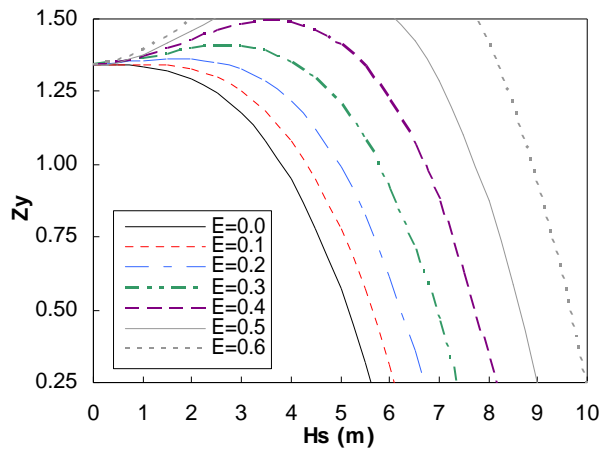
Figure 7.26: Cost intersection lines for $Z_x = 1$

From this figure it follows that when the extra costs ratio is high the irregular placement is the cheaper placement. For this comparison the extra costs ratio is only used for the costs of smoothening the under layer and toe. It is also possible to compare the total constant costs of different types of armour layer and use the difference as the value for the extra costs. In that way also the indirect construction costs and even the allowable maintenance costs per time period can be included.

For the choice of the placement method the view of the client on maintenance is also important. When the client does not want to spend money on maintenance (harbour of Barcelona) it is not recommended to use the irregular method, because the exact behaviour of the layer is insecure, even if the used blocks are bigger than required.

8 Conclusions and Recommendations

8.1 Conclusions

The main objective of this research is to assess the impact of different placement methods, with different packing densities, on the stability of Antifer-block armour layers. This is done by experimental research in the wave-flume of the Fluid mechanics laboratory of the Faculty of Civil Engineering and Geosciences at Delft University of Technology. A total of 17 experiments were performed with different placement methods and packing densities. The Antifer-blocks were placed by hand on a trunk-section with a slope of 1:1.5 and a stable toe.

The placement methods can be divided into the irregular, figure 8.1, and the regular placement methods. The irregular placement method was performed with the Antifer-blocks placed per layer and placed per row. Four types of regular placement methods were tested: the column, figure 8.2, the filled pyramid, figure 8.3, the closed pyramid, figure 8.4 and the double pyramid placement method, figure 8.5. Primarily the column and the double pyramid placement method were placed with an attempt to spread the blocks over the slope, which resulted in the sliding down and a more irregular positioning of blocks. The column method was also tested with the columns placed under an angle to gain more insight in the influence of oblique incoming waves. The size of the openings to the under layer, of the double pyramid placement method, influences the reflection coefficient. Therefore this placement method was also placed with the second layer shifted more upwards (expressed in nominal diameter).
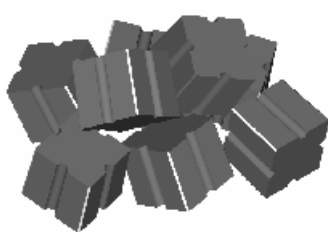

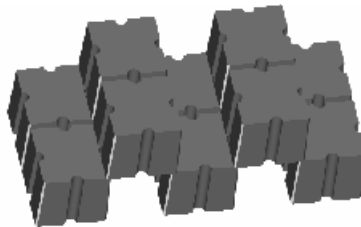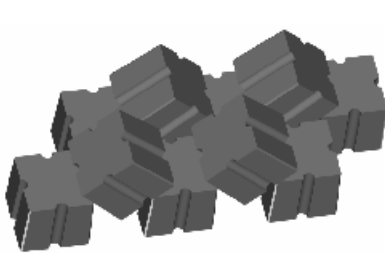Figure 8.1: Irregular   Figure 8.2: Column   Figure 8.3: Filled pyramid
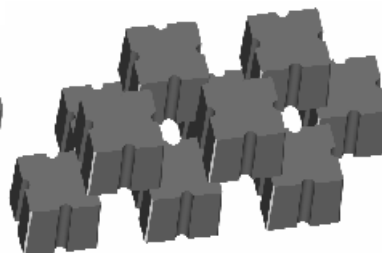

Figure 8.4: Closed pyramid   Figure 8.5: Double pyramid

The placed layers were tested with eight irregular wave series with an increasing significant wave height per wave series. After each wave series photos were taken, which were compared by using the overlay technique. In this way different block movements could be counted within different reference areas, which determined the stability of the layer. Also the reflection coefficients per wave series were calculated. During the last wave series water overtopped the breakwater, which caused the formation of a berm at the leeside. The length of this berm was an indication for the amount of overtopped water.

In table 8.1 the packing densities, ψ_s, the obtained stability values, K_D, and the obtained reflection coefficients from the first wave series, C_r, are presented for the performed experiments. It is mentioned for regular placements (regular grid) if the individual blocks were positioned irregular. For the double pyramid method also the upward shift of the second layer is mentioned. The obtained data is presented per packing density group and per group the most stable method is presented first. The stability values are based on wave heights before failure. For regular placements this is for zero displacements. The stability values for the irregular placement method are calculated for less than 5% displacements within a reference area of SWL (Still Water Level) $\pm 5 \cdot D_n$.

Packing density around 45%				
Placement method	Experiment	ψ_s (%)	K_D	C_r
Closed pyramid	14	44.8	4.1	0.34
Packing densities around 50%				
Placement method	Experiment	ψ_s (%)	K_D	C_r
Column	6	49.1	16.3	0.36
Column (under an angle)	8	50.0	9.4	0.36
Closed pyramid	1	49.7	6.4	0.34
Double pyramid (0-? $\cdot D_n$)	12	49.1	4.0	0.31
Filled pyramid	4	49.1	-	0.31
Packing densities around 55%				
Placement method	Experiment	ψ_s (%)	K_D	C_r
Double pyramid (½ $\cdot D_n$)	11	54.3	16.4	0.29
Closed pyramid	13	54.3	16.0	0.35
Double pyramid (¾ $\cdot D_n$)	15	53.9	15.9	0.31
Double pyramid (? -¼ $\cdot D_n$)	10	53.2	15.7	0.31
Double pyramid (0-? $\cdot D_n$)	17	53.5	13.2	0.32
Irregular (placed per layer)	16	57.4	9.7	0.29
Irregular (placed per row)	2	57.0	9.4	0.30
Column (irregular pos.)	3	54.2	4.0	0.31
Packing densities around 60%				
Placement method	Experiment	ψ_s (%)	K_D	C_r
Double pyramid (0-? $\cdot D_n$)	9	58.5	23.7	0.33
Double pyramid (irregular pos.)	7	58.5	16.7	0.31
Irregular (placed per layer)	5	61.1	16.3	0.33

Table 8.1: Results of performed experiments

General conclusions

- The placement of Antifer-blocks over the slope without any contact between the blocks results in the sliding down and a more irregular positioning of the blocks. Therefore the blocks can not be placed within a square grid and is it very difficult to obtain a prescribed packing density for irregular placed blocks.

- The first displacements mainly occur around the Still Water Level. This underlines the importance of the chosen reference area for the damage calculation. A larger reference area leads to a smaller damage ratio.

- For similar packing densities the regular positioned placement methods are more stable than the irregular positioned placement methods. A disadvantage is that they require accurate placing and a smooth under layer and toe.

- Higher packing densities for equal placement methods results in higher stability-values and higher reflection coefficients, see table 8.1 and figure 8.6.

- There is a positive correlation between the reflection and the overtopping. High reflection coefficients during the first wave series resulted in a long berm length, which indicates high overtopping during the last wave series.

Conclusions per method

- Because the blocks tend to settle, the lowest obtained packing density for the irregular placement method was 57%. The movement ratios for the irregular placement method are far higher than for the regular methods.

- The regular positioned column placement method is very stable. However, the reflection coefficients and the overtopping are very high. The irregular positioned column method is less stable, but the damage development is very slow and the reflection coefficients are average. Oblique incoming waves have a negative influence on the stability of both column placement methods and the high pressures on the toe should not be underestimated.

- The filled pyramid method is very unstable, because there is no integration within the second layer and between both layers.

- The closed pyramid method has high reflection coefficients for all packing densities because the layer has no openings to the under layer. It is the only method which could be tested with a packing density around 45%, where it approached a single layer placement and showed a slow damage development.

- The double pyramid method is very stable for packing densities around 55% and higher. When the blocks are positioned more irregular (less accurate) the stability-value and the reflection coefficient decrease. The reflection coefficients are the lowest when the second layer is shifted half a nominal diameter upwards. In figure 8.6 the obtained reflection coefficients, for the first wave series, are presented for different packing densities and different upward shifts of the second layer. The first number in the legend presents the experiment number and the second the upward shift of the second layer (expressed in nominal diameter).
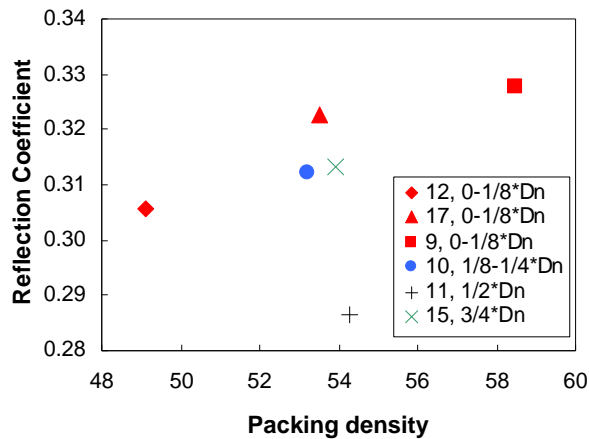
Figure 8.6: Reflection coefficients for the double pyramid placement method

- Overall it can be concluded that, when the under layer and the toe are smooth and the blocks can be placed accurate, the best performing placement methods are the closed pyramid placement method for packing densities around 45% and 50% and the double pyramid placement method for packing densities around 55% and 60%.

The eventual choice of the placement method and packing density depends on the allowed reflection and/or overtopping and the construction costs. The construction costs are divided into the production costs, the placement costs and the constant costs. The production costs are determined by the required volume of concrete per square meter and the costs per cubic meter produced block, X, which is assumed to be constant. The placement costs are determined by the number of required blocks per square meter and the costs per placed block, Y, which depends mainly on the block volume. The constant costs, D, are expressed as costs per square meter and are determined by, for example, the required smoothness of the under layer and toe. Because X is a constant the costs per placed block and the constant costs can be expressed as a ratio of X. This results in the placement costs ratio; $Z = Y / X$ and the constant costs ratio; $E = D / X$. For full understanding of the conclusions from the cost analysis it is recommended to read chapter 7.

Conclusions from cost analysis

- Lower packing densities with lower accompanying stability values lead to bigger required blocks, more required concrete, but fewer required blocks.

- The construction costs are for low design wave heights mainly determined by the placement costs and for high design wave heights by the production costs. When the placement costs or the packing density with accompanying stability value increases the minimum costs also increase and are obtained at a higher design wave height.

- For equal constant costs and equal or small differences in placement costs the placement with the higher packing density and accompanying stability value is cheaper for high design wave heights. When the placement costs decrease for both placements or only for the placement with the higher packing density, then the placement with the higher packing density becomes also cheaper for lower wave heights.

- For the cost comparison of the placements x and y, with different packing densities, stability values and constant costs, the following formula is derived. When the real placement costs ratio for placement y is lower than Z_y the costs for this placement are lower.

$$Z_y = \frac{\left(\dfrac{H_s^3}{\cot\alpha \cdot \Delta^3}\right) \cdot \left(\psi_{sx} \cdot K_{Dx}^{-1/3} - \psi_{sy} \cdot K_{Dy}^{-1/3}\right) + \left(\dfrac{H_s^3}{\cot\alpha \cdot \Delta^3}\right)^{2/3} \cdot \dfrac{E_x - E_y}{n} + \psi_{sx} \cdot K_{Dx}^{2/3} \cdot Z_x}{\psi_{sy} \cdot K_{Dy}^{2/3}}$$

8.2   Recommendations

- It was found that oblique incoming waves have a negative influence on the stability of the column placement method. It is assumed that they also negatively influence the stability of the double pyramid placement method because this placement fails when the blocks move to the side. Therefore it is recommended to perform 3D model tests with oblique incoming waves.

- The experiments were all performed for the trunk section. The placement on the roundhead is different, because the surface is round and the radius is bigger at the toe. Therefore it is recommended to test the stability behaviour of the different placement methods for the roundhead and for the transition between the trunk and the roundhead.

- It is concluded from the obtained reflection coefficients and the measured berm length on the leeside, which is an indicator for the amount of overtopped water, that there is a positive correlation between the reflection coefficient and the overtopping. It is recommended to perform overtopping tests for the different placements to obtain the exact relation between the reflection coefficients and overtopping.

- The cost analysis and resulting formulas give a general view of the influence on the costs of the type of placement method and the packing density with accompanying stability value. It is recommended to validate the equations for different projects and to obtain reliable values for the extra constant costs and the placement costs ratios. When the equations and obtained data are then applied in the design phase this may result in the realisation of cheaper breakwaters.

- The regular placement methods, especially the column placement method, perform high pressures on the toe. This may lead to instability of the toe and subsequent sliding down of the second layer. Therefore it is recommended to investigate the required toe stability, how this can be obtained and the extra constant costs for the application.

- The applied scaling procedure led to small viscous scale effects, because the flow inside the core was not fully turbulent, which might have influenced the stability. The aeration scale effect could lead to small variations in the energy dissipation, which might have influenced the reflection coefficients. Therefore tests on larger scale are recommended.

- The regular placement methods can also be constructed with plain cubes. The costs for the moulds for plain cubes are lower than for Antifer-blocks. Therefore it is recommended to perform the regular placement methods with plain cubes and to compare the obtained results and subsequent costs with the results found in this research.

- The obtained stability values, K_D, in this thesis for the irregular placement are higher than prescribed in the CEM, 2006 and by GÜNBAK, 1999, because of the use of a different damage level. Therefore it is recommended for the design of a breakwater armoured with Antifer-blocks to make sure, before choosing the stability value, which damage level is wanted.

References

BURCHARTH, H.F., LIU, Z. AND TROCH, P. (1999) Scaling of core material in rubble mound breakwater model tests, *Proceedings of the COPEDEC V, Cape Town, South Africa*, 1518-1528

CHEGINI, V AND AGHTOUMAN, P. (2001) An Investigation on the Stability of Rubble Mound Breakwaters with Armour Layers of Antifer Cubes, *International Conference in Ocean Engineering ICOE 2001, December 11-14, 2001*

DE ROUCK, J., WENS, F., VAN DAMME, L. AND LEMMERS, J. (1987) Investigations into the merits of the Haro® -Breakwater armour unit, *Proceedings of Coastal & Port Engineering in Developing Countries Vol.1*, 1054-1068

DE VRIES, M. (1977) Waterloopkunidg onderzoek: collegehandleiding b80 (Hydraulic model investigation: college manual b80), *second edition, Technische Hogeschool Delft, Delft* (in Dutch)

GÜNBAK, A.R. (1999) Antifer cubes on rubble mound breakwaters, *Proceedings of the COPEDEC V, Cape Town, South Africa,* 1450-1455

GÜNBAK, A.R. (2000) Use of rock, tetrapod, antifer, accropode, core-lock armor units on the rubble mound breakwaters, *Pianc seminar for development and cooperation, Buenos Aires, Argentina,*

HOLTHUIJSEN, L.H. (2002) Hand-out lectures on wind waves, *Delft university of Technology, Delft*

HUDSON, R.Y. AND DAVIDSON, D.D. (1975) Reliability of Rubble mound breakwater stability models, *2nd symposium on modelling techniques, American Society of Civil Engineers, Vol 2*, 1603-1622

HUDSON, R.Y. (1959) Laboratory investigations of rubble mound breakwaters, *WES Report, Vicksburg, USA*

HUDSON, R.Y., HERRMANN, F.A., SAGER, R.A., WHALIN, R.W., KEULEGAN, G.H., CHATHAM C.E. AND HALES, L.Z. (1979) Coastal hydraulic models, *Special Report, US Army Corps of Engineering, Coastal Engineering Research Centre, No. 5*.

HUGHES, S.A. (1993) Physical models and laboratory techniques in coastal engineering, *Coastal Engineering Research Center, Waterways Experiment Station, USA*

JONES, C., TRINDADE, J. AND TAE BUM, L. (1998) Recent Experience – Antifer cube units in breakwater construction, *PORTS '98,* 1179-1188

LOSADA, M.A., DESIRE, J.M. AND ALEJO, L.M. (1986) Stability of blocks as breakwater armor units, *Journal of Structure Engineering, ASCE 112 (11),* 2392-2401.

MAQUET, J.F. (1985) Port of Antifer, France, *Design and construction of mounds for breakwaters and coastal protection*, Bruun. P., 696-703

SCHIERECK, G.J. (2001) Introduction to bed, bank and shore protection, *Delft University of Technology, Faculty of Civil Engineering and Geo Sciences, Delft, The Netherlands*
VAN DER MEER, J.W. (1988a) Rock Slopes and Gravel Beaches under Wave attack, *PhD Thesis, Delft University of Technology, Delft, The Netherlands*

VAN DER MEER, J.W. (1988b) Stability of cubes, tetrapods and accropodes, *Proceedings of the Conference on Breakwaters '88 Eastbourne, Institution of Civil Engineers, Thomas Telford, London, UK*, 71-80

VAN DER MEER, J.W. (1999) Design of concrete armour layers, *Proceedings of the International Conference on Coastal Structures, Santander, Spain,* 213-221

VAN GENT, M.R.A. AND SPAAN, G.B.H. (1998) Golfbrekers met een enkele toplaag van kubussen, *Report H3387, Delft Hydraulics, Delft, The Netherlands*

YAGCI, O. AND KAPDASLI, S. (2002) Alternative placement technique for antifer blocks used on breakwaters, *Ocean Engineering 30 (2003)*, 1433-1451

YAGCI, O., KAPDASLI, S. AND CIGIZOGLU, H.K. (2003) The stability of the antifer units used on breakwaters in case of irregular placement, *Ocean Engineering 31 (2004)*, 1111-1127

YALCINER, A.C., ERGIN, A., KAHYAOGLU, I.C. AND YUNCU, H. (1999) 3D Experimental study on the stability coefficients for breakwaters armoured with antifer blocks under irregular waves, *Proceedings of the COPEDEC V, Cape Town, South Africa,* 1458-1469

Manuals
BRITISH STANDARD (1991) *part 6349*
COASTAL ENGINEERING MANUAL (2006) *Chapter V*

Oral information
Van der Hoeven, R. (2007)
Van Gent, M.R.A. (2006)

Appendix I; Properties of the materials

Antifer layer
A total of 50 Antifer-blocks were weighed both dry and under water to determine the material properties, see table A1 and figure A1.

$M_{50,dry}$ [g]	$M_{50,wet}$ [g]	ρ_s [kg/m³]	V [cm³]	D_{n50} [mm]	D_{n85} / D_{n15} [-]
162.66	97.84	2507	64.89	40.18	1.008

Table A1: Summary of properties
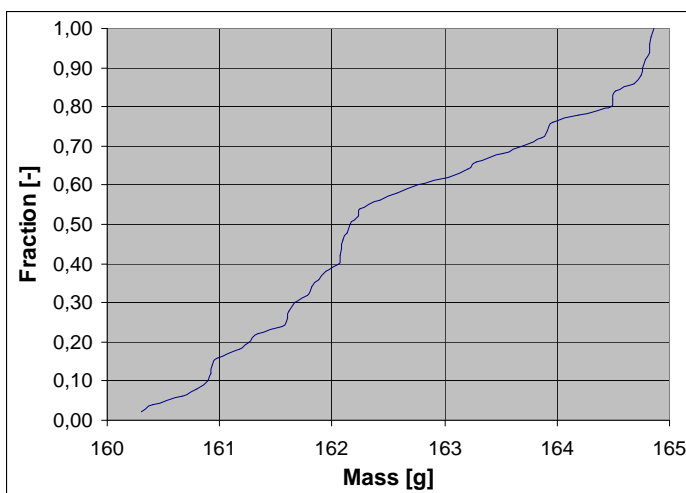
Figure A1: Weight distribution of the Antifer-blocks

Under layer
A total of 100 under layer stones were weighed both dry and under water to determine the material properties, see table A2 and figure A2.

$M_{50,dry}$ [g]	$M_{50,wet}$ [g]	ρ_s [kg/m³]	V [cm³]	D_{n50} [mm]	D_{n85} / D_{n15} [-]
20.624	12.875	2663	7.55	19.63	1.214

Table A2: Summary of properties
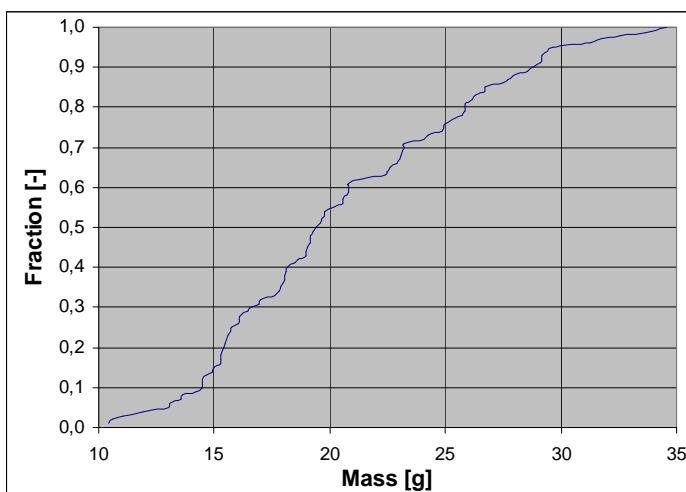
Figure A2: Weight distribution of the under layer stones

Core

A total of 100 core stones were weighed both dry and under water to determine the material properties, see table A3 and figure A3.

$M_{50,dry}$ [g]	$M_{50,wet}$ [g]	ρ_s [kg/m³]	V [cm³]	D_{n50} [mm]	D_{n85}/D_{n15} [-]
3.470	2.556	2643	1.31	10.75	1.342

Table A3: Summary of properties
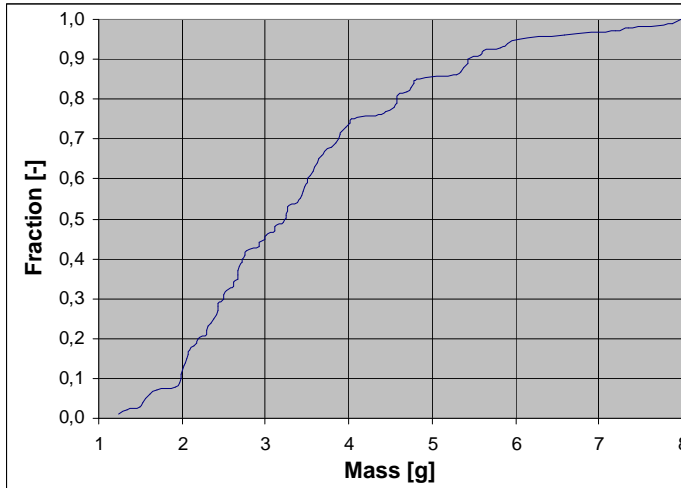
Figure A3: Weight distribution of the core stones

Toe

A total of 70 toe stones were weighed both dry and under water to determine the material properties, see table A4 and figure A4.

| $M_{50,dry}$ [g]	$M_{50,wet}$ [g]	ρ_s [kg/m³]	V [cm³]	D_{n50} [mm]	D_{n85}/D_{n15} [-]
172.67	82.62	2678	64.48	39.61	1.230

Table A4: Summary of properties
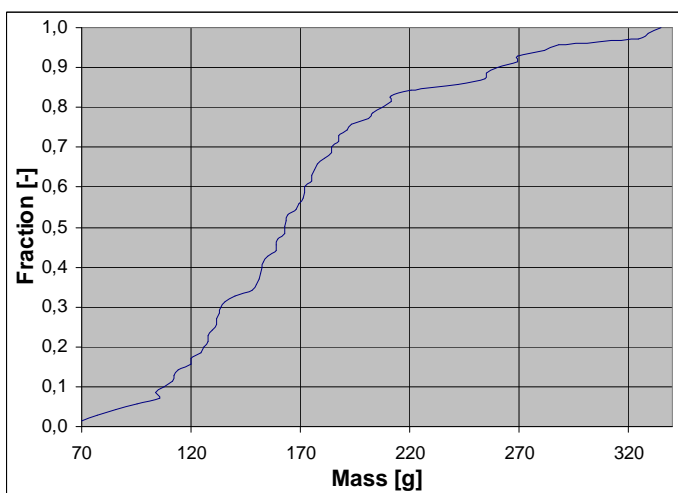
Figure A4: Weight distribution of the toe stones

Appendix II; Overview performed experiments
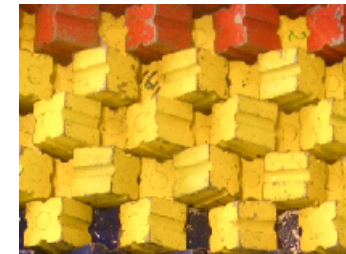
Experiment 1, $\psi_s = 49.7\%$

Experiment 2, $\psi_s = 57.0\%$

Experiment 3, $\psi_s = 54.2\%$

Experiment 4, $\psi_s = 49.1\%$

Experiment 5, $\psi_s = 61.1\%$
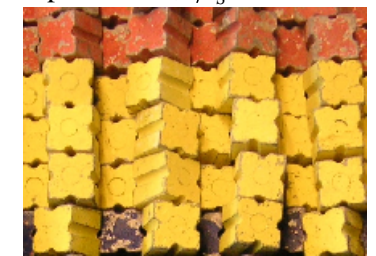
Experiment 6, $\psi_s = 49.1\%$
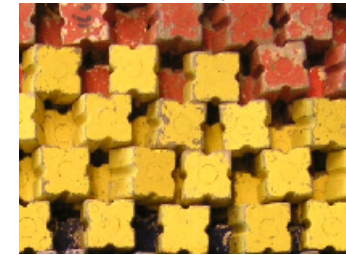
Experiment 7, $\psi_s = 58.5\%$

Experiment 8, $\psi_s = 50.0\%$
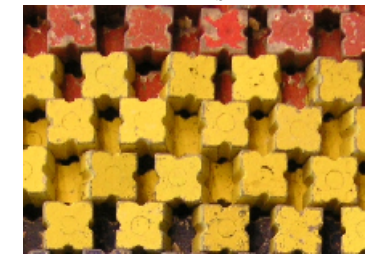
Experiment 9, $\psi_s = 58.5\%$
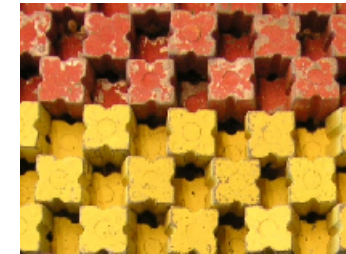
Experiment 10, $\psi_s = 53.2\%$
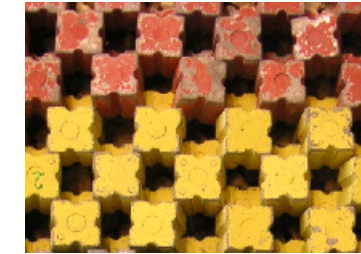
Experiment 11, $\psi_s = 54.3\%$
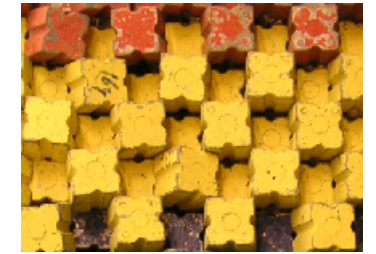
Experiment 12, $\psi_s = 49.1\%$
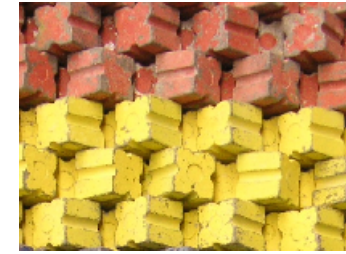
Experiment 13, $\psi_s = 54.3\%$

Experiment 14, $\psi_s = 44.8\%$
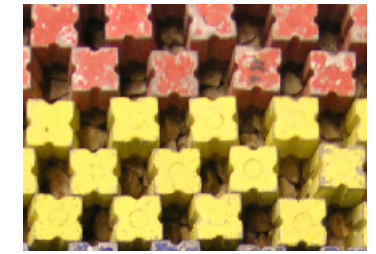
Experiment 15, $\psi_s = 53.9\%$

Experiment 16, $\psi_s = 57.4\%$
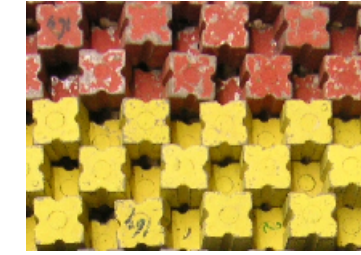
Experiment 17, $\psi_s = 53.5\%$

Appendix III; Obtained data